PHYSICS OF COMPACT OBJECTS
AND THEIR BINARY INTERACTIONS

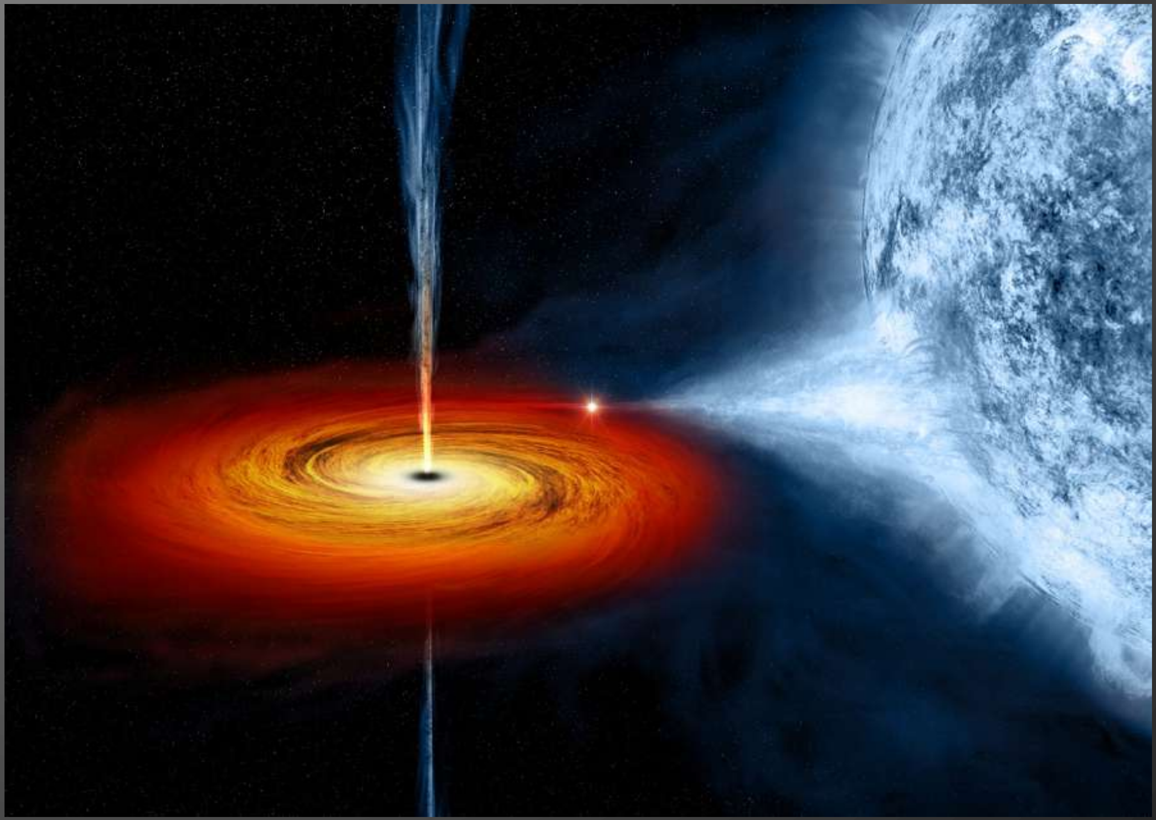

AALBORG UNIVERSITY

Thomas Tauris – Physics, Aalborg University

Last Week

Summary

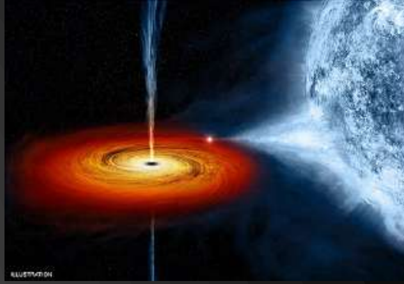

- Stellar mass BHs have spins: $0.1 < a_* < 0.99 \quad \wedge \quad a_* \equiv \frac{c\,J}{GM^2}$
- BH spins can be determined via the continuum-fitting model
- TODAY! BH spins can also be measured in merging BH binaries (LIGO)
- The two classes of BHs (transient vs persistent) have different spins
- The fast spins of the persistent BHs are natal
- The BH spins seem to be correlated with the jet power

Literature

- Shapiro & Teukolsky (1983), Chapter 12 (14)
- McClintock, Narayan & Steiner (2013)
- Fabian & Lasenby (2015)
- Tauris & van den Heuvel (2023), Chapter 7.6

Programme

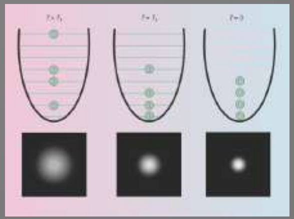



- ∗ **Introduction**
- ∗ **Degenerate Fermi Gases**

  Non-relativistic and extreme relativistic electron / (n,p,e^-) gases
- ∗ **White Dwarfs**

  Structure, cooling models, observations
- ∗ **Neutron Stars**

  Structure and equation-of-state
- ∗ **Radio Pulsars**

  Characteristics, spin evolution, magnetars, observations
- ∗ **Binary Evolution and Interactions**

  X-ray binaries, accretion, formation of millisecond pulsars, recycling
- ∗ **Black Holes**

  Observations, characteristics and spins
- ∗ **Gravitational Waves**

  Sources and detection, kilonovae
- ∗ **Exam**

Gravitational Waves
– sources and detection

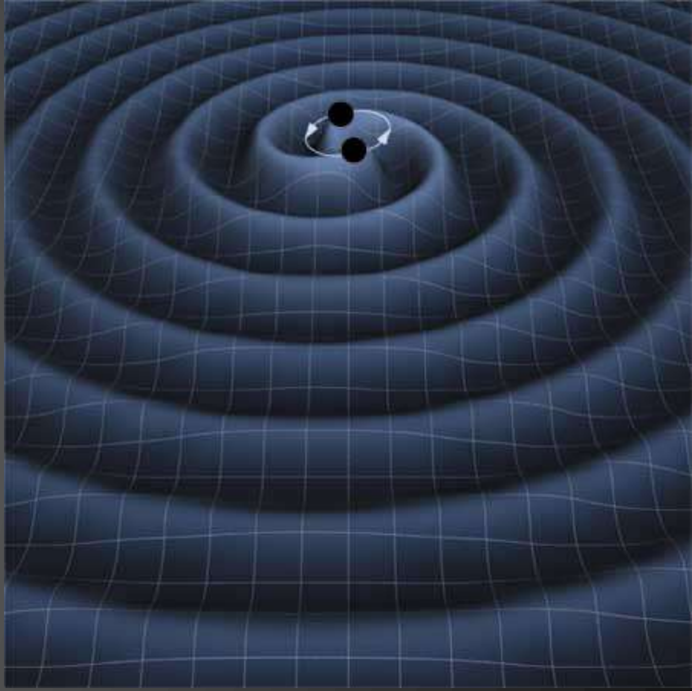

- Concepts and emission of GWs
- Detection of GWs – LIGO, LISA, PTA
- Astrophysical sources
  - Burst emission sources (extra galactic)
  - Continuous emission sources (Galactic)
- Merger timescale
- GW150914 (first BHBH merger)
- GW170817 (first NSNS merger)
- Results from GWTC-3 (LIGO O1–O3)
- Kilonovae
- aLIGO detection rates
  - Population synthesis
  - Challenges

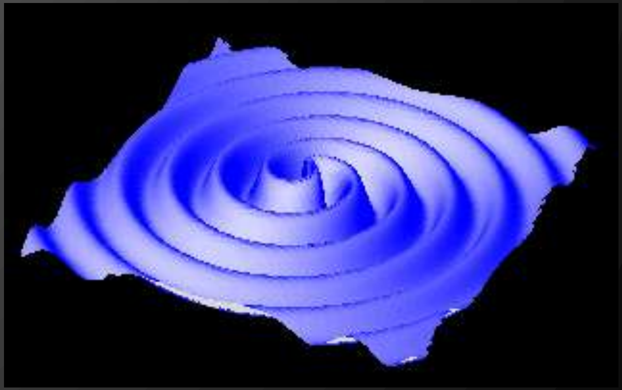

Introduction

The last 400 years of astronomy were about
”seeing” a silent movie.
LIGO is delivering the ”sound track”.

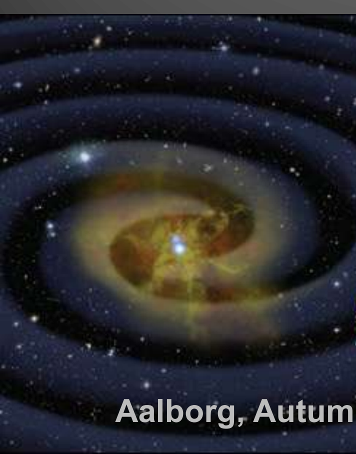

slide by Norbert Wex

Gravity regimes

(1) Quasi-stationary weak-field regime

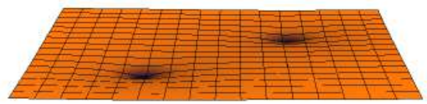

(2) Quasi-stationary strong-field regime

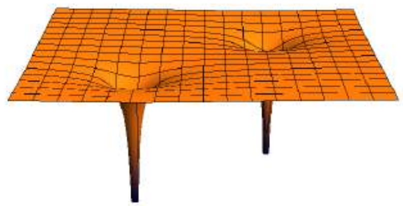

(3) Radiative regime

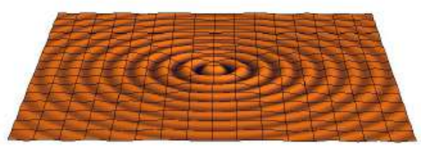

(4) Highly relativistic regime

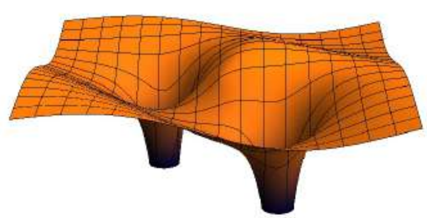

Solar system experiments

Binary pulsar experiments

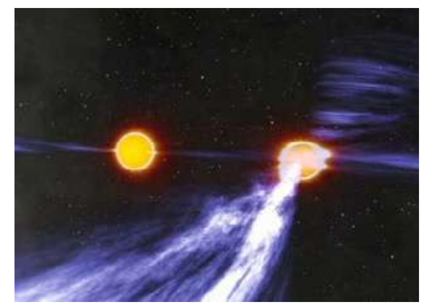

GW astronomy

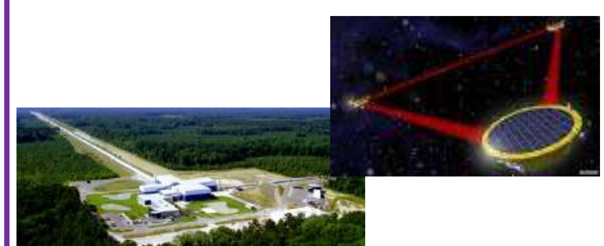

General relativity in a nutshell

- Imagine space as a stretched rubber sheet
- A mass on the surface will cause a deformation
- Another mass dropped onto the sheet will roll towards that mass

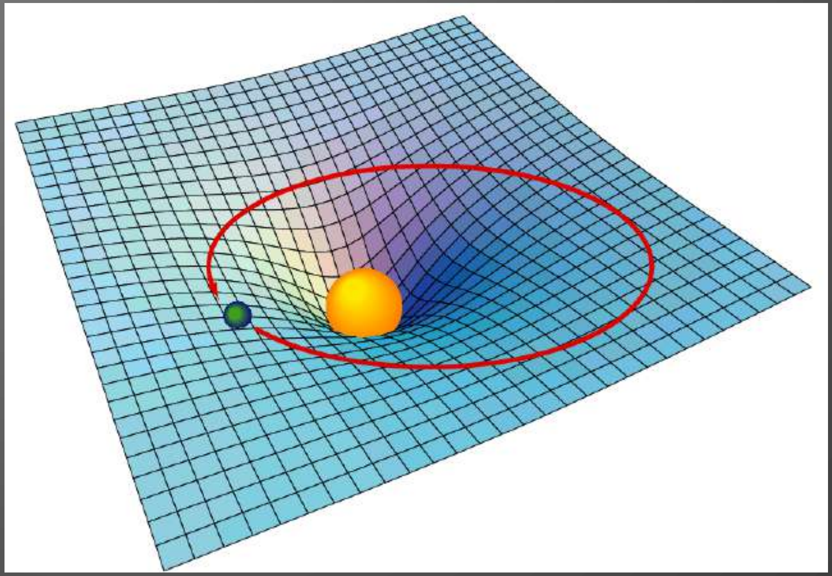

”The curvature of space determines how matter should move - and matter determines the curvature of space”

(Einstein’s field equations explained by John Wheeler)

Einstein's field equations

How does the distribution of mass-energy determine the geometry ?

$$G_{\mu\nu} = K\,T_{\mu\nu}$$ strain (curvature) = const. x stress (mass, energy)

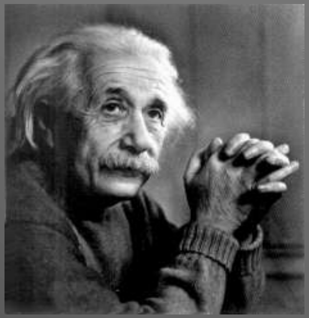

space-time curvature tensor

stress-energy tensor (source term)

scalar constant ”effectiveness of distorting space-time”

$$G_{\mu\nu} = \frac{8\pi G}{c^4} T_{\mu\nu} - \Lambda g_{\mu\upsilon}$$

(cosmological constant)

Metric

Semi-Riemannian geometry (curved space):

$$ds^2 = g_{\mu\upsilon}\, dx^{\mu} dx^{\upsilon}$$

$$g_{\mu\upsilon} = \begin{pmatrix} g_{00} & g_{01} & g_{02} & g_{03} \\ g_{10} & g_{11} & g_{12} & g_{13} \\ g_{20} & g_{21} & g_{22} & g_{23} \\ g_{30} & g_{31} & g_{32} & g_{33} \end{pmatrix}$$

metric tensor

Minkowski flat space:

$$ds^2 = -c^2 dt^2 + dx^2 + dy^2 + dz^2$$

(special relativity)

Weak field vacuum limit

Consider a small pertubation from a flat space-time:

Let the metric tensor be: $g_{\mu\upsilon} = \eta_{\mu\upsilon} + h_{\mu\upsilon}$ where $\eta_{\mu\upsilon} = \begin{pmatrix} -1 & 0 & 0 & 0 \\ 0 & 1 & 0 & 0 \\ 0 & 0 & 1 & 0 \\ 0 & 0 & 0 & 1 \end{pmatrix}$

and $|h_{\mu\upsilon}| << 1$ is a small pertubation

For a specific coordinate system it can be shown that

$$\nabla^2 h_{\mu\upsilon} - \frac{\partial^2 h_{\mu\upsilon}}{\partial t^2} = 0$$

is a solution to Einstein's field eq. (the equation for a plane wave)

Analogue to Hooke's law:

$$F = -kx$$

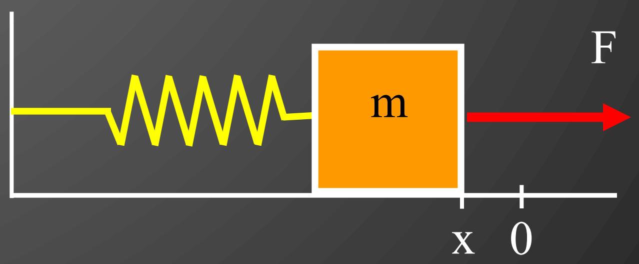

"force" "displacement"

source curvature

$$T_{\mu\nu} = \frac{c^4}{8\pi G} G_{\mu\upsilon}$$

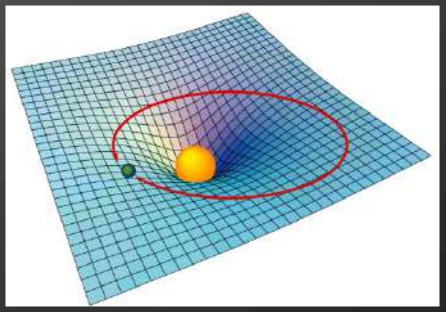

Nature of the gravitational waves

- The emitted waves carry information of the changes in the gravitational field of the source as a result of a change in the distribution of mass, energy and momentum
- Gravitational waves propagate with the speed of light (the graviton has zero rest mass)
- They give rise to fluctuations in the metric where they pass through
- The waves' force field is transverse to its propagation direction and has quadrupolar symmetry (i.e. the graviton has S=2)

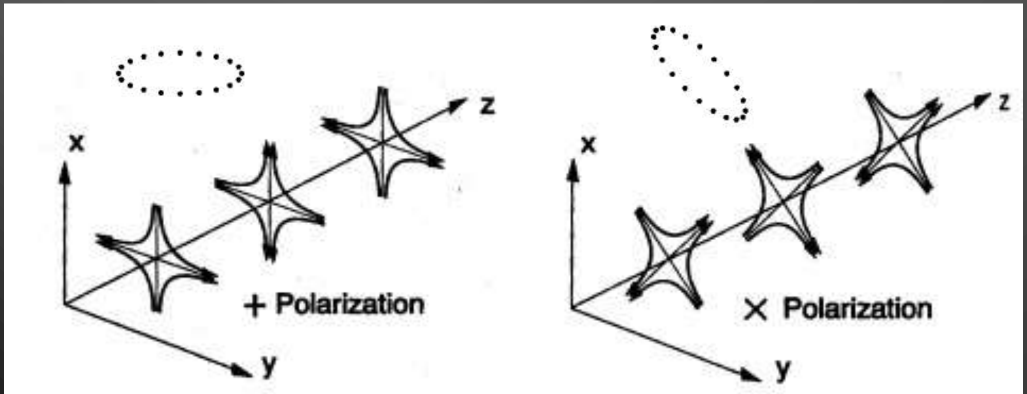

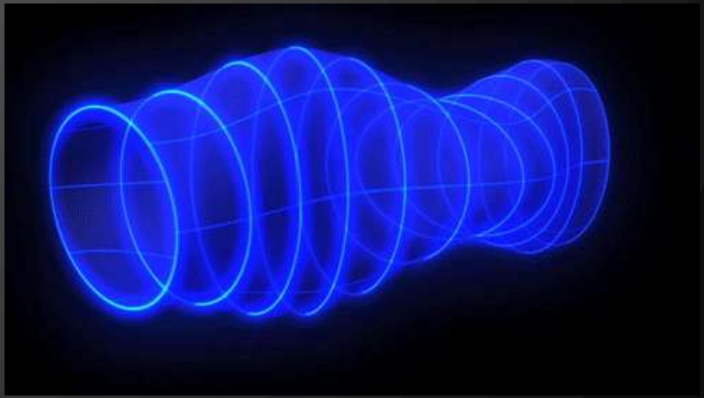

Gravitational wave emission

A time-varying quadrupole moment* gives rise to emission of gravitational waves with a strain amplitude:

$$h_{\mu\upsilon} \approx \frac{2G}{c^4 d}\,\ddot{Q}_{\mu\upsilon}$$

quadrupole moment

distance to source

(Newtonian/quadrupole approximation)

* an asymmetric distribution of mass with respect to the rotation axis:

☐ no gravitational waves

✓ gravitational waves

Gravitational waves – How are they created?

<u>Acceleration of charged particles</u> ⇒ <u>electromagnetic waves</u>:

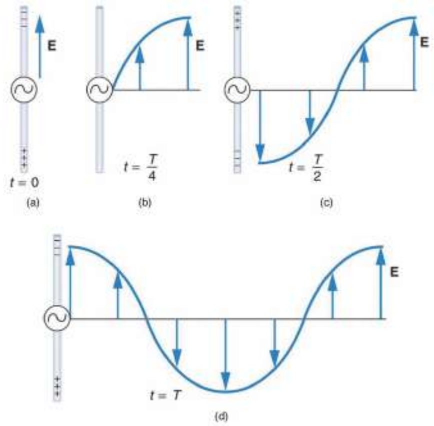

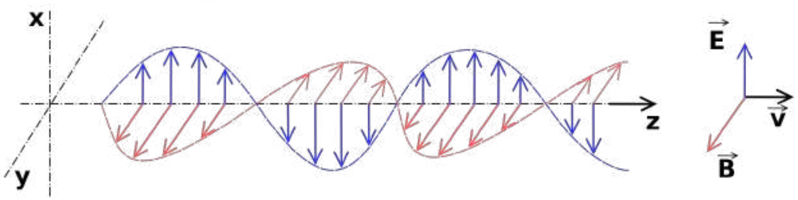

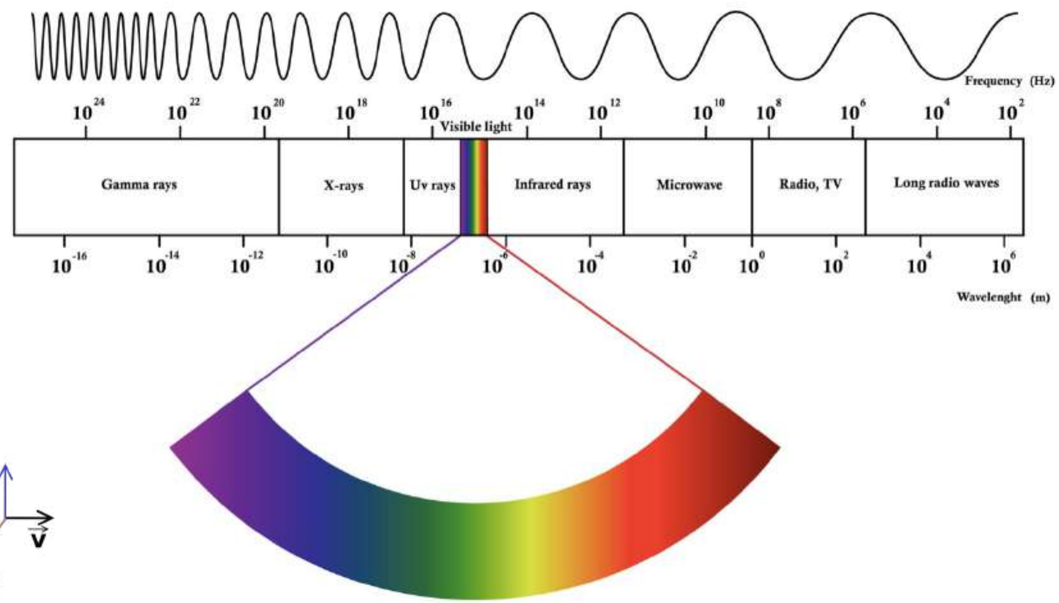

<u>Acceleration of masses</u> ⇒ <u>gravitational waves</u>:

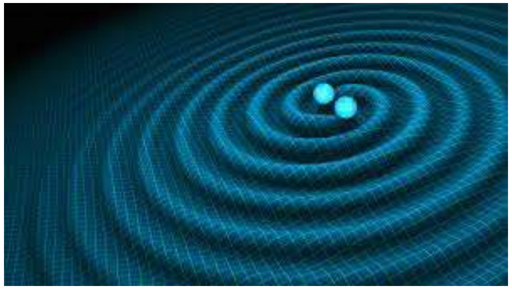

The physical meaning of "h"

Remember:

$$ds^2 = g_{\mu\nu}\,dx^\mu dx^\nu = (\eta_{\mu\nu} + h_{\mu\nu})\,dx^\mu dx^\nu$$

Consider the following geometry:

$$ds = L + \delta L \qquad dx = L$$

$$dy = dz = dt = 0$$

$$h_{xx} = h$$

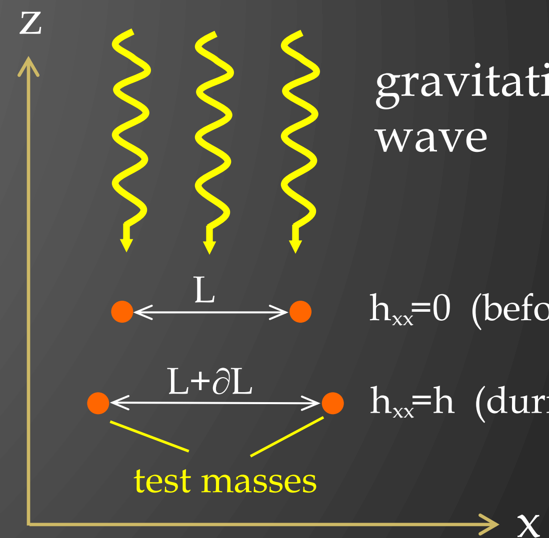

$$(L + \delta L)^2 = (1+h)\,L^2 \quad \Leftrightarrow \quad \frac{\delta L}{L} \approx \frac{h}{2}$$

the wave (strain) amplitude is twice the relative length change

The effect on Leonardo da Vinci

Beware, only space is deformed - not matter!

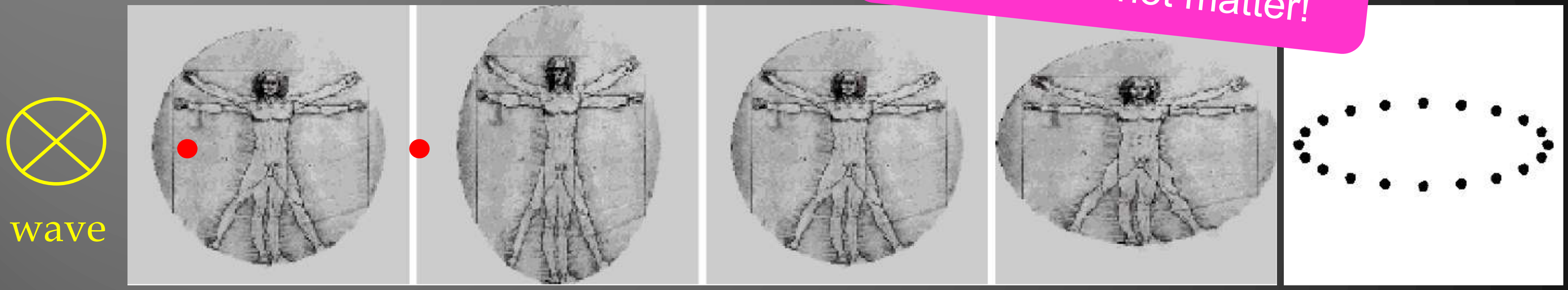

L $L-\delta L$ L $L+\delta L$

$$\frac{\delta L}{L} = \tfrac{1}{2} h \approx 10^{-21}$$ for many astrophysical sources

NS-NS collision at 200 Mpc

The value of h for astrophysical sources

$$h_{\mu\upsilon} = \frac{2G}{c^4 d}\ddot{Q}_{\mu\upsilon}$$

order-of-magnitude estimate

$$Q \sim MR^2 \quad \Rightarrow \quad \ddot{Q} \sim \frac{MR^2}{T^2} \sim Mv^2$$

where (M,R,T,v) are characteristic values of the source

$$h \sim \frac{2G}{c^4 d} Mv^2 = \frac{2G}{c^2}\frac{M}{d}\left(\frac{v}{c}\right)^2 \sim 1.0\times 10^{-19}\,\frac{M/M_{\odot}}{d/Mpc}\left(\frac{v}{c}\right)^2$$

$$h = \begin{cases} 10^{-17} & \text{at outskirts of our Milky Way (10 kpc)} \\ 10^{-20} & \text{at the Virgo cluster of galaxies (15 Mpc)} \\ 10^{-21} & \text{at 200 Mpc} \\ 10^{-22} & \text{at the Hubble distance (3 Gpc)} \end{cases}$$

Gravitational wave luminosity

$$h_{\mu\upsilon} = \frac{2G}{c^4 d}\,\ddot{Q}_{\mu\upsilon}$$

wave amplitude

inner product (scalar)

$$F = \frac{c^3}{32\pi G}\langle \dot{h}_{\mu\upsilon}\,\dot{h}_{\mu\upsilon}\rangle$$

energy flux detected

$$L = r^2 \int F\, d\Omega$$

luminosity

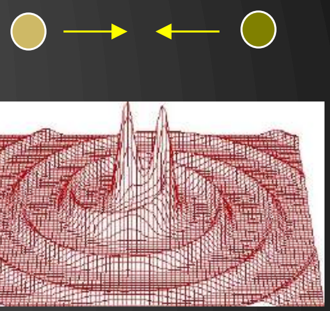

$$\Rightarrow \quad \boxed{L_{gwr} \equiv \frac{dE}{dt} = \frac{G}{5c^5}\langle \dddot{Q}_{\mu\upsilon}\,\dddot{Q}_{\mu\upsilon}\rangle}$$

Gravitational wave luminosity

$$L_{gwr} \equiv \frac{dE}{dt} = \frac{G}{5c^5}\langle \dddot{Q}_{\mu\upsilon}\,\dddot{Q}_{\mu\upsilon}\rangle$$

order-of-magnitude estimate

$$Q \sim MR^2 \quad \Rightarrow \quad \dddot{Q} \sim \frac{MR^2}{T^3} \sim \frac{Mv^3}{R}$$

where (M,R,T,v) are characteristic values of the source

1 mm mountain on a neutron star:

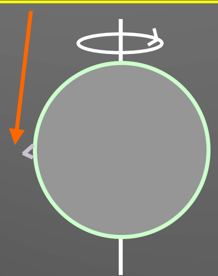

$M=1.4\,M_\odot$
$R=10$ km, $\Delta r=1$ mm
$\Omega=2\pi\nu=1000$ rad/s

$L_{gwr}=10^{36}$ erg/s

$$L_{gwr} \equiv \frac{|\,dE\,|}{dt} = \frac{32G}{5c^5}\, I^2 \varepsilon^2\, \Omega^6$$

$$\varepsilon = \frac{a-b}{(a+b)/2} \approx \frac{\Delta r}{R} \qquad I \sim MR^2$$

steel rod:

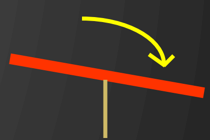

$M=140.000$ kg
$R=20$ meters
$v=300$ m/s

$L_{gwr}=10^{-24}$ erg/s

a factor of $\sim 10^{60}$ in difference!!!

Merging neutron star / black hole binaries

$$L_{gwr} \cong \frac{G}{5c^5}\langle \dddot{Q}_{\mu\upsilon}\,\dddot{Q}_{\mu\upsilon}\rangle$$

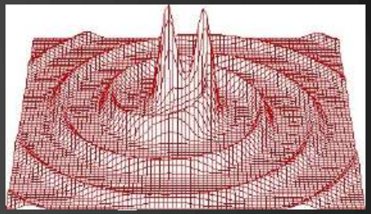

$$Q = \frac{1}{2}\mu a^2 \begin{pmatrix} \cos(2\varphi)+const & \sin(2\varphi)+const \\ \sin(2\varphi)+const & -\cos(2\varphi)+const \end{pmatrix}$$

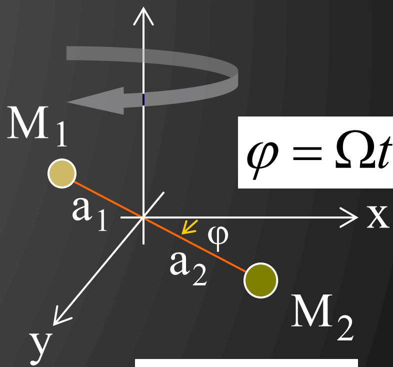

$$\varphi = \Omega t$$

$$\boxed{L_{gwr}(n,e) = \frac{32}{5}\frac{G^4}{c^5}\frac{M^3\mu^2}{a^5}\,g(n,e)}$$

Fourier decomposition factor
(harmonic number, eccentricity)

$$M = M_1 + M_2$$

$$M_1 a_1 = M_2 a_2 = \mu a$$

$$\mu = \frac{M_1 M_2}{M_1 + M_2}$$

$$a = -\frac{GM\mu}{2E_{orb}} \quad \Rightarrow \quad \dot{a} = \frac{GM\mu}{2E_{orb}^2}\dot{E}_{orb} \quad \wedge \quad |\dot{E}_{orb}| = L_{gwr}$$

orbital decay!

$$\dot{a} = -\frac{GM\mu}{2E_{orb}^2} L_{gwr}$$

$$\frac{1}{a}\frac{da}{dt} = -\frac{1}{E}\frac{dE}{dt}\bigg|_{e=0} f(e)$$

$$L_{gwr} \cong \frac{32}{5}\frac{G^4}{c^5}\frac{M^3\mu^2}{a^5}\,\frac{\overbrace{1+(73/24)e^2+(37/96)e^4}}{\left(1-e^2\right)^{7/2}}$$

$$\dot{a} \cong \frac{64}{5}\frac{G^3}{c^5}\frac{M^2\mu}{a^3}\,\frac{1+(73/24)e^2+(37/96)e^4}{\left(1-e^2\right)^{7/2}}$$

$\Downarrow$

$$\boxed{\tau(a_0,e_0) \cong \frac{12}{19}\frac{C_0{}^4}{\beta}\int_0^{e_0}\frac{e^{29/19}[1+(121/304)e^2]^{1181/2299}}{\left(1-e^2\right)^{3/2}}\,de}$$

Merger timescale

determine C_0 from initial condition: $a=a_0$, $e=e_0$

$$\beta \equiv \frac{64}{5}\frac{G^3}{c^5}M^2\mu$$

$$a(e) = \frac{C_0 e^{12/19}}{(1-e^2)}[1+(121/304)e^2]^{870/2299}$$

For a circular binary:

$$\tau_{gwr}^{circ} = \frac{a_0^4}{4\beta}$$

Gravitational waves do exist!

PSR B1913+16 (Hulse-Taylor pulsar, P_{orb}=7.75 hr, ecc=0.61)

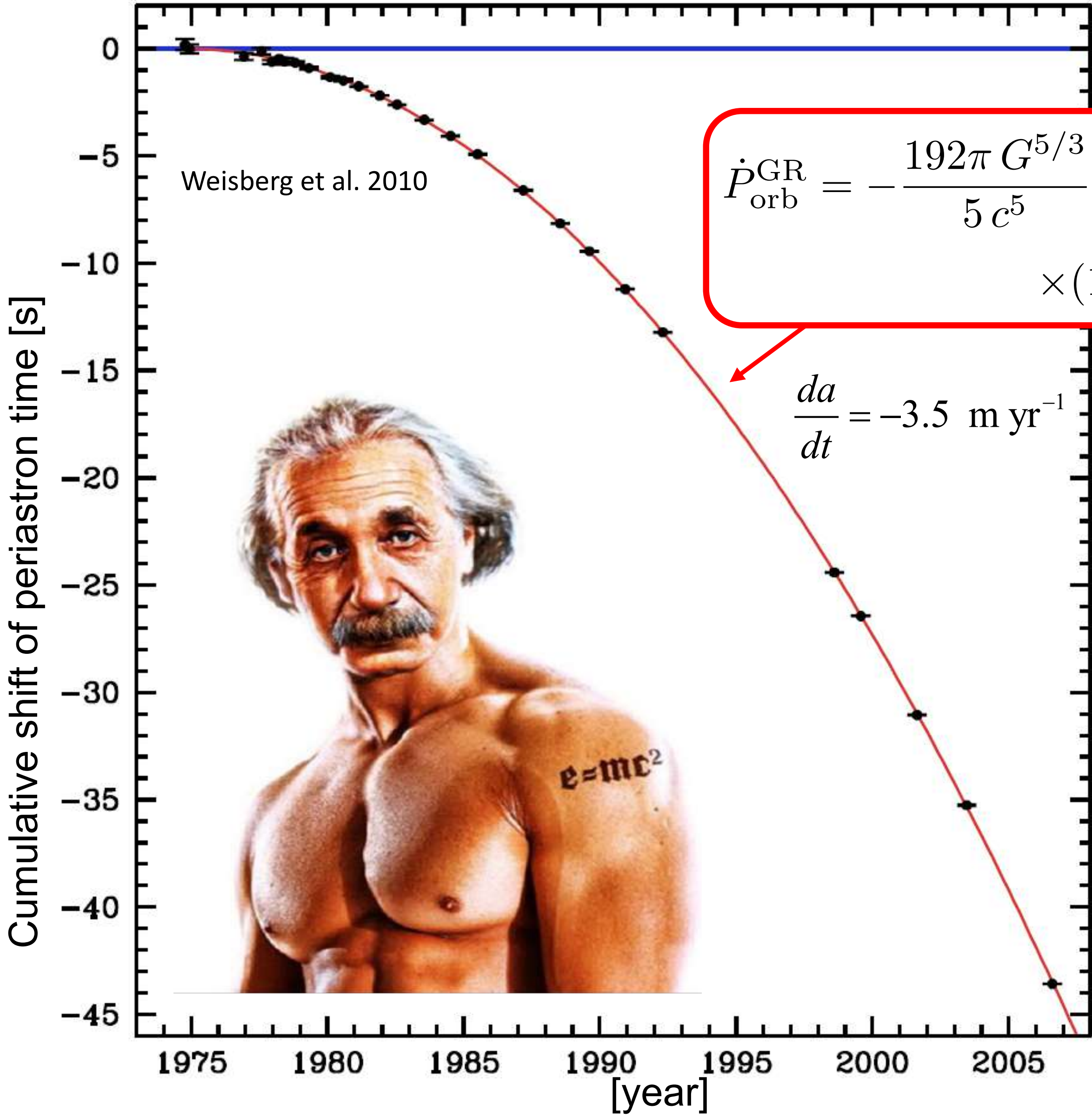

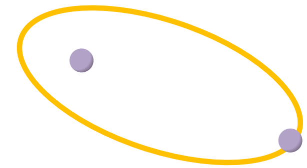

Peters (1964)

$$\dot{P}_{\rm orb}^{\rm GR} = -\frac{192\pi\, G^{5/3}}{5\, c^5} \left(\frac{P_{\rm orb}}{2\pi}\right)^{-5/3} \left(1 + \frac{73}{24}e^2 + \frac{37}{96}e^4\right) \times (1-e^2)^{-7/2}\, M_1 M_2\, (M_1+M_2)^{-1/3}$$

Collision in
τ = 301 mill. yr

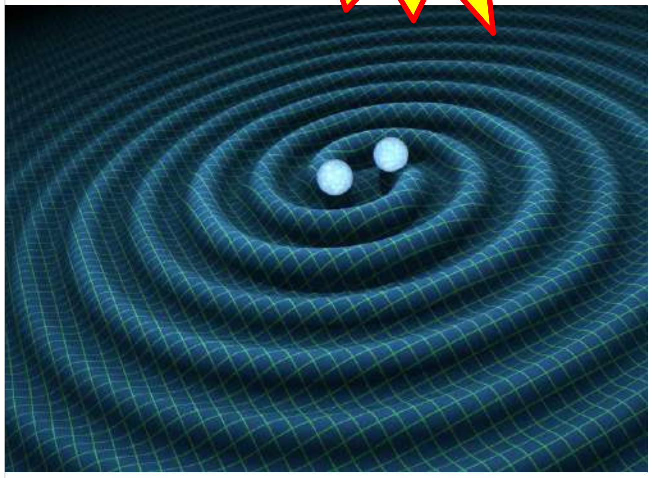

$$L_{\rm GW} = 7\times 10^{24}\ {\rm W} \qquad (L_{{\rm GW},\odot} = 5000\ {\rm W})$$

Tauris & van den Heuvel (2023)

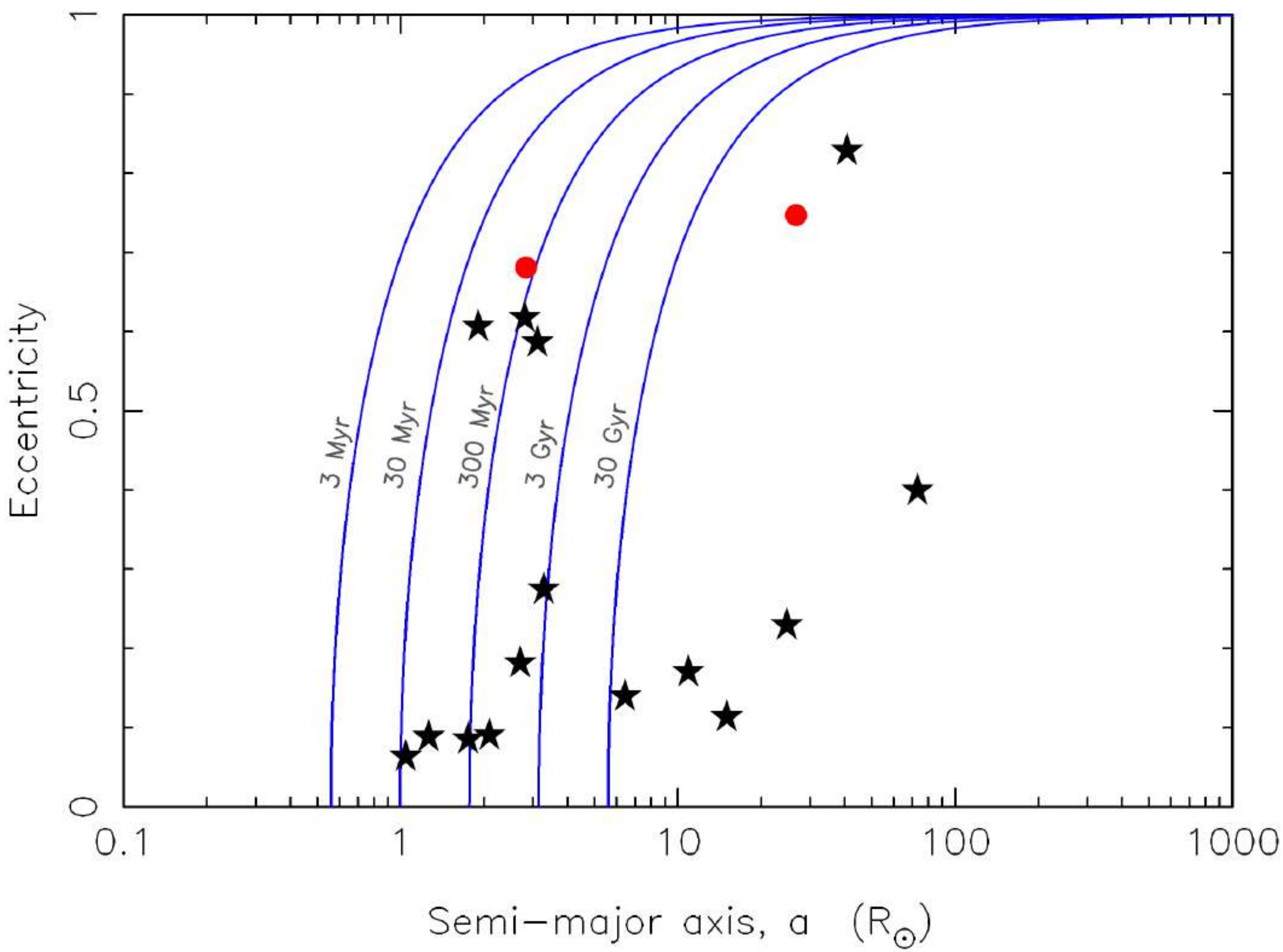

Note:
ecc ≅ 0.7
$\Rightarrow \tau_{GW} \downarrow$ x 10

Gravitational wave detection

$f_{\mathrm{gwr}} = 2\, f_{\mathrm{orb}}$ (ecc.=0)

GWs in second harmonic (n=2)

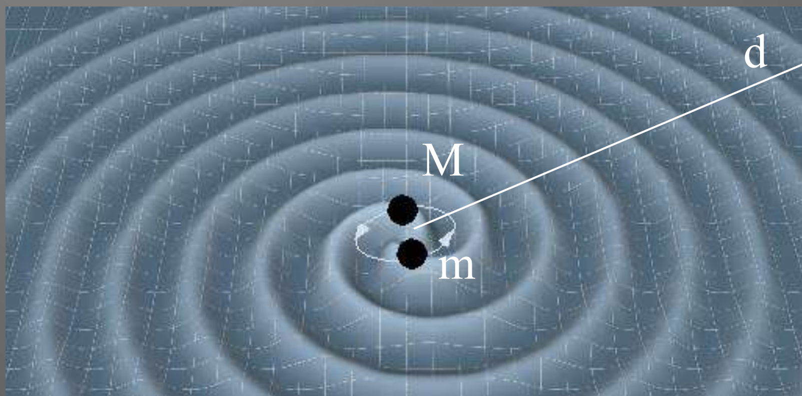

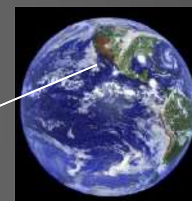

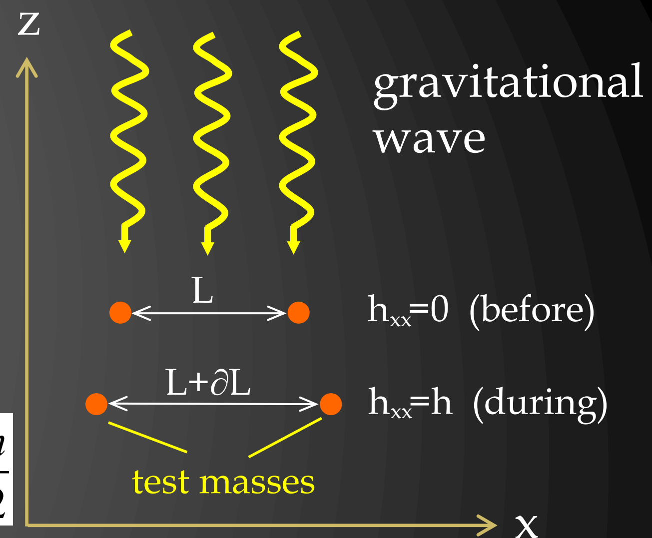

$$\frac{\delta L}{L} \approx \frac{h}{2}$$

the wave amplitude is twice the relative length change

strain (amplitude):

$$h(n,e) = \left(\tfrac{1}{2}\left[h^2_{+,\max} + h^2_{\times,\max}\right]\right)^{1/2} = \left[\frac{16\pi G}{c^3 \omega^2_{\mathrm{gwr}}} \frac{L_{\mathrm{gwr}}(n,e)}{4\pi d^2}\right]^{1/2}$$

$$= 1.0 \times 10^{-21} \frac{\sqrt{g(n,e)}}{n} \left(\frac{Mm\,(M+m)^{-1/3}}{\mathrm{M}_\odot^{5/3}}\right) \left(\frac{P_{\mathrm{orb}}}{1\,\mathrm{hr}}\right)^{-2/3} \left(\frac{d}{1\,\mathrm{kpc}}\right)^{-1}$$

massive

tight

nearby

scale factor (Fourier decomposition factor)

LIGO Laser Interferometer Gravitational wave Observatory

wave amplitude: h ~ 10^{-21}

measurement accuracy to achieve: $\Delta L \sim 10^{-16}$ cm (1/1000 the diameter of a proton!)

$\Rightarrow$ interferometer arm length: $L = \Delta L/h \sim 4$ km

aLIGO observations began in 2015

aVIRGO observations began in 2016

KAGRA joined in 2020

Gravitational wave observatories

LIGO

GEO

Virgo

KAGRA

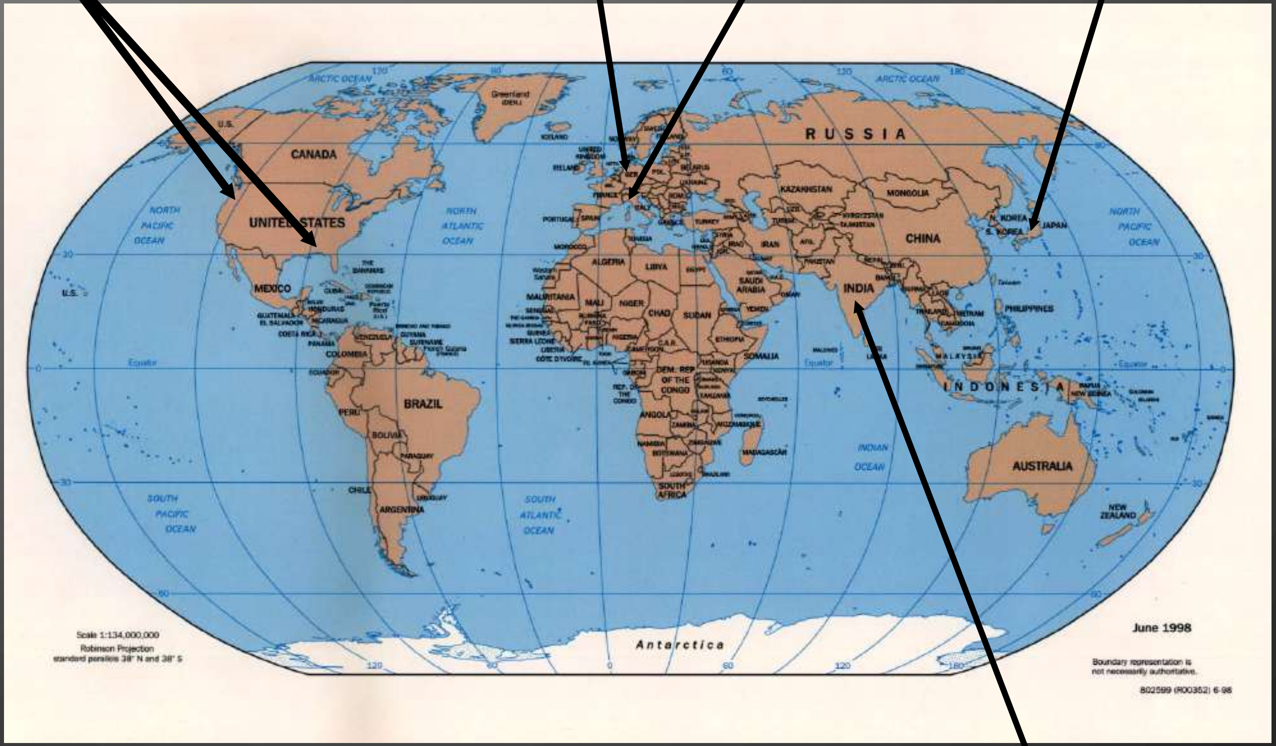

Angular resulution below 5-10 deg^2.

INDIGO

Merger rate of double neutron star binaries in a Milky Way-like galaxy: 3–10 Myr^{-1}

advanced LIGO

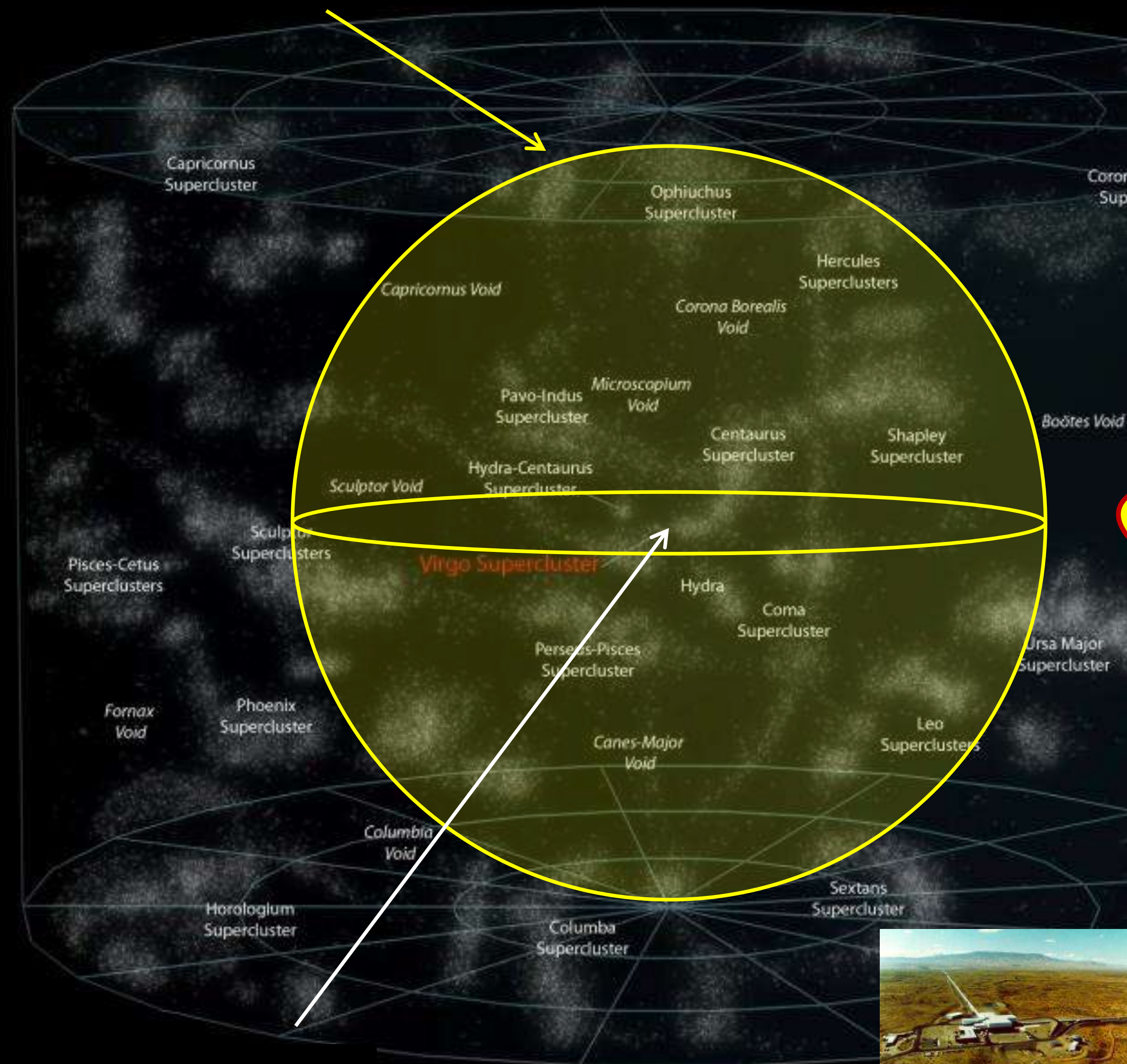

You are here!

Range:
NSNS merger 200 Mpc
NSBH merger 600 Mpc
BHBH merger 5.0 Gpc
(Z=0.8)

Detection rate:
3-10 per year
(Milky Way: 3-10 Myr^{-1})

Highly uncertain

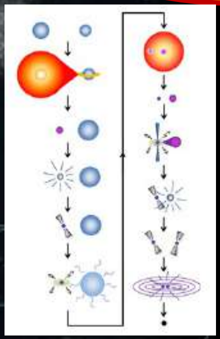

Main uncertainties:
CE evolution, kicks

Sensitivity of LIGO/VIRGO

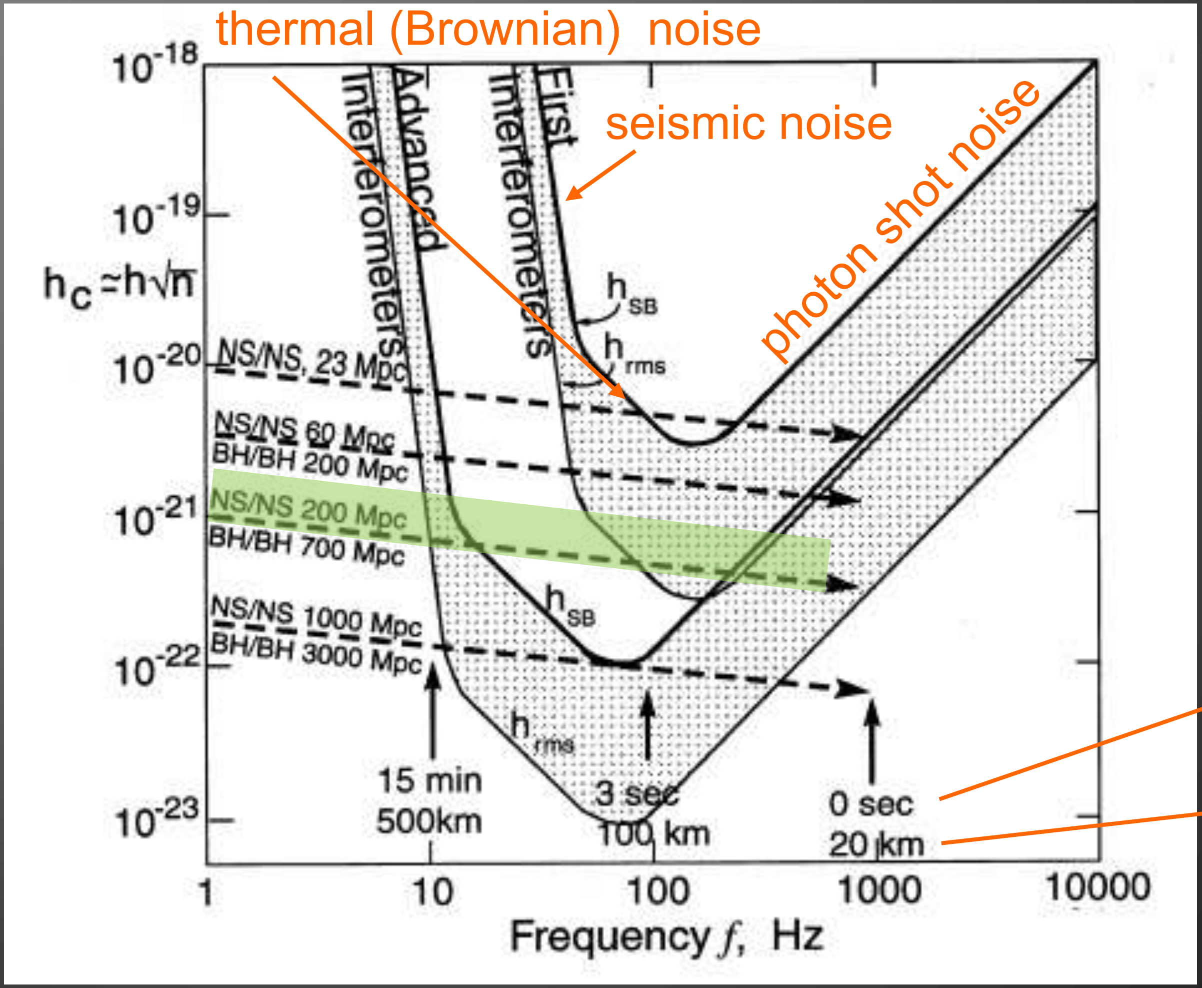

Laser interferometer
- how to achieve $\Delta L \sim 10^{-16}$ cm ?

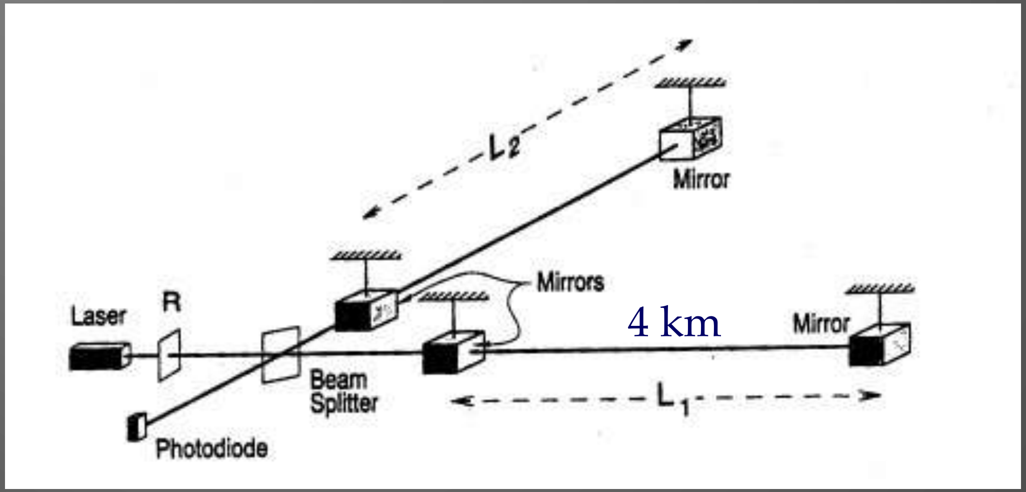

Michelson-Morley interferometer

Sensitivity noise: photon, thermal and seismic.
5 cm wide laser beam shining on 10^{17} atoms.
Light is reflected 100 times $|\longleftrightarrow|$

$$\Delta I_{pd} \propto \Delta\Phi \propto \Delta L \propto h(t)$$

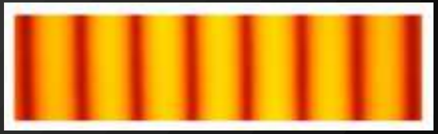

Waveform and dependence on inclination and eccentricity

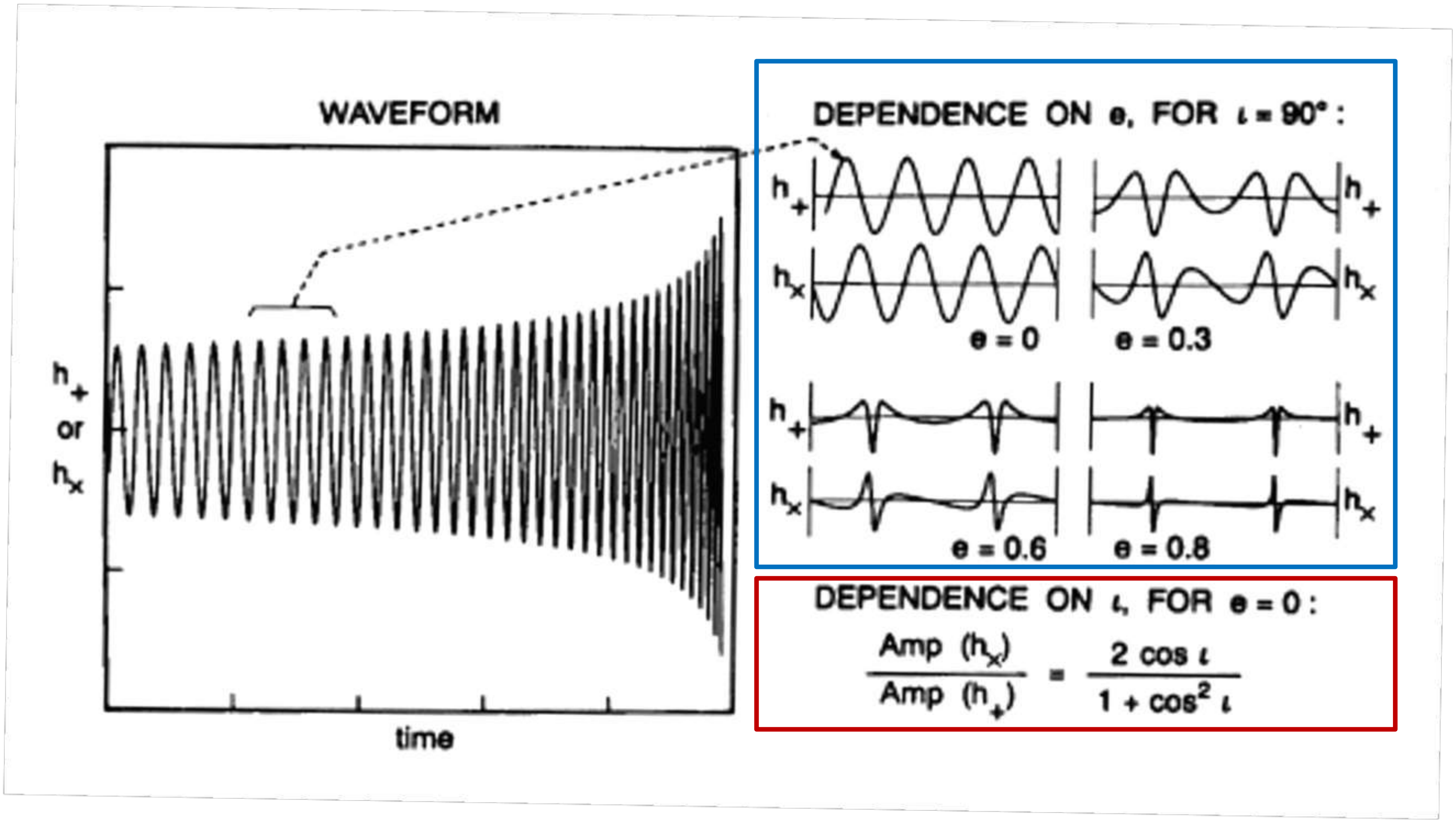

Chirp mass

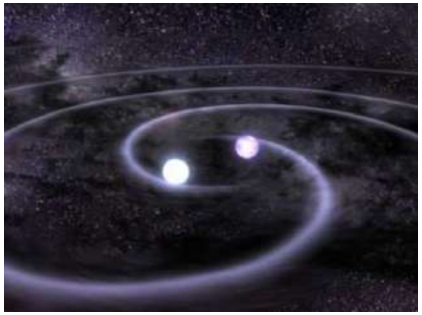

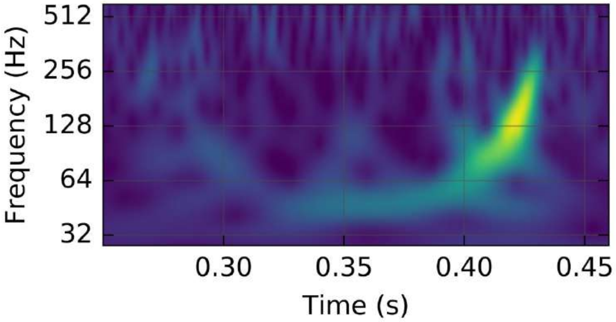

$$\mathcal{M} = \frac{(m_1 m_2)^{3/5}}{M^{1/5}} \simeq \frac{c^3}{G}\left[\frac{5}{96}\pi^{-8/3} f^{-11/3} \dot{f}\right]^{3/5} \qquad (\mathcal{M}^{5/3} = \mu M^{2/3})$$

The chirp mass determines how fast the signal sweeps (”chirps”) through the frequency band. It can be determined to within 1% error.

$$f_{GW}(t) = \frac{1}{8\pi} 5^{3/8} \left[\frac{c^3}{G M_{chirp}}\right]^{5/8} \frac{1}{(t_{merge} - t)^{3/8}}$$

$$h(t) = \frac{1}{r}\left[\frac{5 G^5 M_{chirp}^5}{c^{11}}\right]^{1/4} \frac{1}{(t_{merge} - t)^{1/4}}$$

Riles (2013)

Note, this expression breaks down as $r \rightarrow 0$ $(v/c) \rightarrow 1$

Detected Black Hole and Neutron Star Mergers

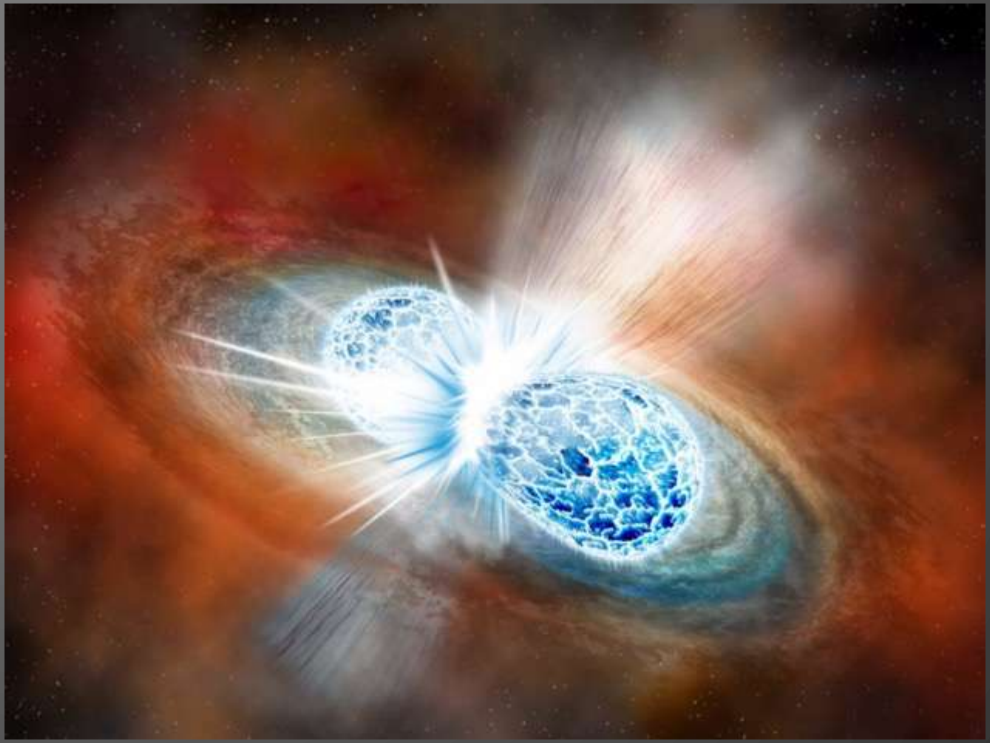

A brief chirp from a galaxy 1.4 billion light years away…

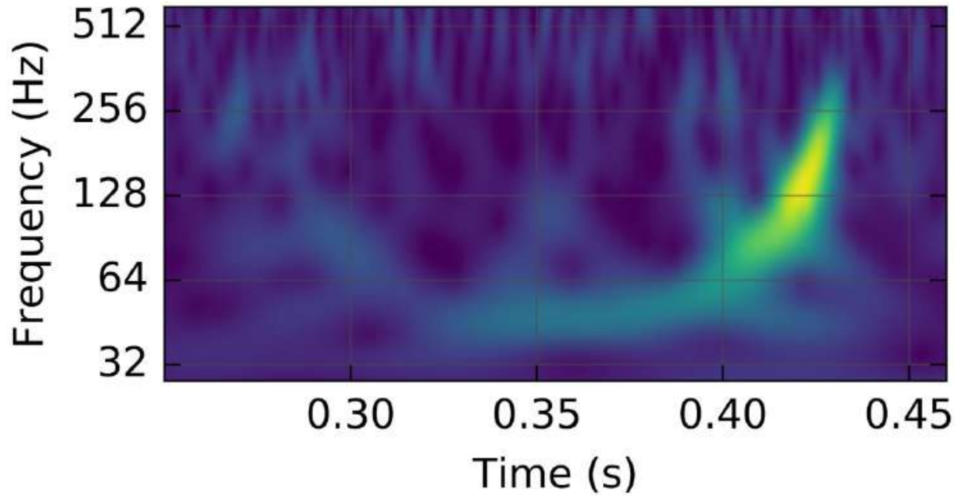

Detection of gravitational waves!

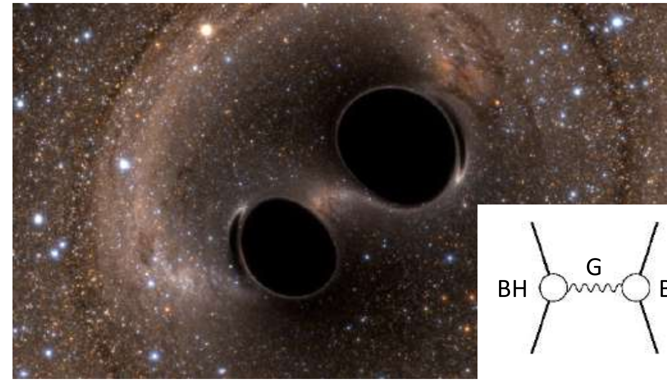

GW150914, GW151012, GW151226, GW170104, GW170608, GW170729, GW170809, GW170814, GW170817, GW170818, GW170823, (O3…….)

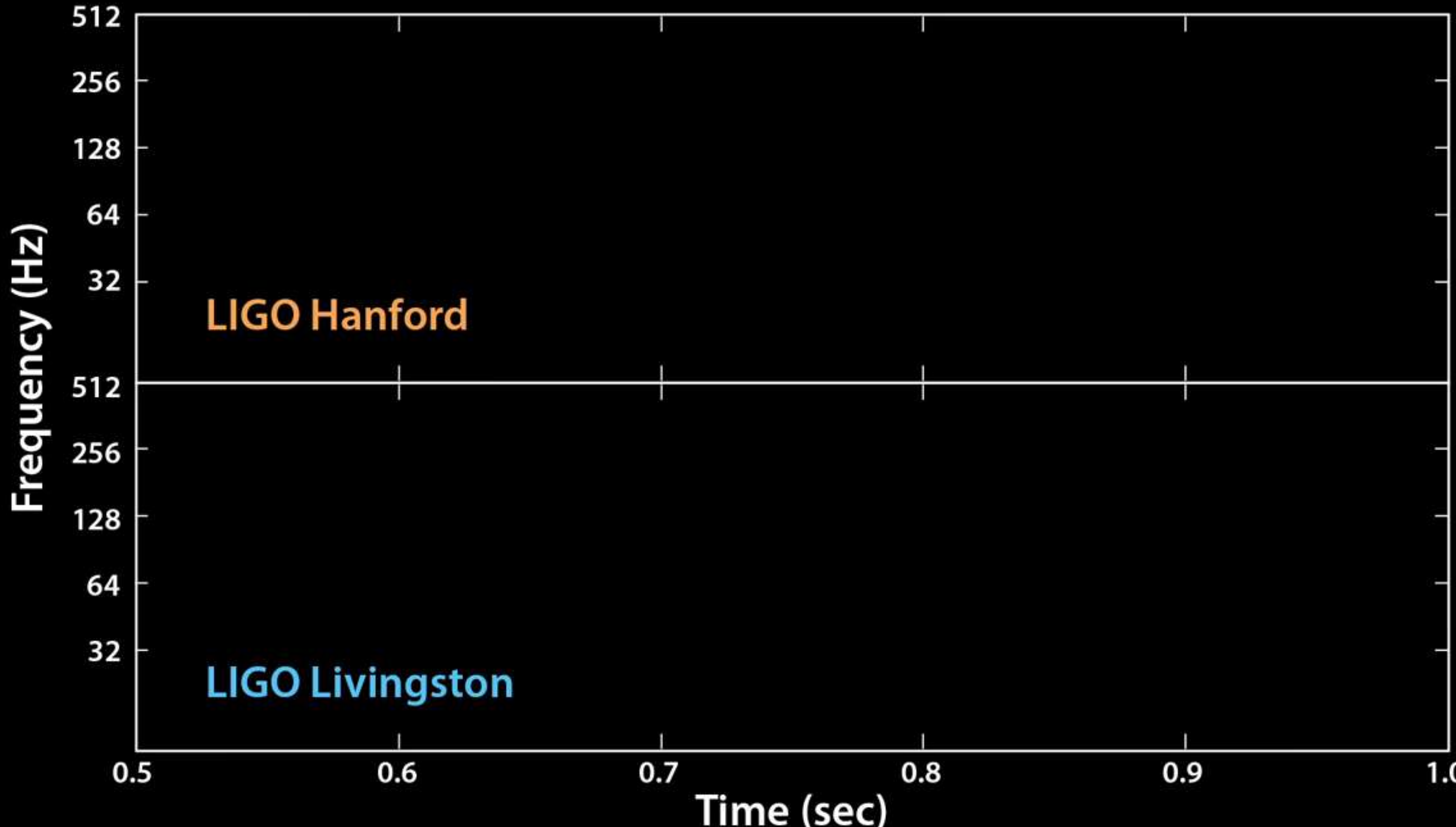
512
256
128
64
32
LIGO Hanford
512
256
128
64
32
LIGO Livingston
Frequency (Hz)
0.5
0.6
0.7
0.8
0.9
1.0
Time (sec)

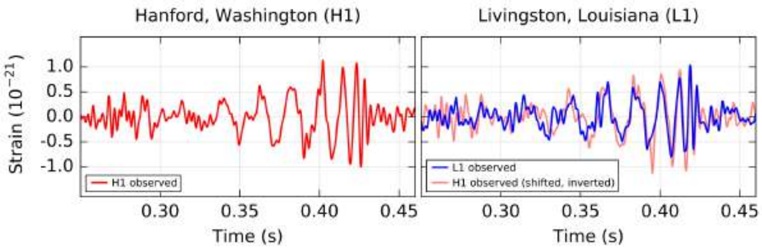

$$\mathcal{M} = \frac{(m_1 m_2)^{3/5}}{M^{1/5}} \simeq \frac{c^3}{G}\left[\frac{5}{96}\pi^{-8/3} f^{-11/3} \dot{f}\right]^{3/5}$$

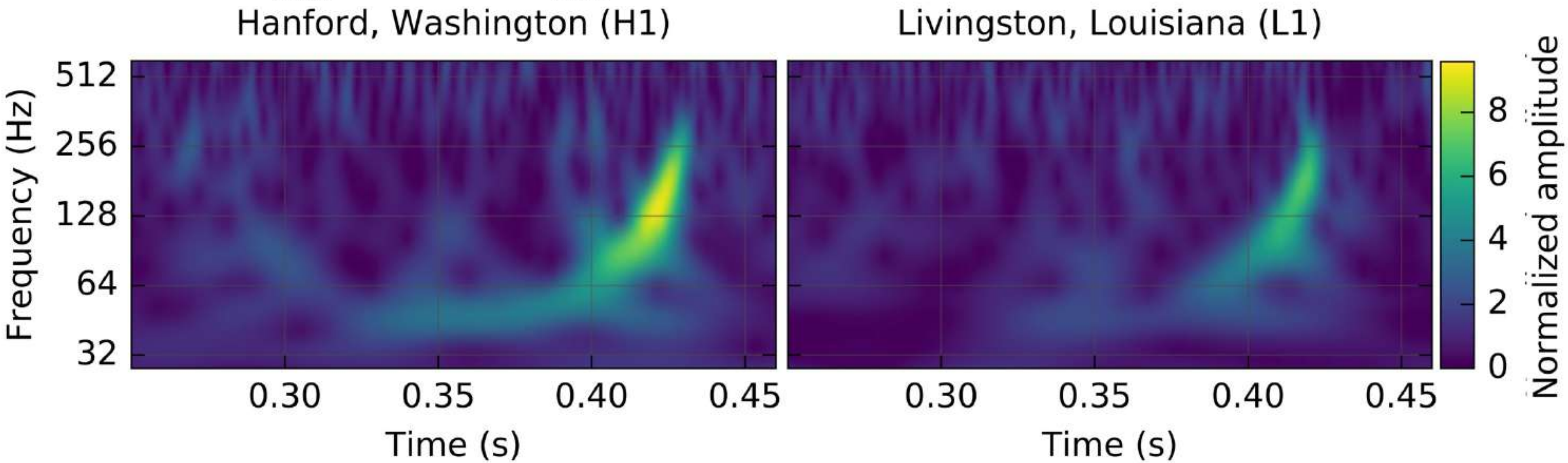

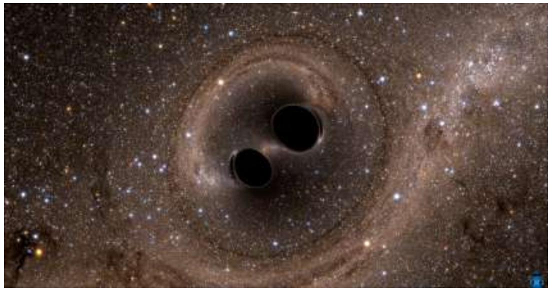

Collision of two black holes:

36 M_{sun} + 29 M_{sun} ≠ 65 M_{sun}

M_{merger} = 62 M_{sun} ! (3 $M_{sun} \cdot c^2$ emitted as GWs)

35–250 Hz (8 cycles)

$h_{top} = 3.4 \times 10^{-22}$

Z=0.09 (400 Mpc = 1.4 bill. light years)

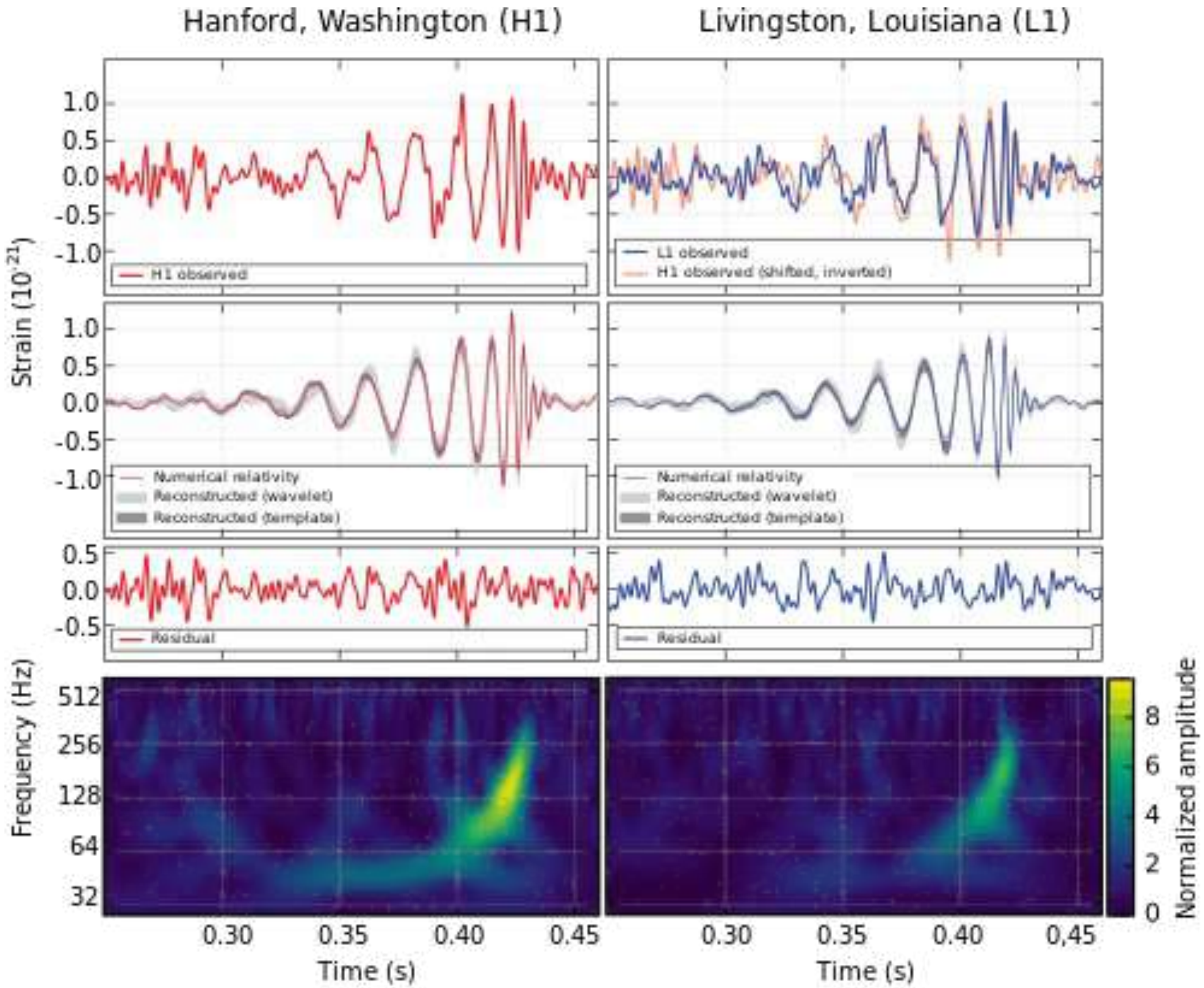

$$\mathcal{M} = \frac{(m_1 m_2)^{3/5}}{M^{1/5}} \simeq \frac{c^3}{G}\left[\frac{5}{96}\pi^{-8/3} f^{-11/3} \dot{f}\right]^{3/5}$$

Chirp mass = 29 M_{sun}

Must be BH-BH merger!
(also the GW freq. at merger points to radii equal to Schwarzchild radii of massive BHs)

GW150914 and the revolution

The ring-down

Typical value

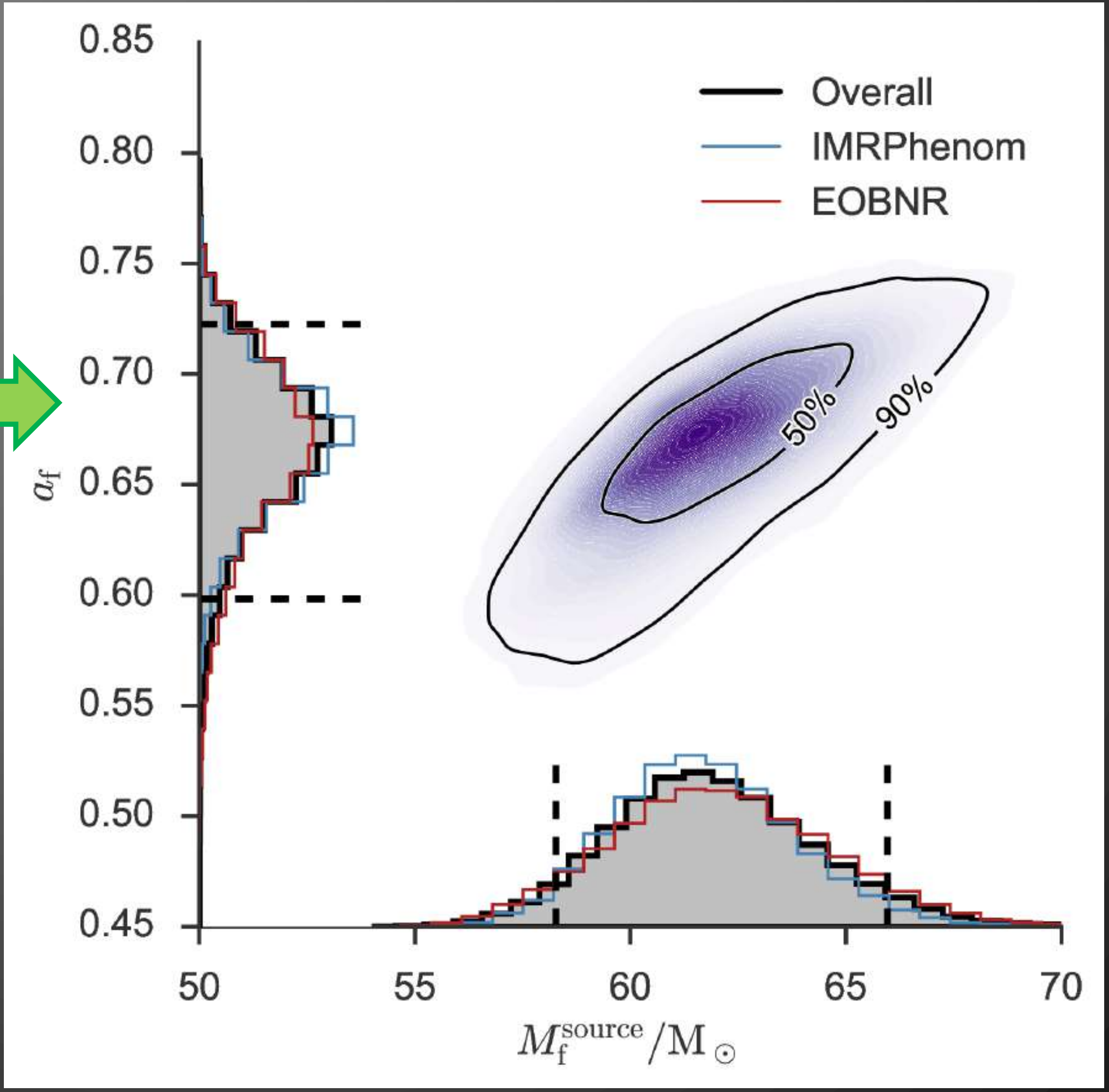

3 phases:

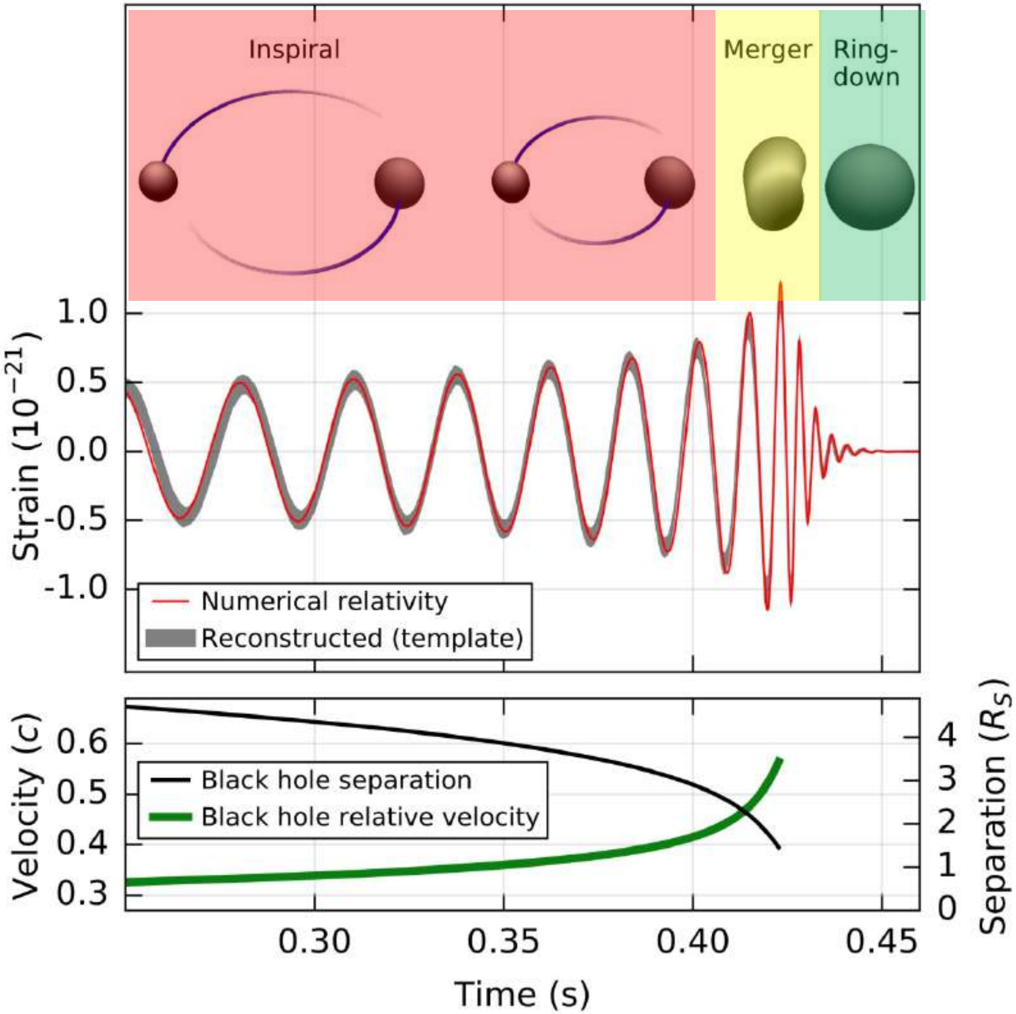
Inspiral
Merger
Ring-down
1.0
0.5
0.0
-0.5
-1.0
Strain (10^{-21})
Numerical relativity
Reconstructed (template)
Velocity (c)
0.6
0.5
0.4
0.3
Black hole separation
Black hole relative velocity
4
3
2
1
0
Separation (R_S)
0.30
0.35
0.40
0.45
Time (s)

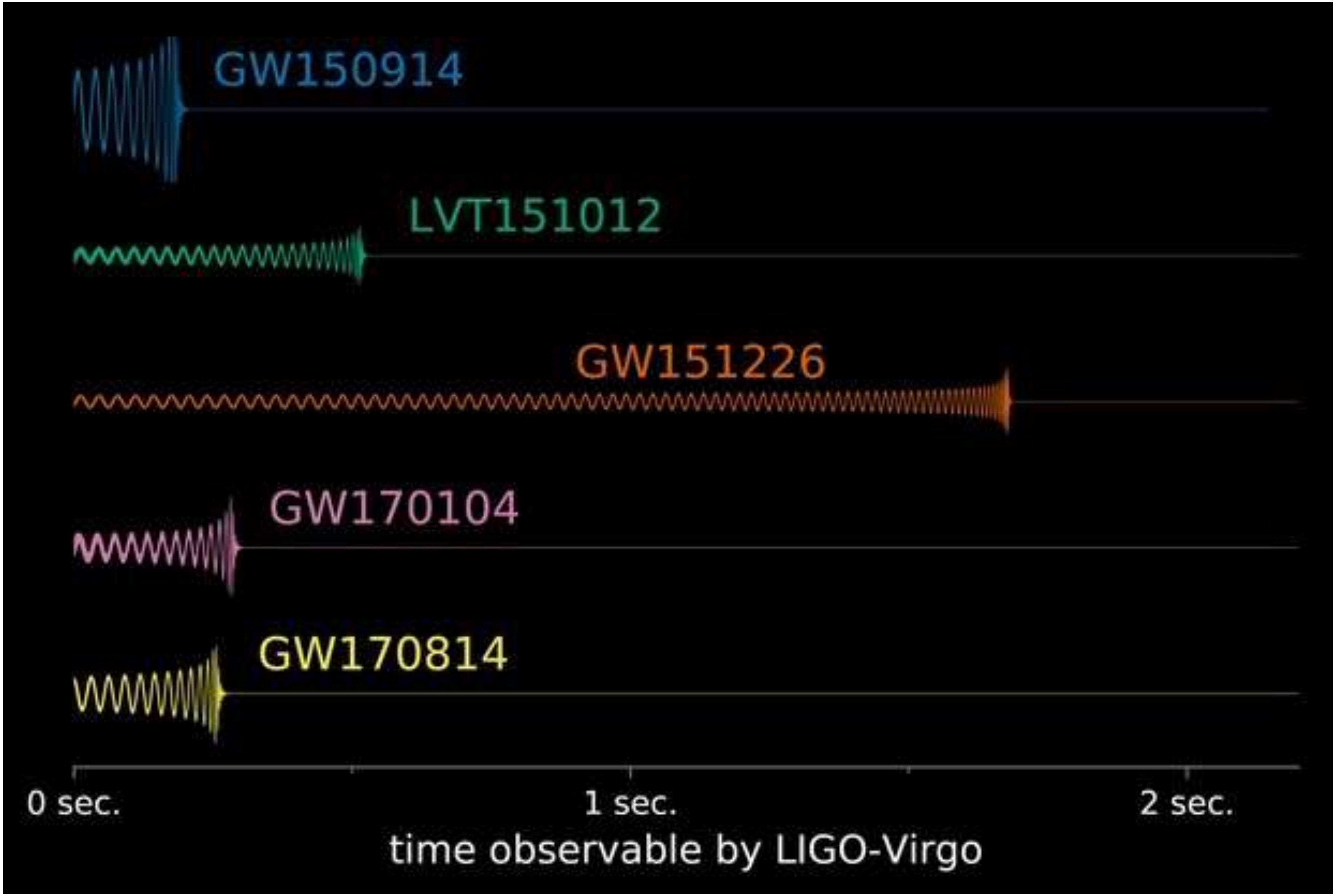
GW150914
LVT151012
GW151226
GW170104
GW170814
0 sec.
1 sec.
2 sec.
time observable by LIGO-Virgo

DETECTIONS SO FAR (Nov. 2022)

<u>11* events</u> in O1 and O2

10 BH+BH mergers
1 NS+NS merger

<u>~ 80 events</u> in O3a + O3b

?	x	BH+BH mergers	75
	y	NS+NS mergers	1(3)
	z	BH+NS mergers	2(3)
		mass gap	2(3)

- **We predict ~10 times more detections of mixed BH/NS mergers compared to double NS mergers**

Observational selection bias against?

Mainly BHBH mergers
(selection effect: detection vol. ~ $M_{chirp}^{5/2}$)

NSNS
BHNS

very massive

q ~ 0.10

See GWTC-3 Population analysis

Event	M ($M_\odot$)	$\mathcal{M}$ ($M_\odot$)	m_1 ($M_\odot$)	m_2 ($M_\odot$)	$\chi_{\rm eff}$	D_L (Gpc)	z	M_f ($M_\odot$)	χ_f	$\Delta\Omega$ (deg²)	SNR
GW190408_181802	$42.9^{+4.1}_{-2.9}$	$18.3^{+1.8}_{-1.2}$	$24.5^{+5.1}_{-3.4}$	$18.3^{+3.2}_{-3.5}$	$-0.03^{+0.13}_{-0.19}$	$1.58^{+0.40}_{-0.59}$	$0.30^{+0.06}_{-0.10}$	$41.0^{+3.8}_{-2.7}$	$0.67^{+0.06}_{-0.07}$	140	$15.3^{+0.2}_{-0.3}$
GW190412	$38.4^{+3.8}_{-3.7}$	$13.3^{+0.4}_{-0.3}$	$30.0^{+4.7}_{-5.1}$	$8.3^{+1.6}_{-0.9}$	$0.25^{+0.08}_{-0.11}$	$0.74^{+0.14}_{-0.17}$	$0.15^{+0.03}_{-0.03}$	$37.3^{+3.9}_{-3.9}$	$0.67^{+0.05}_{-0.06}$	21	$18.9^{+0.2}_{-0.3}$
GW190413_052954	$56.9^{+13.1}_{-8.9}$	$24.0^{+5.4}_{-3.7}$	$33.4^{+12.4}_{-7.4}$	$23.4^{+6.7}_{-6.3}$	$0.01^{+0.29}_{-0.33}$	$4.10^{+2.41}_{-1.89}$	$0.66^{+0.30}_{-0.27}$	$54.3^{+12.4}_{-8.4}$	$0.69^{+0.12}_{-0.13}$	1400	$8.9^{+0.4}_{-0.8}$
GW190413_134308	$76.1^{+15.9}_{-10.6}$	$31.9^{+7.3}_{-4.6}$	$45.4^{+13.6}_{-9.6}$	$30.9^{+10.2}_{-9.6}$	$-0.01^{+0.24}_{-0.28}$	$5.15^{+2.44}_{-2.34}$	$0.80^{+0.30}_{-0.31}$	$72.8^{+15.2}_{-10.5}$	$0.69^{+0.10}_{-0.12}$	520	$10.0^{+0.4}_{-0.5}$
GW190421_213856	$71.8^{+12.5}_{-8.6}$	$30.7^{+5.5}_{-3.9}$	$40.6^{+10.4}_{-6.6}$	$31.4^{+7.5}_{-8.2}$	$-0.05^{+0.23}_{-0.26}$	$3.15^{+1.37}_{-1.42}$	$0.53^{+0.18}_{-0.21}$	$68.6^{+11.7}_{-8.1}$	$0.68^{+0.10}_{-0.11}$	1000	$10.7^{+0.2}_{-0.4}$
GW190424_180648	$70.7^{+13.4}_{-9.8}$	$30.3^{+5.7}_{-4.2}$	[illegible]	[illegible]	$0.15^{+0.22}_{-0.22}$	$2.55^{+1.56}_{-1.33}$	$0.45^{+0.22}_{-0.21}$	$67.1^{+12.5}_{-9.2}$	$0.75^{+0.08}_{-0.09}$	26000	$10.4^{+0.2}_{-0.4}$
GW190425	$3.4^{+0.3}_{-0.1}$	$1.44^{+0.02}_{-0.02}$	$2.0^{+0.6}_{-0.3}$	$1.4^{+0.3}_{-0.3}$	$0.06^{+0.11}_{-0.05}$	$0.16^{+0.07}_{-0.07}$	$0.03^{+0.01}_{-0.02}$	–	–	9900	$12.4^{+0.3}_{-0.4}$
GW190426_152155	$7.2^{+3.5}_{-1.5}$	$2.41^{+0.08}_{-0.08}$	$5.7^{+4.0}_{-2.3}$	$1.5^{+0.8}_{-0.5}$	$-0.03^{+0.33}_{-0.30}$	$0.38^{+0.19}_{-0.16}$	$0.08^{+0.04}_{-0.03}$	–	–	1400	$8.7^{+0.5}_{-0.6}$
GW190503_185404	$71.3^{+9.3}_{-8.0}$	$30.1^{+4.2}_{-4.0}$	$42.9^{+9.2}_{-7.8}$	$28.5^{+7.5}_{-7.9}$	$-0.02^{+0.20}_{-0.26}$	$1.52^{+0.71}_{-0.66}$	$0.29^{+0.11}_{-0.11}$	$68.2^{+8.7}_{-7.5}$	$0.67^{+0.09}_{-0.12}$	94	$12.4^{+0.2}_{-0.3}$
GW190512_180714	$35.6^{+3.9}_{-3.4}$	$14.5^{+1.3}_{-1.0}$	$23.0^{+5.4}_{-5.7}$	$12.5^{+3.5}_{-2.5}$	$0.03^{+0.13}_{-0.13}$	$1.49^{+0.53}_{-0.59}$	$0.28^{+0.09}_{-0.10}$	$34.2^{+3.9}_{-3.4}$	$0.65^{+0.07}_{-0.07}$	230	$12.2^{+0.2}_{-0.4}$
GW190513_205428	$53.6^{+8.6}_{-5.9}$	$21.5^{+3.6}_{-1.9}$	$35.3^{+9.6}_{-9.0}$	$18.1^{+7.3}_{-4.2}$	$0.12^{+0.29}_{-0.18}$	$2.16^{+0.94}_{-0.80}$	$0.39^{+0.14}_{-0.13}$	$51.3^{+8.1}_{-5.8}$	$0.69^{+0.14}_{-0.12}$	490	$12.9^{+0.3}_{-0.4}$
GW190514_065416	$64.2^{+16.6}_{-9.6}$	$27.4^{+6.9}_{-4.3}$	$36.9^{+13.4}_{-7.3}$	$27.5^{+8.2}_{-7.7}$	$-0.16^{+0.28}_{-0.32}$	$4.93^{+2.76}_{-2.41}$	$0.77^{+0.34}_{-0.33}$	$61.6^{+16.0}_{-9.2}$	$0.64^{+0.11}_{-0.14}$	2400	$8.2^{+0.3}_{-0.6}$
GW190517_055101	$61.9^{+10.0}_{-9.6}$	$26.0^{+4.2}_{-4.0}$	$36.4^{+11.8}_{-7.8}$	$24.8^{+6.9}_{-7.1}$	$0.53^{+0.20}_{-0.19}$	$2.11^{+1.79}_{-1.00}$	$0.38^{+0.26}_{-0.16}$	$57.8^{+9.4}_{-9.1}$	$0.87^{+0.05}_{-0.07}$	460	$10.7^{+0.4}_{-0.6}$
GW190519_153544	$104.2^{+14.5}_{-14.9}$	$43.5^{+6.8}_{-6.8}$	$64.5^{+11.3}_{-13.2}$	$39.9^{+11.0}_{-10.6}$	$0.33^{+0.19}_{-0.22}$	$2.85^{+2.02}_{-1.14}$	$0.49^{+0.27}_{-0.17}$	$98.7^{+13.5}_{-14.2}$	$0.80^{+0.07}_{-0.12}$	770	$15.6^{+0.2}_{-0.3}$
GW190521	$157.9^{+37.4}_{-20.9}$	$66.9^{+15.5}_{-9.2}$	$91.4^{+29.3}_{-17.5}$	$66.8^{+20.7}_{-20.7}$	$0.06^{+0.31}_{-0.37}$	$4.53^{+2.30}_{-2.13}$	$0.72^{+0.29}_{-0.29}$	$150.3^{+35.4}_{-20.4}$	$0.73^{+0.11}_{-0.14}$	940	$14.2^{+0.3}_{-0.3}$
GW190521_074359	$74.4^{+6.8}_{-4.6}$	$31.9^{+3.1}_{-2.4}$	[illegible]	[illegible]	$0.09^{+0.10}_{-0.13}$	$1.28^{+0.38}_{-0.57}$	$0.25^{+0.06}_{-0.10}$	$70.7^{+6.4}_{-4.2}$	$0.72^{+0.05}_{-0.07}$	500	$25.8^{+0.1}_{-0.2}$
GW190527_092055	$58.5^{+27.9}_{-10.6}$	$24.2^{+11.9}_{-4.4}$	$36.2^{+18.1}_{-9.5}$	$22.8^{+12.7}_{-8.1}$	$0.13^{+0.29}_{-0.28}$	$3.10^{+4.85}_{-1.64}$	$0.53^{+0.61}_{-0.25}$	$55.9^{+26.4}_{-10.1}$	$0.73^{+0.12}_{-0.16}$	3800	$8.1^{+0.4}_{-1.0}$
GW190602_175927	$114.1^{+18.5}_{-15.7}$	$48.3^{+8.6}_{-8.0}$	$67.2^{+16.0}_{-12.6}$	$47.4^{+13.4}_{-16.6}$	$0.10^{+0.25}_{-0.25}$	$2.99^{+2.02}_{-1.26}$	$0.51^{+0.27}_{-0.19}$	$108.8^{+17.2}_{-14.8}$	$0.71^{+0.10}_{-0.13}$	720	$12.8^{+0.2}_{-0.3}$
GW190620_030421	$90.1^{+17.3}_{-12.1}$	$37.5^{+7.8}_{-5.7}$	$55.4^{+15.8}_{-12.0}$	$35.0^{+11.6}_{-11.4}$	$0.34^{+0.21}_{-0.25}$	$3.16^{+1.67}_{-1.43}$	$0.54^{+0.22}_{-0.21}$	$85.4^{+15.9}_{-11.4}$	$0.80^{+0.08}_{-0.14}$	6700	$12.1^{+0.3}_{-0.4}$
GW190630_185205	$58.8^{+4.7}_{-4.8}$	$24.8^{+2.1}_{-2.0}$	$35.0^{+6.9}_{-5.7}$	$23.6^{+5.2}_{-5.1}$	$0.10^{+0.12}_{-0.13}$	$0.93^{+0.56}_{-0.40}$	$0.19^{+0.10}_{-0.07}$	$56.1^{+4.5}_{-4.6}$	$0.70^{+0.06}_{-0.07}$	1300	$15.6^{+0.2}_{-0.3}$
GW190701_203306	$94.1^{+11.6}_{-9.3}$	$40.2^{+5.2}_{-4.7}$	$53.6^{+11.7}_{-7.8}$	$40.8^{+8.3}_{-11.5}$	$-0.06^{+0.23}_{-0.28}$	$2.14^{+0.79}_{-0.73}$	$0.38^{+0.12}_{-0.12}$	$90.0^{+10.8}_{-8.6}$	$0.67^{+0.09}_{-0.12}$	45	$11.3^{+0.2}_{-0.4}$
GW190706_222641	$101.6^{+17.9}_{-13.5}$	$42.0^{+8.4}_{-6.2}$	$64.0^{+15.2}_{-15.2}$	$38.5^{+12.5}_{-12.4}$	$0.32^{+0.25}_{-0.30}$	$5.07^{+2.57}_{-2.11}$	$0.79^{+0.31}_{-0.28}$	$96.3^{+16.7}_{-13.2}$	$0.80^{+0.08}_{-0.17}$	610	$12.6^{+0.2}_{-0.4}$
GW190707_093326	$20.0^{+1.9}_{-1.3}$	$8.5^{+0.6}_{-0.4}$	$11.5^{+3.3}_{-1.7}$	$8.4^{+1.4}_{-1.6}$	$-0.05^{+0.10}_{-0.08}$	$0.80^{+0.37}_{-0.38}$	$0.16^{+0.07}_{-0.07}$	$19.2^{+1.9}_{-1.3}$	$0.66^{+0.03}_{-0.04}$	1300	$13.3^{+0.2}_{-0.4}$
GW190708_232457	$30.8^{+2.5}_{-1.8}$	$13.1^{+0.9}_{-0.6}$	$17.5^{+4.7}_{-2.3}$	$13.1^{+2.0}_{-2.7}$	$0.02^{+0.10}_{-0.08}$	$0.90^{+0.33}_{-0.40}$	$0.18^{+0.06}_{-0.07}$	$29.4^{+2.5}_{-1.7}$	$0.69^{+0.04}_{-0.04}$	14000	$13.1^{+0.2}_{-0.3}$
GW190719_215514	$55.8^{+16.3}_{-10.0}$	$22.7^{+5.9}_{-3.7}$	$35.2^{+16.9}_{-9.9}$	$20.2^{+8.1}_{-6.5}$	$0.35^{+0.28}_{-0.32}$	$4.61^{+2.84}_{-2.17}$	$0.73^{+0.35}_{-0.30}$	$52.9^{+15.8}_{-9.5}$	$0.80^{+0.10}_{-0.16}$	2300	$8.3^{+0.3}_{-1.0}$
GW190720_000836	$21.3^{+4.3}_{-2.3}$	$8.9^{+0.5}_{-0.8}$	$13.3^{+6.6}_{-3.0}$	$7.8^{+2.2}_{-2.2}$	$0.18^{+0.14}_{-0.12}$	$0.81^{+0.71}_{-0.33}$	$0.16^{+0.12}_{-0.06}$	$20.3^{+4.5}_{-2.3}$	$0.72^{+0.06}_{-0.05}$	510	$11.0^{+0.3}_{-0.8}$
GW190727_060333	$65.8^{+10.9}_{-7.4}$	$28.1^{+4.9}_{-3.4}$	$37.2^{+9.4}_{-5.9}$	$28.8^{+6.6}_{-7.9}$	$0.12^{+0.26}_{-0.25}$	$3.60^{+1.59}_{-1.51}$	$0.60^{+0.20}_{-0.22}$	$62.6^{+10.2}_{-7.0}$	$0.73^{+0.10}_{-0.10}$	860	$11.9^{+0.3}_{-0.5}$
GW190728_064510	$20.5^{+4.5}_{-1.3}$	$8.6^{+0.5}_{-0.3}$	$12.2^{+7.1}_{-2.2}$	$8.1^{+1.7}_{-2.6}$	$0.12^{+0.19}_{-0.07}$	$0.89^{+0.25}_{-0.37}$	$0.18^{+0.05}_{-0.07}$	$19.5^{+4.6}_{-1.3}$	$0.71^{+0.04}_{-0.04}$	410	$13.0^{+0.2}_{-0.4}$
GW190731_140936	$67.1^{+15.3}_{-10.2}$	$28.4^{+6.8}_{-4.5}$	$39.3^{+11.8}_{-8.2}$	$28.0^{+8.9}_{-8.4}$	$0.08^{+0.24}_{-0.24}$	$3.97^{+2.56}_{-2.07}$	$0.65^{+0.32}_{-0.30}$	$63.9^{+14.4}_{-9.8}$	$0.71^{+0.10}_{-0.12}$	3000	$8.6^{+0.2}_{-0.5}$
GW190803_022701	$62.7^{+11.8}_{-8.4}$	$26.7^{+5.2}_{-3.8}$	$36.1^{+10.2}$ [illegible]	$26.7^{+7.1}_{-7.6}$	$-0.01^{+0.25}_{-0.26}$	$3.69^{+2.04}_{-1.69}$	$0.61^{+0.26}_{-0.24}$	$59.9^{+11.3}_{-7.9}$	$0.69^{+0.10}_{-0.11}$	1500	$8.6^{+0.3}_{-0.5}$
GW190814	$25.8^{+1.0}_{-0.9}$	$6.09^{+0.06}_{-0.06}$	$23.2^{+1.1}_{-1.0}$	$2.59^{+0.08}_{-0.09}$	$0.00^{+0.06}_{-0.06}$	$0.24^{+0.04}_{-0.05}$	$0.05^{+0.009}_{-0.010}$	$25.6^{+1.0}_{-0.9}$	$0.28^{+0.02}_{-0.02}$	19	$24.9^{+0.1}_{-0.2}$
GW190828_063405	$57.5^{+7.5}_{-4.4}$	$24.8^{+3.3}_{-2.0}$	[illegible]	[illegible]	$0.19^{+0.15}_{-0.16}$	$2.22^{+0.63}_{-0.95}$	$0.40^{+0.09}_{-0.15}$	$54.5^{+6.9}_{-4.0}$	$0.76^{+0.06}_{-0.07}$	520	$16.2^{+0.2}_{-0.3}$
GW190828_065509	$34.1^{+5.5}_{-4.5}$	$13.3^{+1.2}_{-0.9}$	$23.8^{+7.2}_{-7.0}$	$10.2^{+3.5}_{-2.1}$	$0.08^{+0.16}_{-0.16}$	$1.66^{+0.63}_{-0.61}$	$0.31^{+0.10}_{-0.10}$	$32.9^{+5.7}_{-4.5}$	$0.65^{+0.09}_{-0.08}$	640	$10.0^{+0.3}_{-0.5}$
GW190909_114149	$71.2^{+54.3}_{-15.0}$	$29.5^{+17.5}_{-6.3}$	$43.2^{+50.7}_{-12.2}$	$27.6^{+13.0}_{-10.9}$	$-0.03^{+0.44}_{-0.36}$	$4.77^{+3.70}_{-2.66}$	$0.75^{+0.45}_{-0.37}$	$68.3^{+52.5}_{-14.5}$	$0.68^{+0.16}_{-0.18}$	4200	$8.1^{+0.4}_{-0.7}$
GW190910_112807	$78.7^{+9.5}_{-9.0}$	$33.9^{+4.3}_{-3.9}$	$43.5^{+7.6}_{-6.2}$	$35.1^{+6.3}_{-7.0}$	$0.02^{+0.19}_{-0.18}$	$1.57^{+1.07}_{-0.64}$	$0.29^{+0.17}_{-0.11}$	$75.0^{+8.7}_{-8.5}$	$0.70^{+0.08}_{-0.07}$	10000	$14.1^{+0.2}_{-0.3}$
GW190915_235702	$59.5^{+7.5}_{-6.2}$	$25.1^{+3.1}_{-2.6}$	$34.9^{+9.5}_{-6.2}$	$24.4^{+5.5}_{-6.0}$	$0.03^{+0.19}_{-0.24}$	$1.70^{+0.71}_{-0.64}$	$0.32^{+0.11}_{-0.11}$	$56.8^{+7.1}_{-5.8}$	$0.71^{+0.09}_{-0.11}$	380	$13.6^{+0.2}_{-0.3}$
GW190924_021846	$13.9^{+5.1}_{-0.9}$	$5.8^{+0.2}_{-0.2}$	$8.8^{+7.0}_{-2.0}$	$5.0^{+1.3}_{-1.9}$	$0.03^{+0.30}_{-0.09}$	$0.57^{+0.22}_{-0.22}$	$0.12^{+0.04}_{-0.04}$	$13.3^{+5.2}_{-1.0}$	$0.67^{+0.05}_{-0.05}$	380	$11.5^{+0.3}_{-0.4}$
GW190929_012149	$90.6^{+21.2}_{-14.1}$	$34.3^{+8.6}_{-6.5}$	$64.7^{+22.4}_{-18.9}$	$25.7^{+14.4}_{-9.7}$	$0.03^{+0.27}_{-0.27}$	$3.68^{+2.98}_{-1.68}$	$0.61^{+0.38}_{-0.24}$	$87.5^{+20.7}_{-14.1}$	$0.64^{+0.17}_{-0.23}$	1800	$9.8^{+0.8}_{-0.6}$
[illegible]	[illegible]	[illegible]	$12.3^{+12.5}_{-2.3}$	$7.8^{+1.7}_{-3.3}$	$0.14^{+0.31}_{-0.15}$	$0.78^{+0.37}_{-0.33}$	$0.16^{+0.07}_{-0.06}$	$19.3^{+9.3}_{-1.5}$	$0.72^{+0.07}_{-0.06}$	1800	[illegible]

Detection range (NSNS)

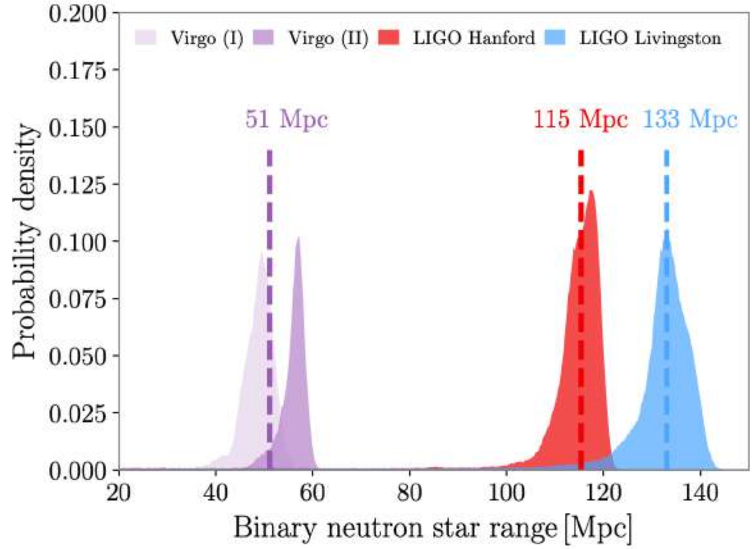

Detection versus time-volume

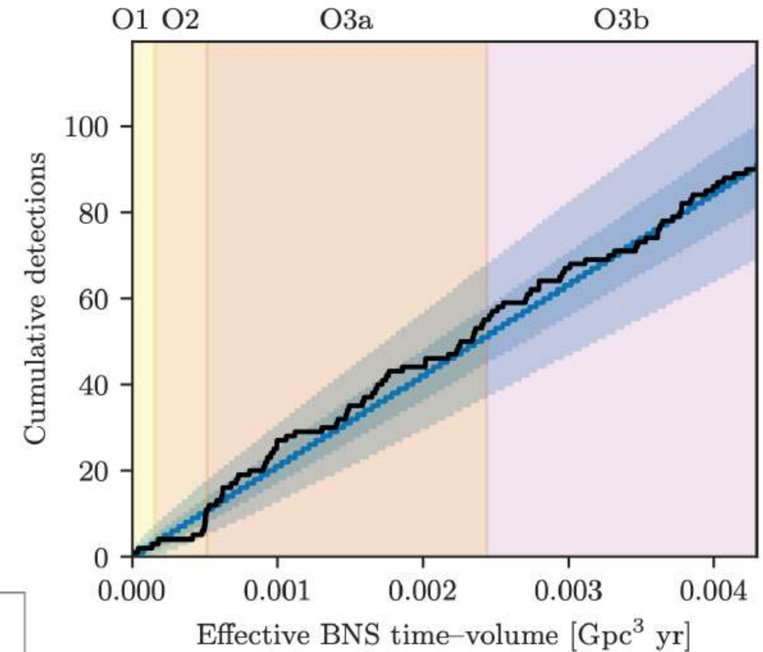

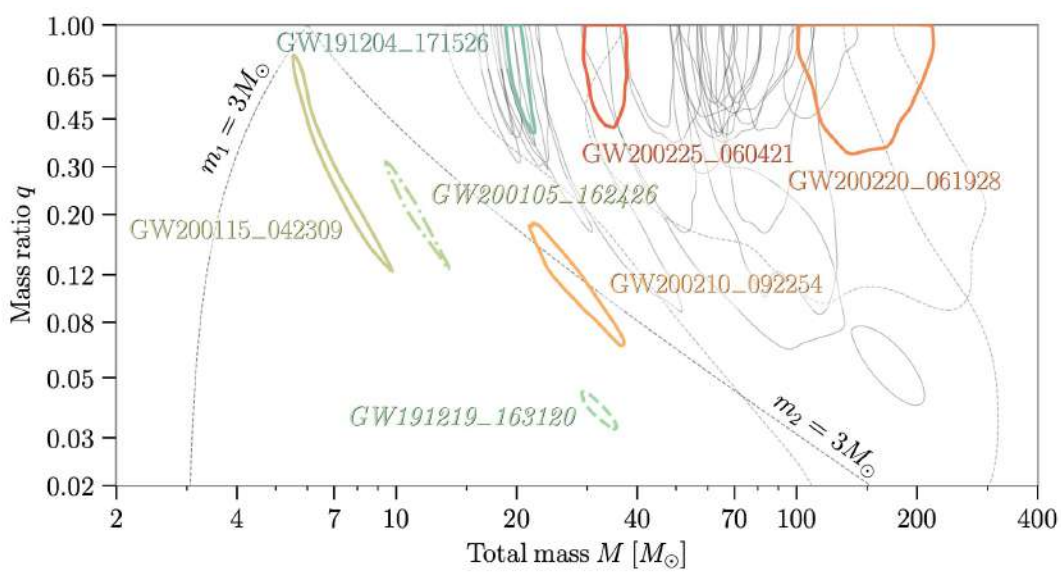

Component masses
Mass ratios
Spins
Distances

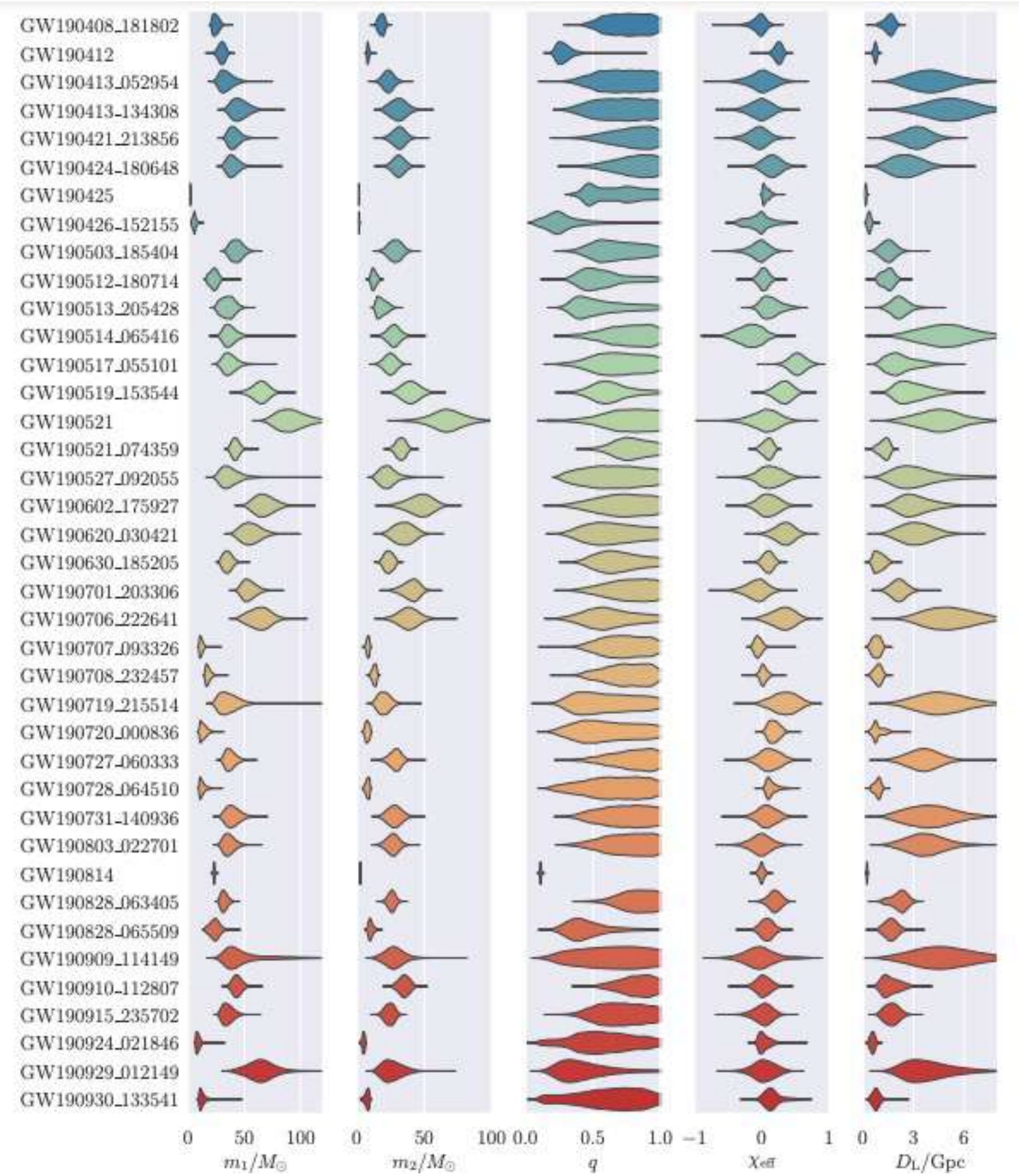

Tauris & van den Heuvel (2023)

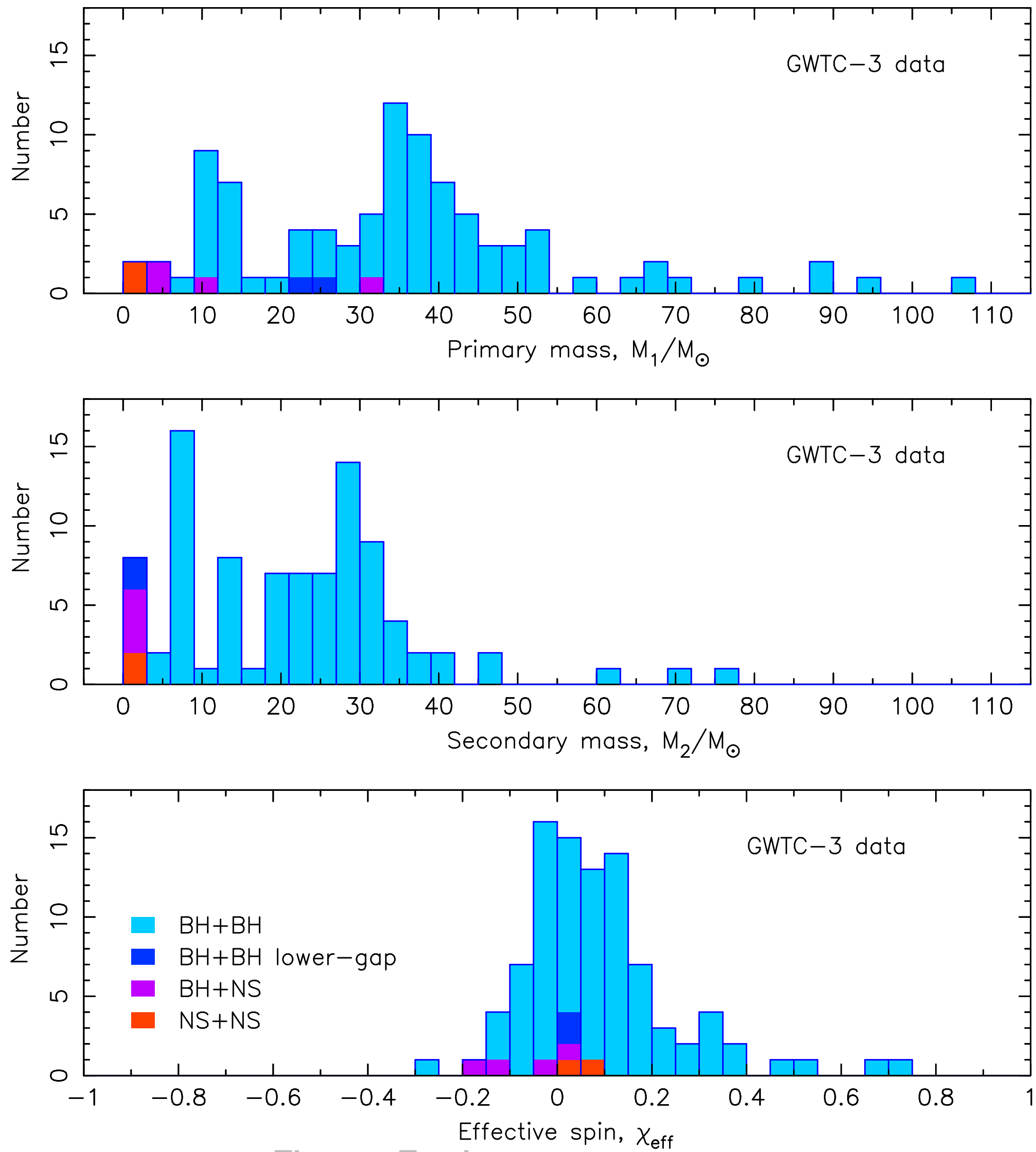

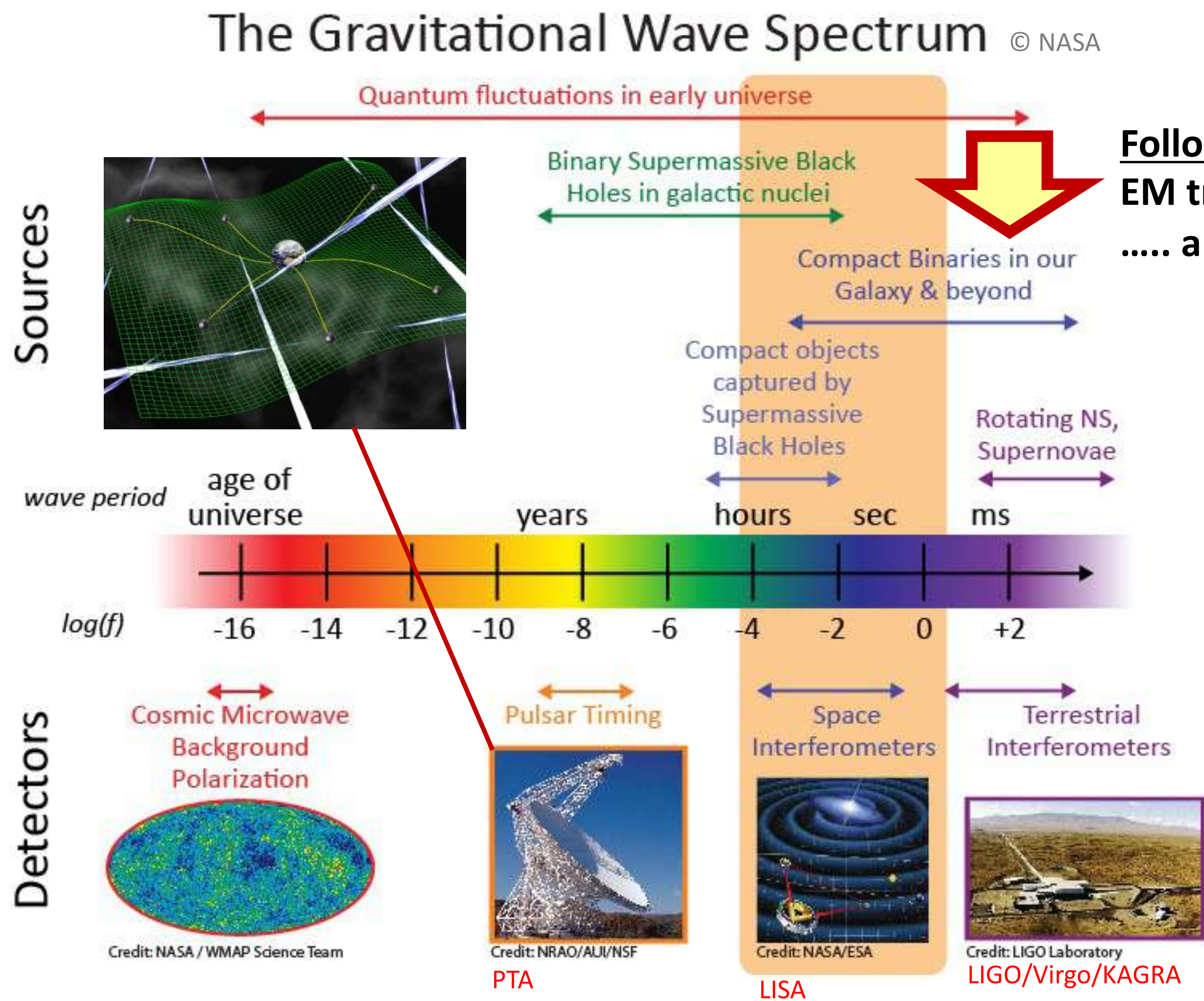

Follow-up:
EM transient counterparts
..... and neutrinos

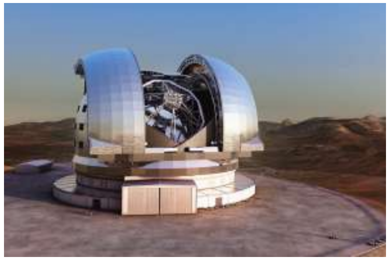

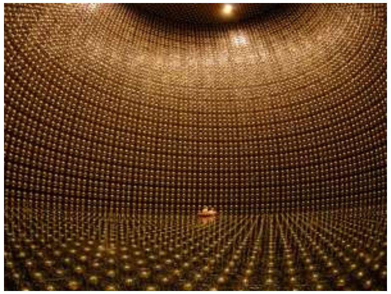

$* \; \Delta E_{GW} < 10^{-8} \, M_{\odot} \, c^2$

high freq. GWs **LIGO: 10 Hz – 1 kHz**

low freq. GWs **LISA: 0.1 mHz – 10 mHz**

I. Transient (one-time) burst events: extragalactic

LIGO ❖ Colliding neutron star + black hole binaries

(LISA may detect these mergers too)

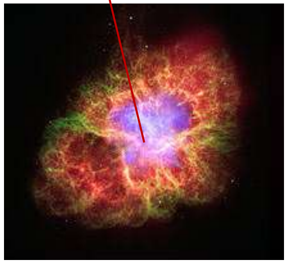

LIGO ❖ Supernova core collapse (Galactic!) *

LISA ❖ Supermassive black hole mergers

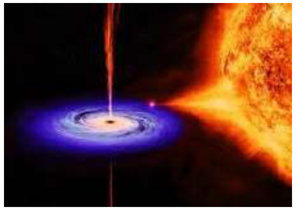

II. Persistent sources (continuous emission): Galactic

LIGO ❖ Pulsars or accreting NS

LISA ❖ Galactic resolved compact binaries (WD, NS, BH)

`Murmurs' from the Big Bang

signals from the early Universe

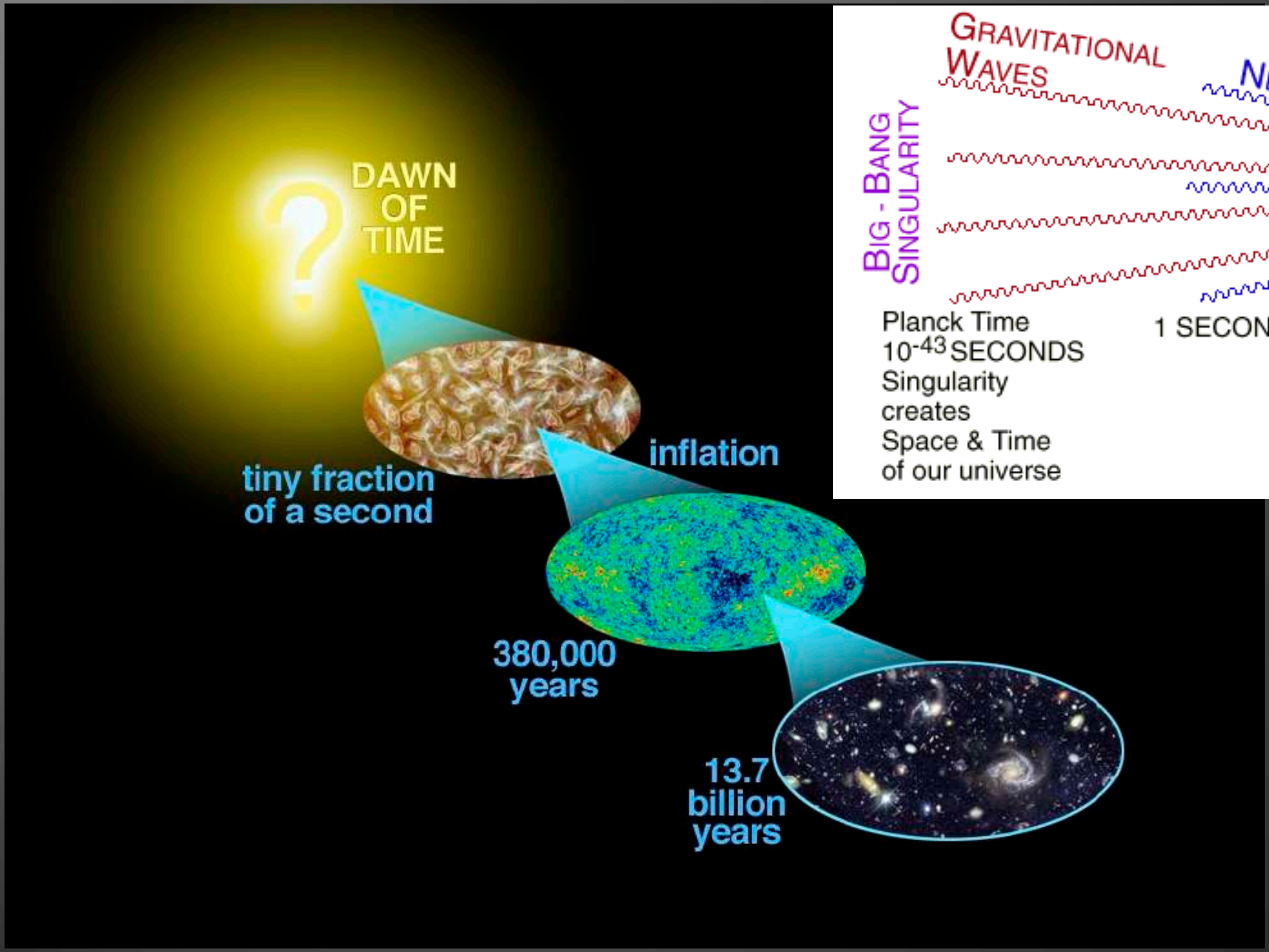

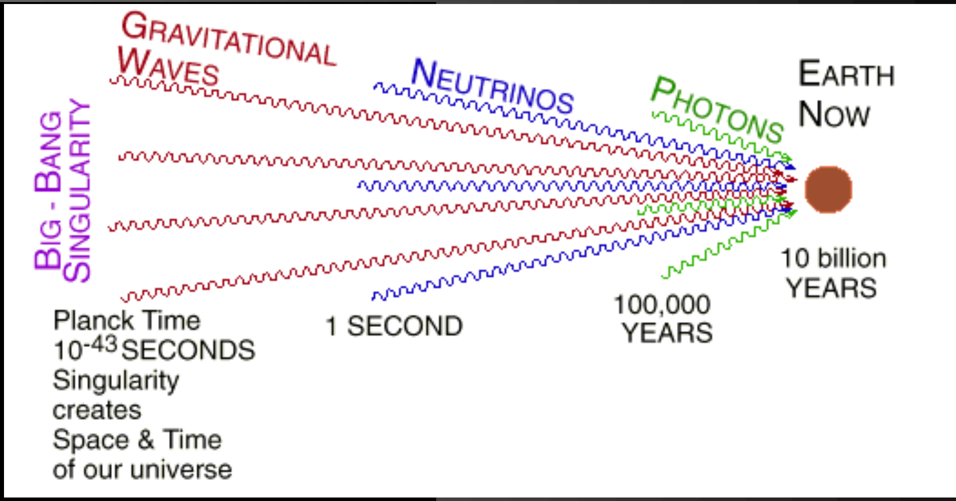

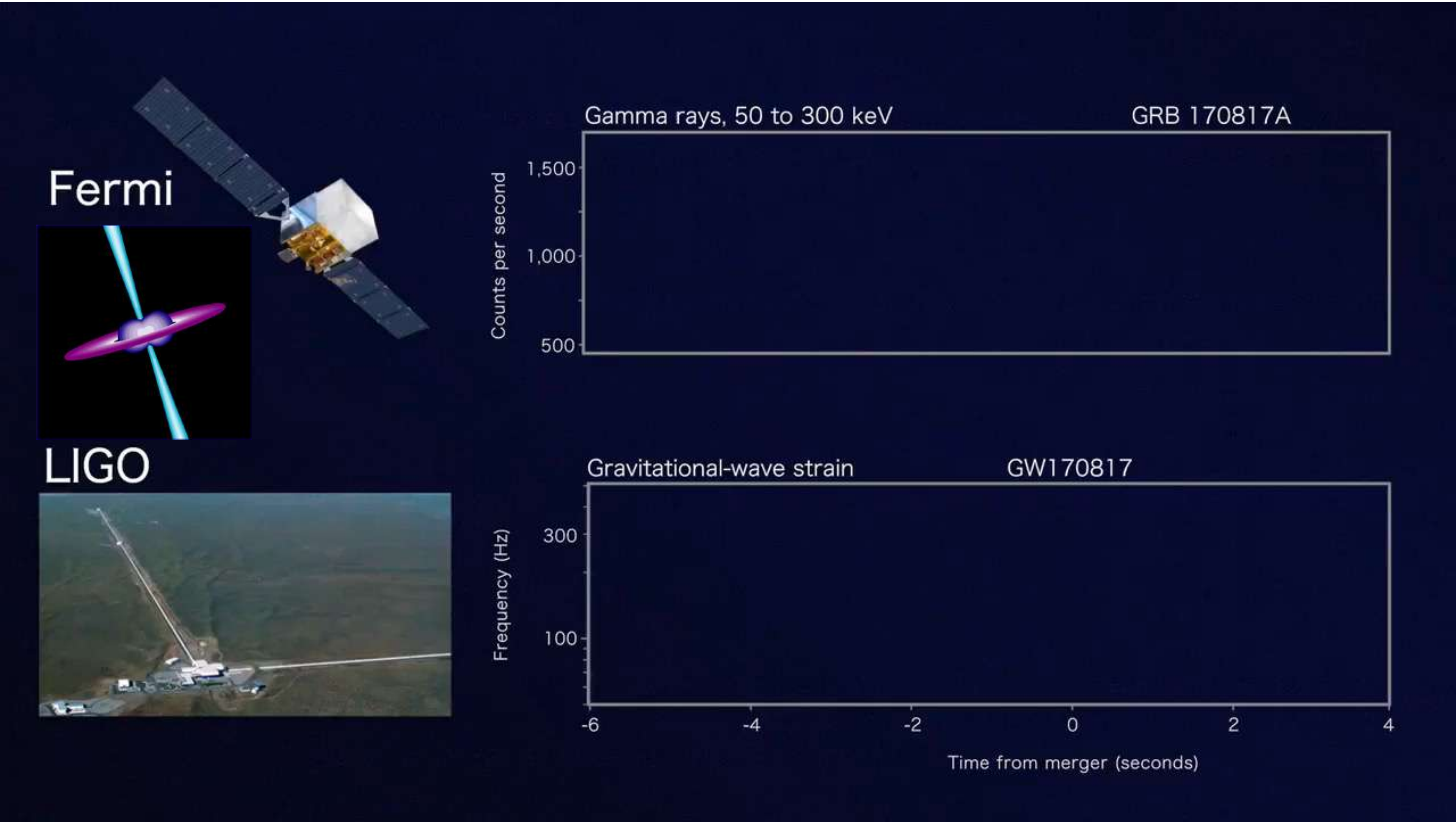
Fermi
LIGO
Gamma rays, 50 to 300 keV
GRB 170817A
Counts per second
1,500
1,000
500
Gravitational-wave strain
GW170817
Frequency (Hz)
300
100
-6
-4
-2
0
2
4
Time from merger (seconds)

New era of **multi-messenger** astrophysics

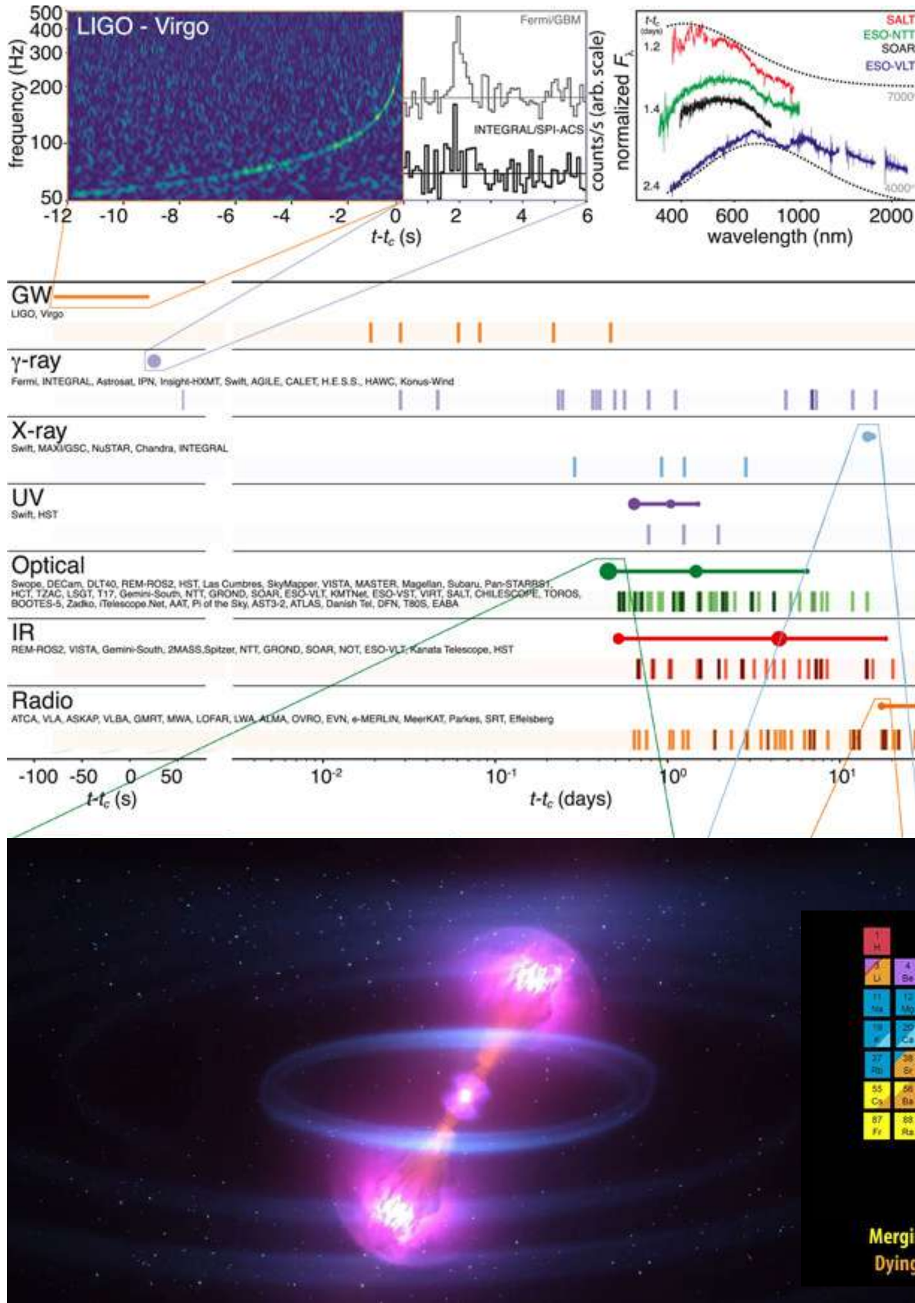

Detection of a **kilonova** (radioactive decay of heavy r-process elements)

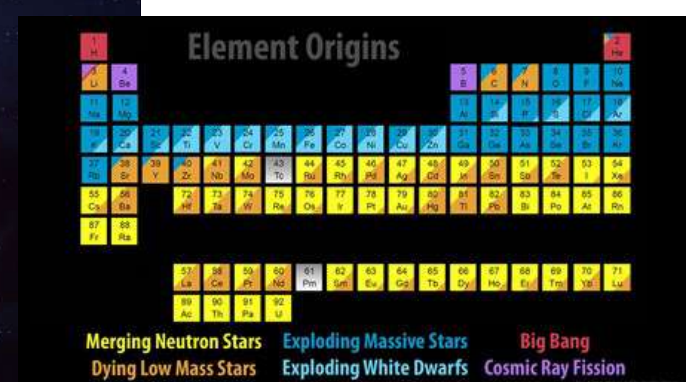

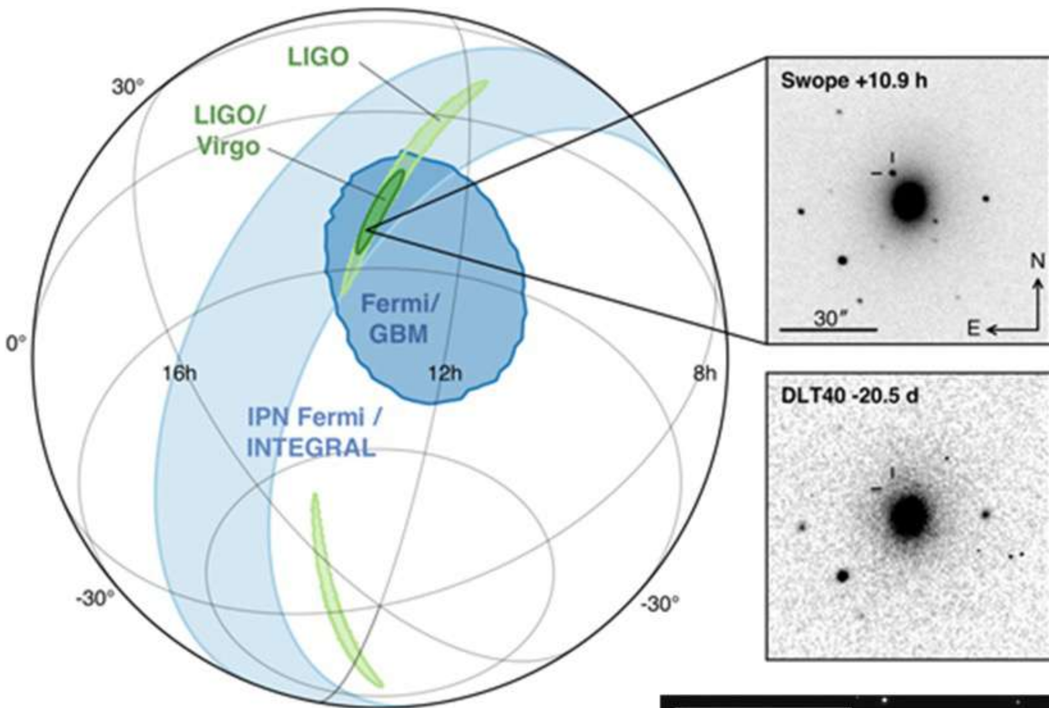

NGC 4993
d = 40 Mpc (z=0.009, 130 mill. ly)

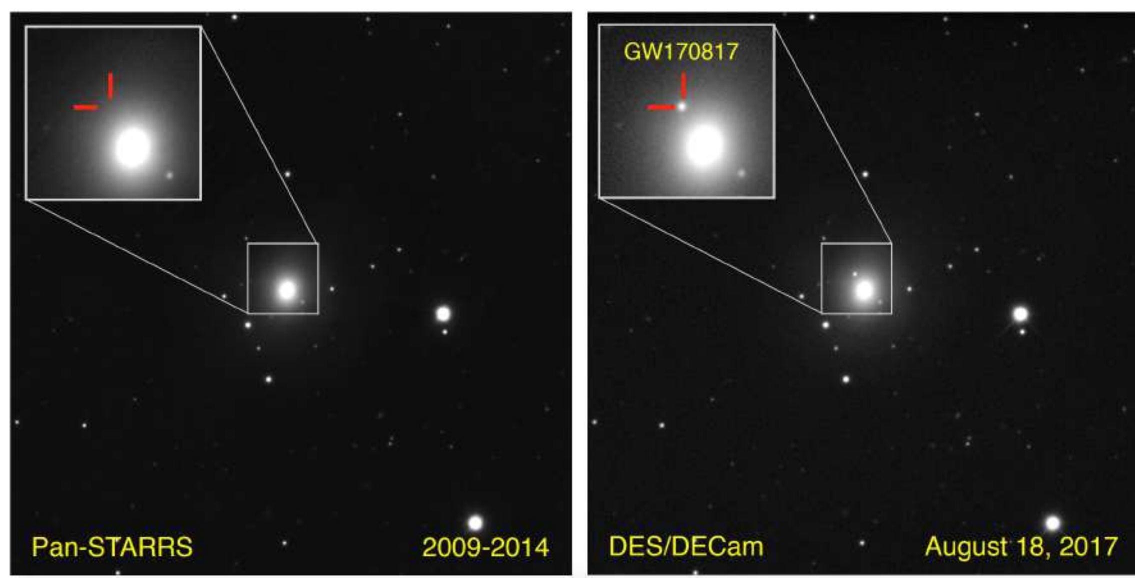

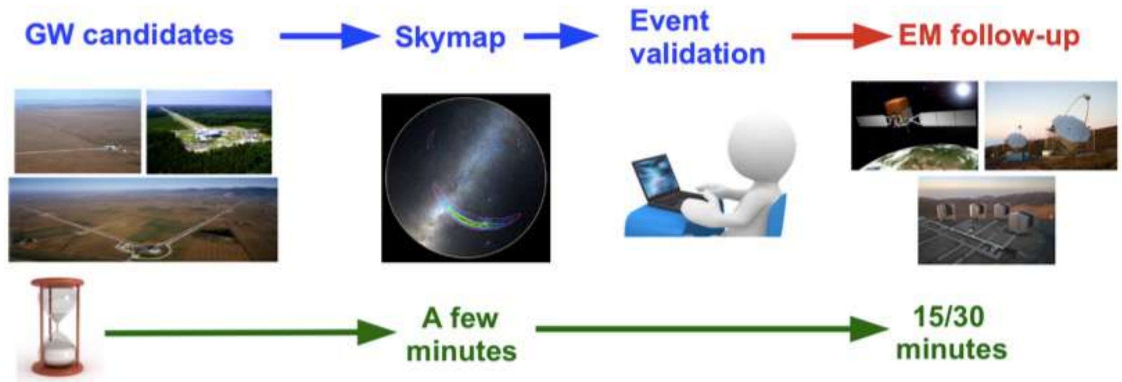

© Patricelli

GW

- mass
- spin
- eccentricity
- luminosity distance
- system orientation
- BH/NS merger-rate density
- evolution over cosmic time (primordial BHs, SMBH seeds)

EM

- sky location
- host galaxy
- redshift
- local environment
- heavy r-process nucleosynthesis
- emission processes (kilonova)
- sGRB (central engine, beaming, jets, afterglow)

NEUTRINOS

- neutrino physics
- central engine
- SN explosions

- **Testing theories of gravity**
- **NS equation-of-state**
- **Cosmology**

© Branchesi

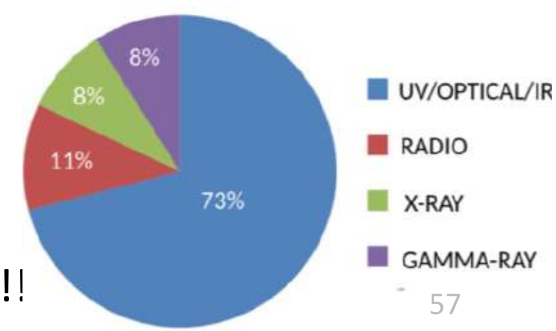

80 MoUs involving 170 instruments!!

- **Tidal deformation and NS EoS**

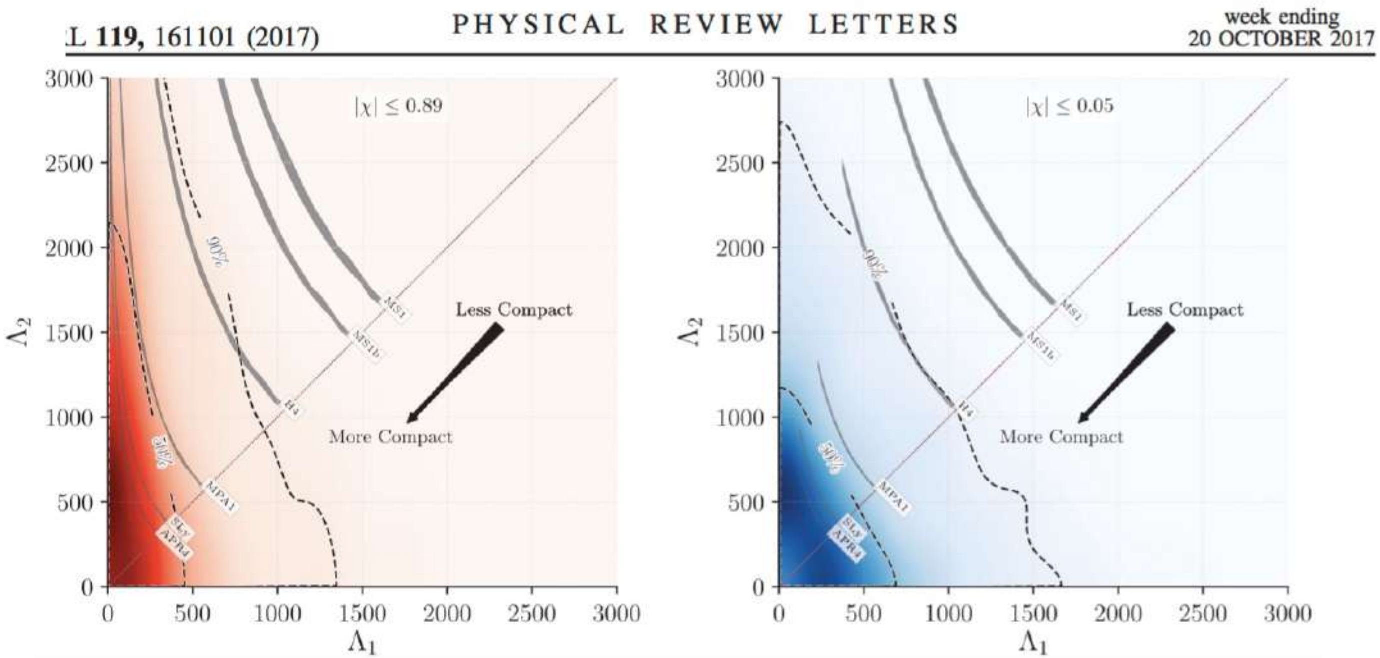

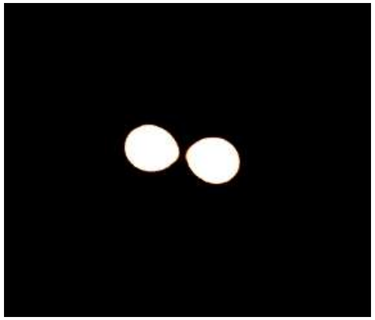

S. Roswogg

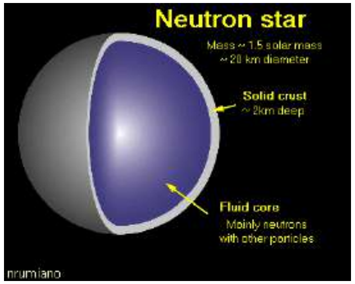

GW phase depends on tidal deformability parameter:

$$\Lambda \propto k\,(R\,/\,M)^5$$

$$\lambda \equiv -\frac{Q_{ij}}{\mathcal{E}_{ij}} \qquad \Lambda \equiv \frac{\lambda}{m^5} = \frac{2}{3}k_2\left(\frac{Gm}{Rc^2}\right)^{-5}$$

$$\tilde{\Lambda} = \frac{16}{13}\frac{(12q+1)\Lambda_1 + (12+q)q^4\Lambda_2}{(1+q)^5}$$

$$q = m_2/m_1 \le 1$$

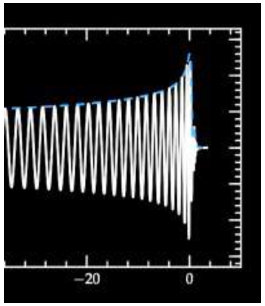

Flanagan & Hinderer (2008)

RECIPE

- Binary stellar evolution
- Population synthesis
  (input distributions and stellar grids)
- Galactic star formation rate
  (formation history of massive binaries)
- Galactic potentials
  (to probe location of mergers in host galaxies)
- Extrapolation to local Universe
  (scaling-law of galaxy number density)

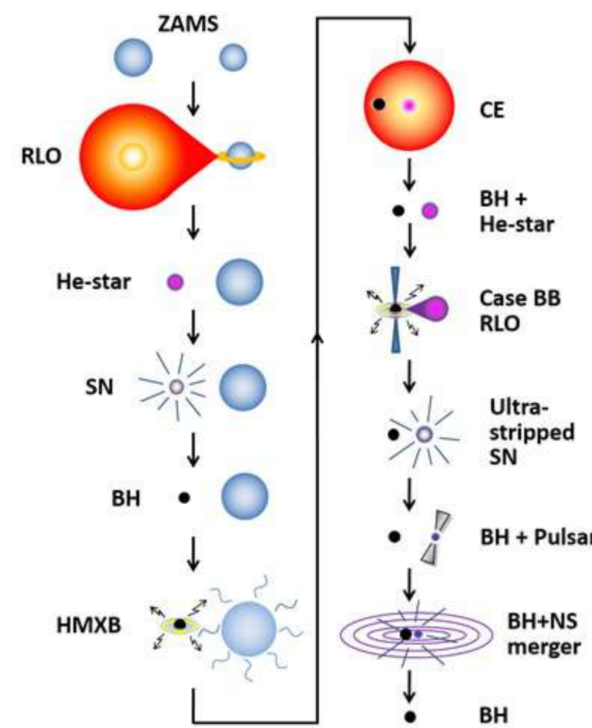

Notes on POP. SYNTHESIS

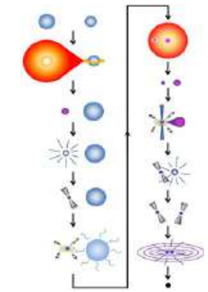

1. Reproduction of LIGO rates is *no* success criterion on its own
2. Can Galactic sources be reproduced? (properties of HMXBs, DNSs, etc.)
3. Is the input physics reasonable? Is the evolution self consistent? *
4. Watch out for papers that claim they can explain everything!

* E.g. Stellar evolution (Z)
Klencki et al. (2020)

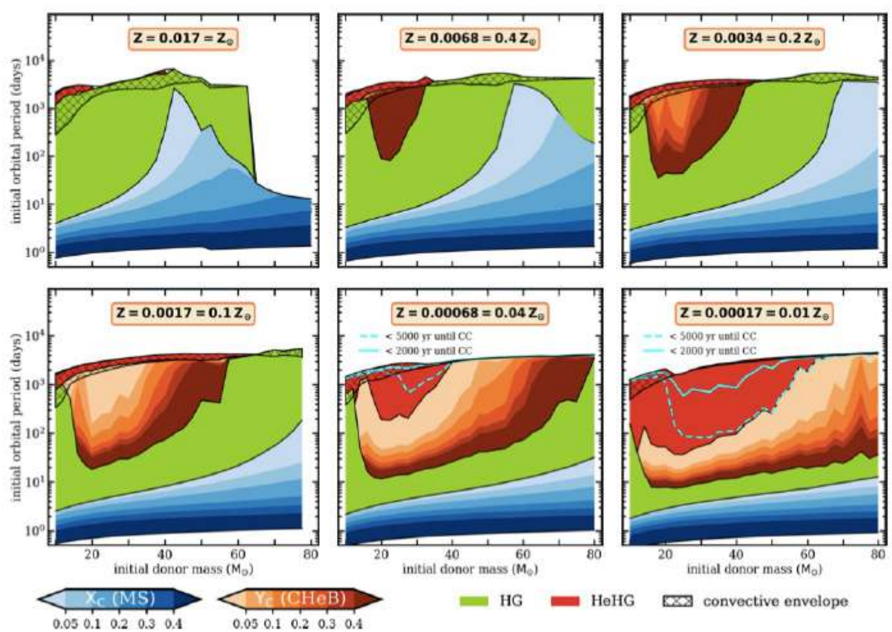

Kruckow et al. (2018), MNRAS

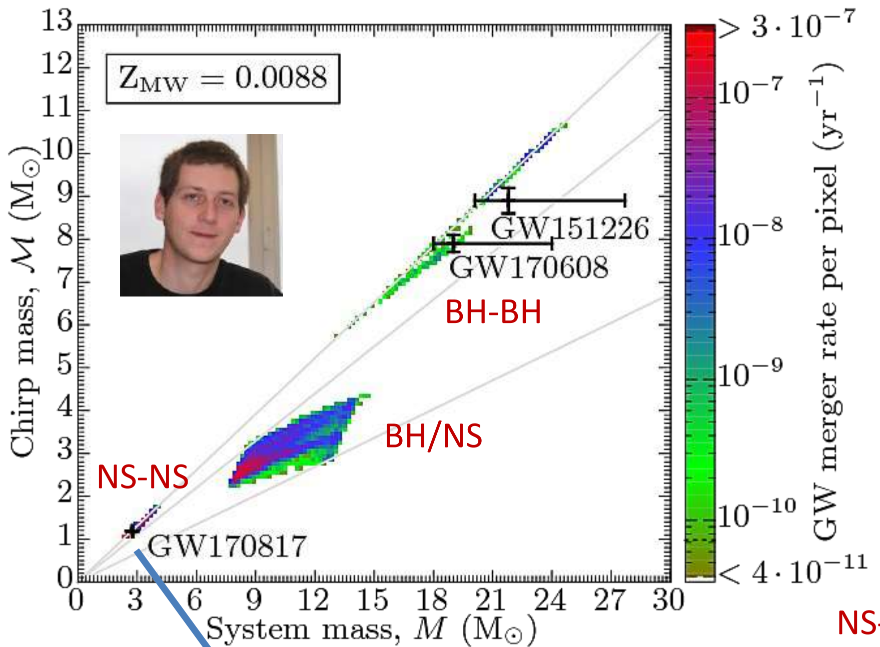

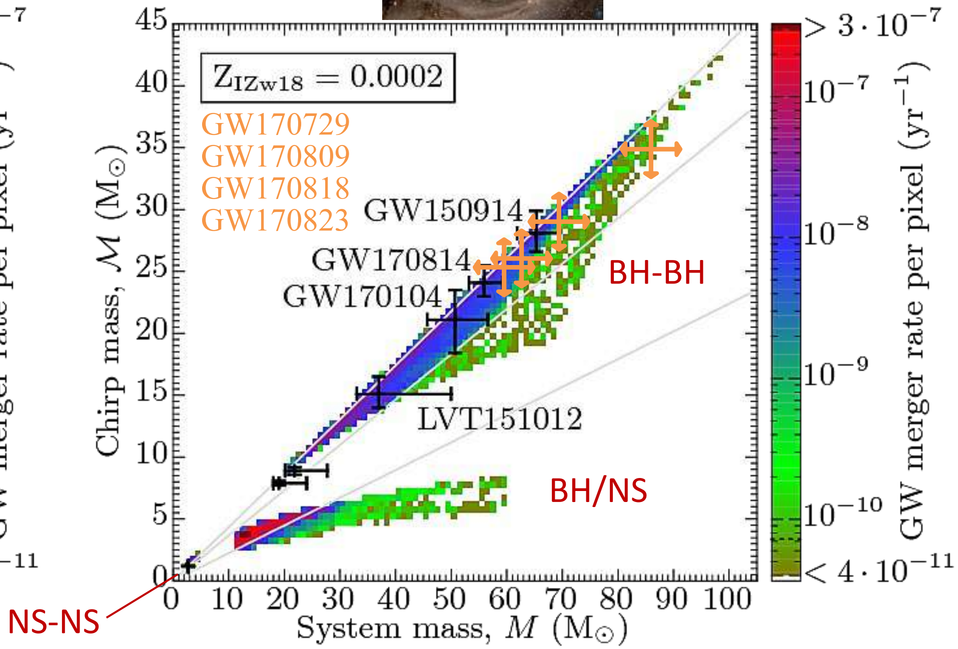

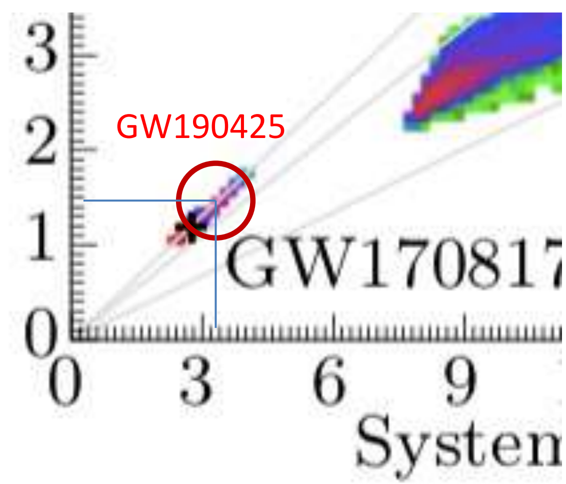

GW190425

$M_{chirp} = 1.44\ M_{sun}$

$M_{total} = 3.3\ M_{sun}$

($\chi < 0.05$)

GW170817:

$R = 1540 +/-{}^{3200}_{1220}\ Gpc^{-3}\ yr^{-1}$

GW190425:

$R = 1090 +/-{}^{1720}_{800}\ Gpc^{-3}\ yr^{-1}$

GWTC-2 rate:

$R = 320 +/-{}^{490}_{240}\ Gpc^{-3}\ yr^{-1}$

GWTC-3 rate:

$R = 99 +/-{}^{260}_{86}\ Gpc^{-3}\ yr^{-1}$

Eccentricity, e

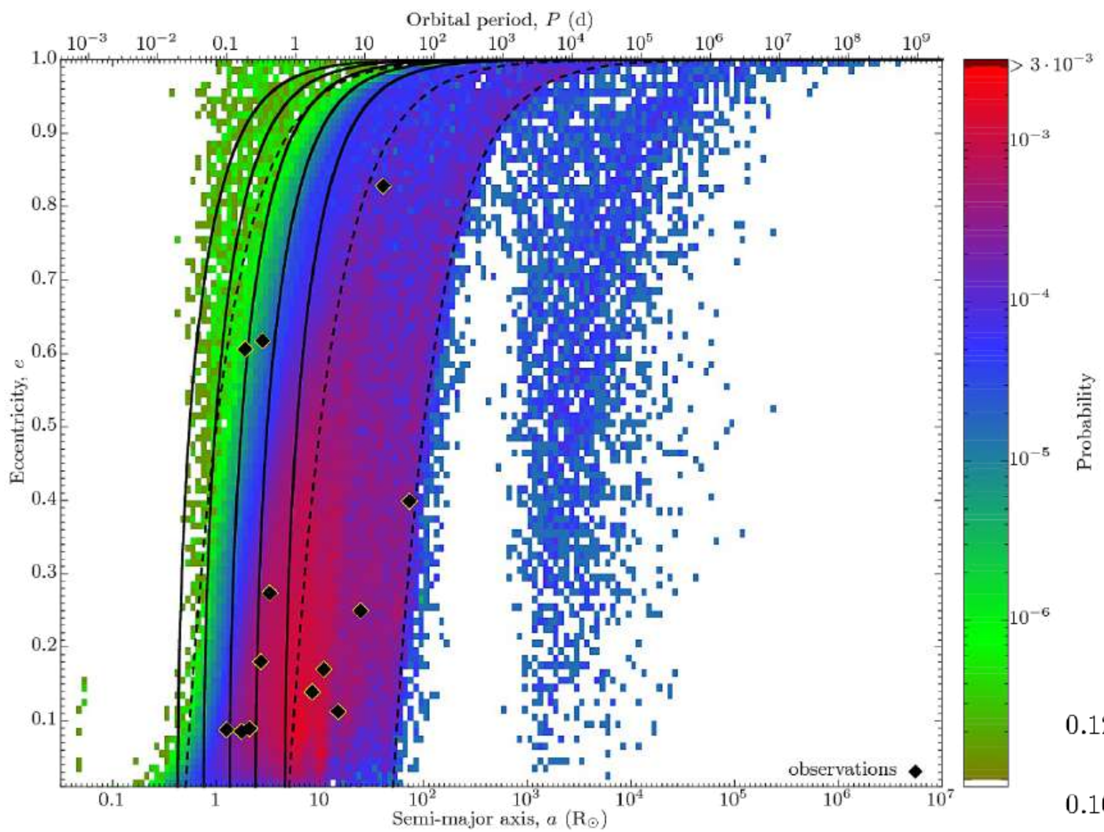

Semi-major axis, a (R_{sun})

Kruckow, Tauris, et al. (2018), MNRAS

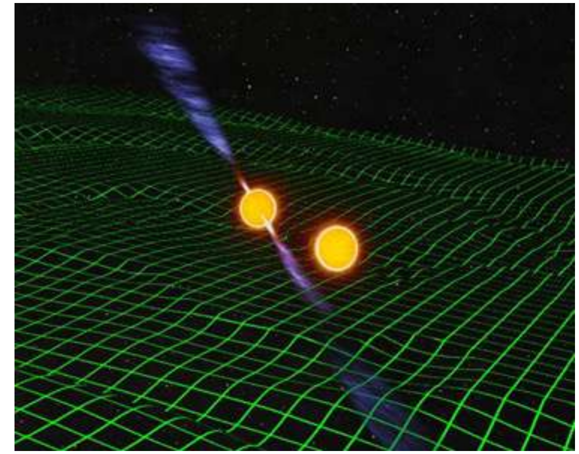

Do not trust population synthesis if it cannot reproduce observed Galactic DNS systems

NS mass ratios

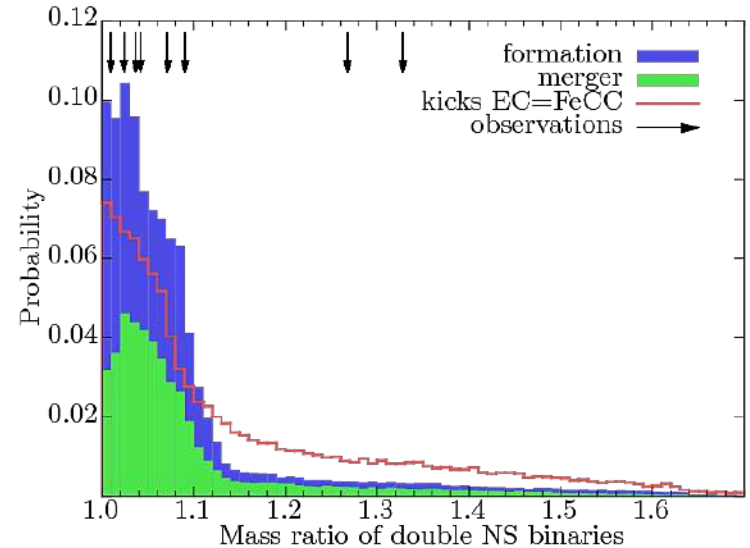

Important calibration data!!!

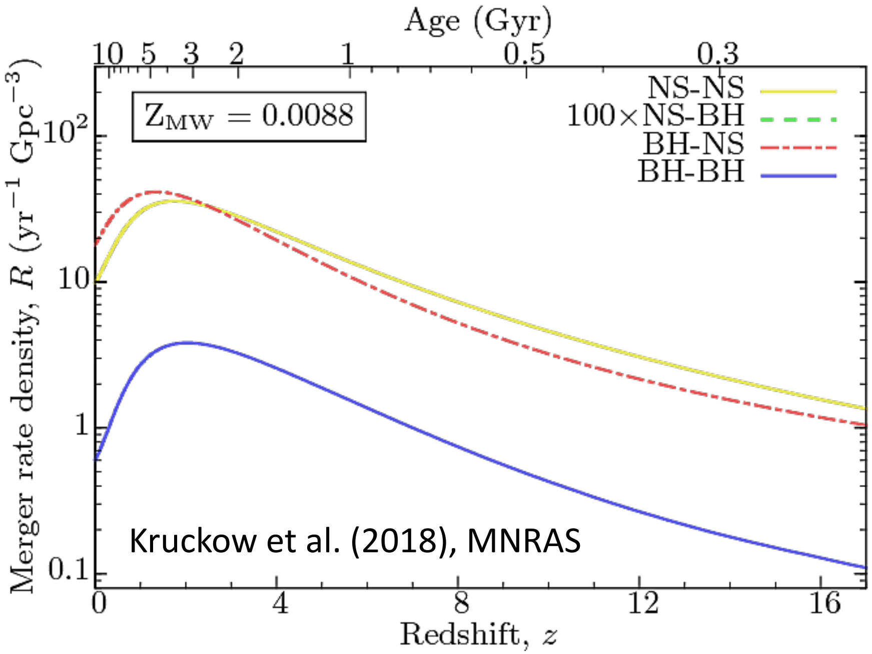

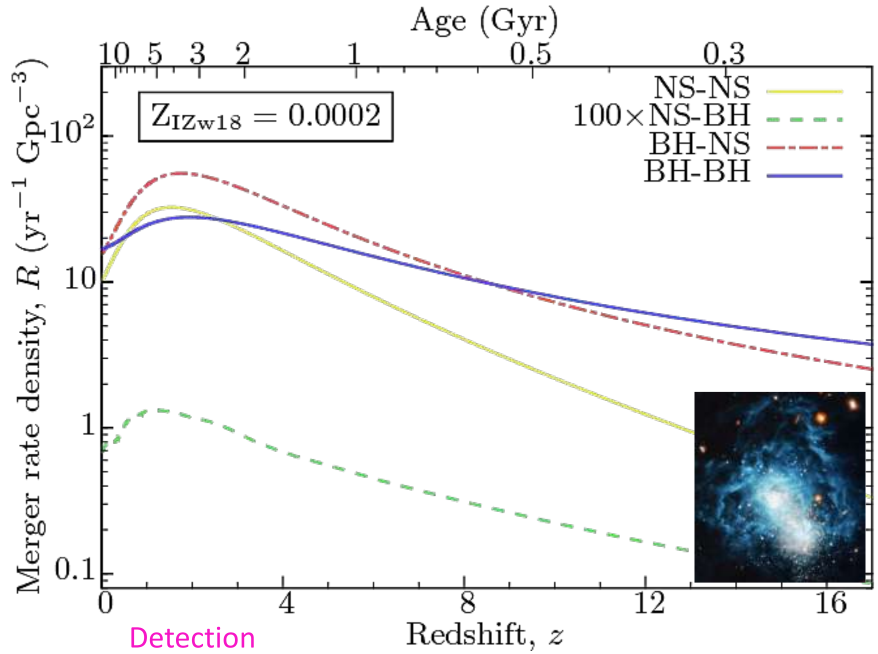

Detection rates

local Universe

Z_{MW}	$\langle M^{2.5} \rangle$	$R_{z=0}$	R_D	R_{cSFR}	$R_{D,cSFR}$
NS-NS	1.36 $M_\odot^{2.5}$	9.85×10^0 yr^{-1} Gpc^{-3}	0.28 yr^{-1}	3.47×10^1 yr^{-1} Gpc^{-3}	0.98 yr^{-1}
NS-BH	20.0 $M_\odot^{2.5}$	0.00×10^0 yr^{-1} Gpc^{-3}	0.00 yr^{-1}	0.00×10^0 yr^{-1} Gpc^{-3}	0.00 yr^{-1}
BH-NS	15.7 $M_\odot^{2.5}$	1.80×10^1 yr^{-1} Gpc^{-3}	5.88 yr^{-1}	4.72×10^1 yr^{-1} Gpc^{-3}	15.43 yr^{-1}
BH-BH	233 $M_\odot^{2.5}$	6.01×10^{-1} yr^{-1} Gpc^{-3}	2.92 yr^{-1}	3.08×10^0 yr^{-1} Gpc^{-3}	14.95 yr^{-1}
Z_{IZw18}	$\langle M^{2.5} \rangle$	$R_{z=0}$	R_D	R_{cSFR}	$R_{D,cSFR}$
NS-NS	1.27 $M_\odot^{2.5}$	1.00×10^1 yr^{-1} Gpc^{-3}	0.27 yr^{-1}	3.28×10^1 yr^{-1} Gpc^{-3}	0.87 yr^{-1}
NS-BH	32.3 $M_\odot^{2.5}$	6.61×10^{-3} yr^{-1} Gpc^{-3}	0.00 yr^{-1}	1.55×10^{-2} yr^{-1} Gpc^{-3}	0.01 yr^{-1}
BH-NS	35.5 $M_\odot^{2.5}$	1.54×10^1 yr^{-1} Gpc^{-3}	11.40 yr^{-1}	5.32×10^1 yr^{-1} Gpc^{-3}	39.34 yr^{-1}
BH-BH	1720 $M_\odot^{2.5}$	1.68×10^1 yr^{-1} Gpc^{-3}	603.02 yr^{-1}	3.45×10^1 yr^{-1} Gpc^{-3}	1235.27 yr^{-1}
optimistic	$\langle M^{2.5} \rangle$	$R_{z=0}$	R_D	R_{cSFR}	$R_{D,cSFR}$
NS-NS	1.31 $M_\odot^{2.5}$	7.09×10^1 yr^{-1} Gpc^{-3}	1.94 yr^{-1}	1.59×10^2 yr^{-1} Gpc^{-3}	4.37 yr^{-1}
NS-BH	19.4 $M_\odot^{2.5}$	0.00×10^0 yr^{-1} Gpc^{-3}	0.00 yr^{-1}	0.00×10^0 yr^{-1} Gpc^{-3}	0.00 yr^{-1}
BH-NS	21.9 $M_\odot^{2.5}$	1.34×10^1 yr^{-1} Gpc^{-3}	6.11 yr^{-1}	2.44×10^1 yr^{-1} Gpc^{-3}	11.17 yr^{-1}
BH-BH	275 $M_\odot^{2.5}$	4.34×10^1 yr^{-1} Gpc^{-3}	248.34 yr^{-1}	1.09×10^2 yr^{-1} Gpc^{-3}	623.03 yr^{-1}

@design sensitivity: 1–5 detections per yr

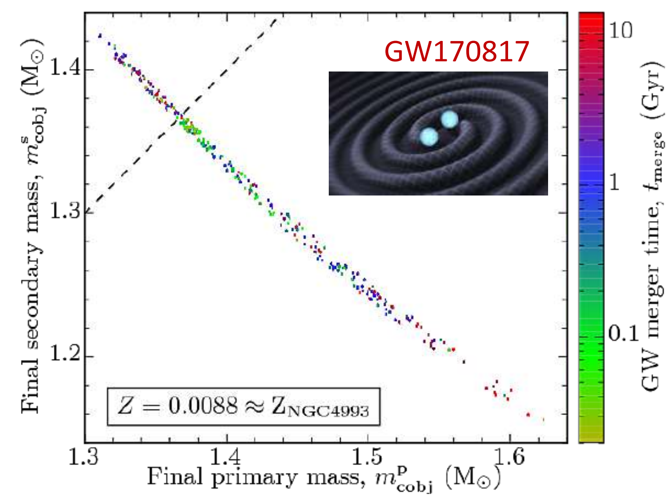

PROGENITORS OF LIGO-VIRGO EVENTS: METALLICITY

Kruckow et al. (2018), MNRAS

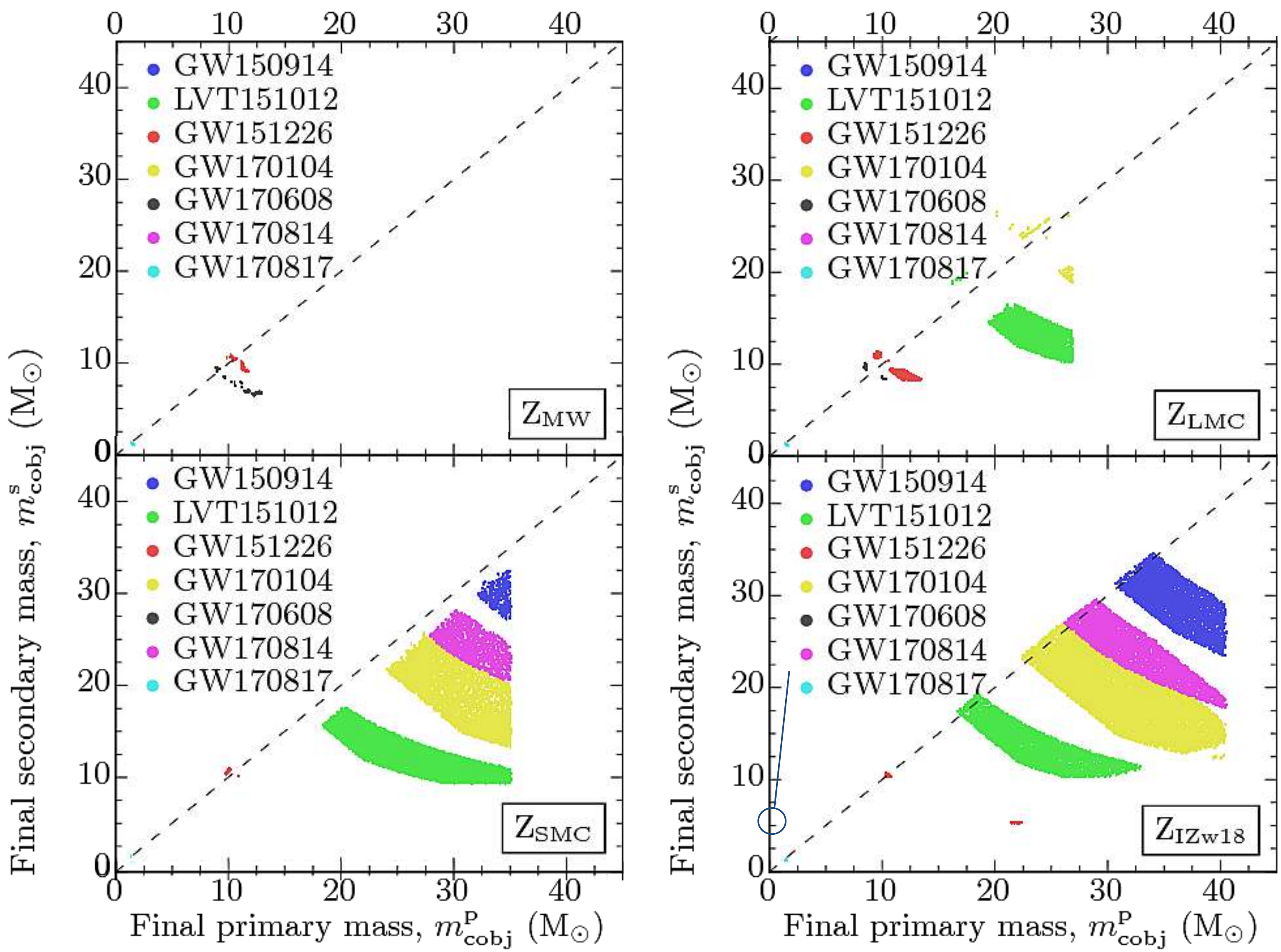

@design sensitivity: 1–5 detections per yr

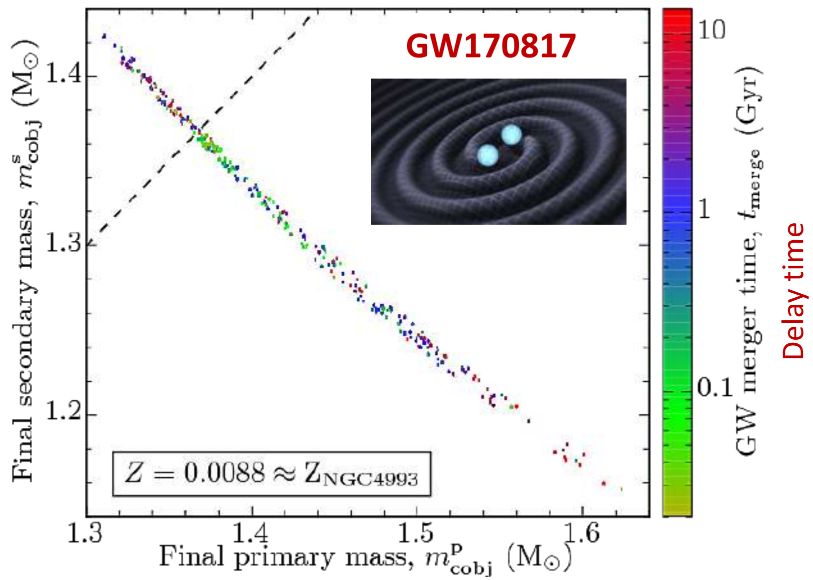

Kruckow, et al. (2018), MNRAS

We find age solutions from <100 Myr to >10 Gyr

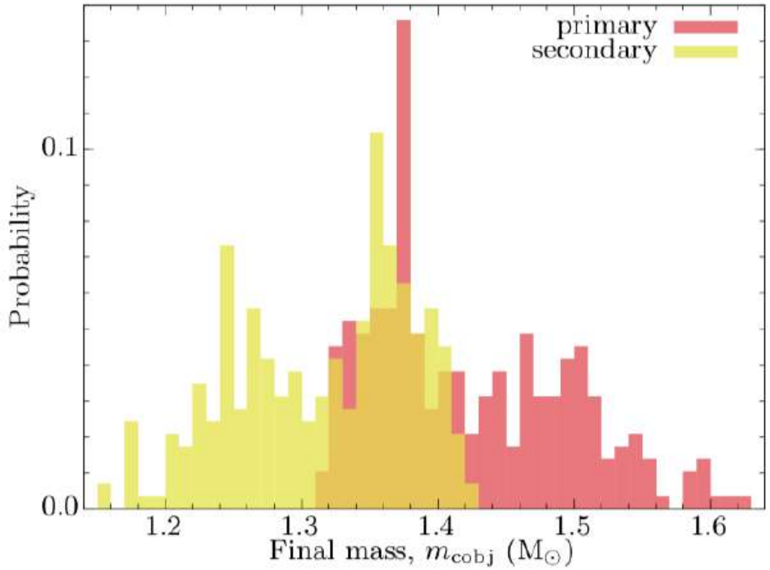

Our NS mass solutions for GW170817 are typical for Galactic DNS systems

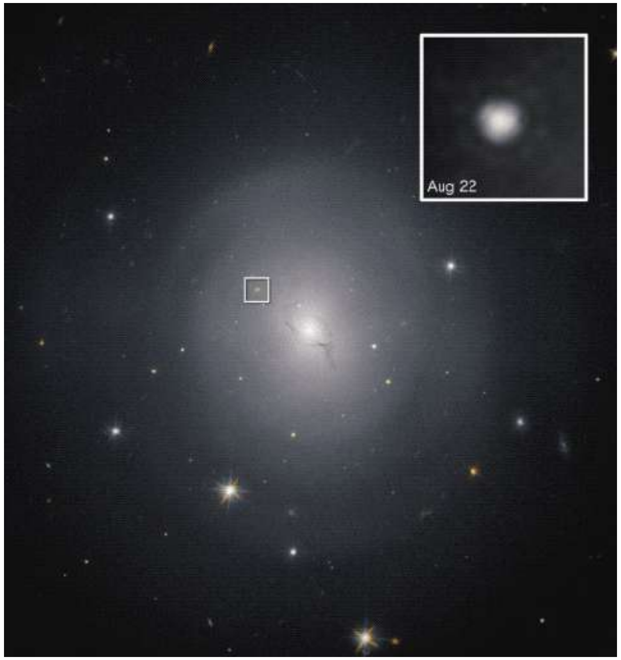

NGC 4993

Kruckow et al. (2018), MNRAS

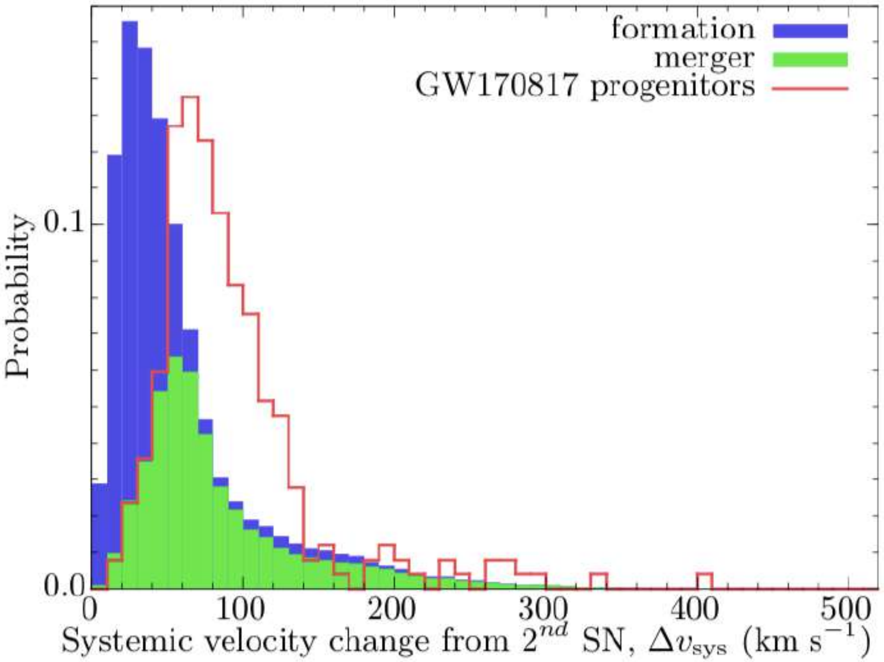

For NGC 4393, the escape velocity at the location of GW170817 is about 350 km s^{-1}(Pan et al. 2017), much larger than the typical systemic velocities we obtain in our simulations.

LIGO network measurements:

$$\chi_{\text{eff}} \equiv \frac{(M_1\vec{\chi}_1 + M_2\vec{\chi}_2)}{M} \cdot \frac{\vec{L}}{|\vec{L}|} = \frac{\chi_1 \cos\theta_1 + q\,\chi_2 \cos\theta_2}{1+q}$$

LIGO run O1+O2:

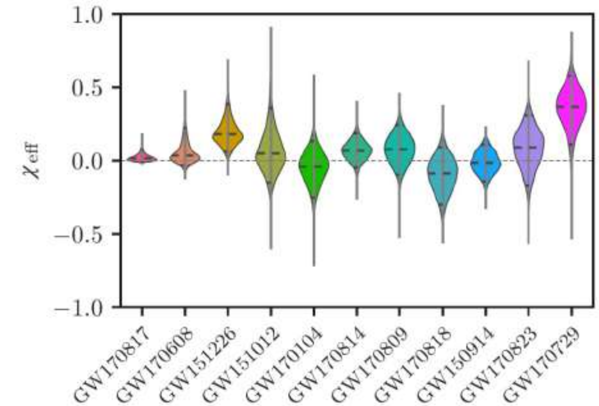

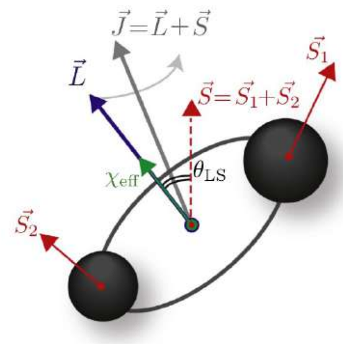

LIGO run O3a:

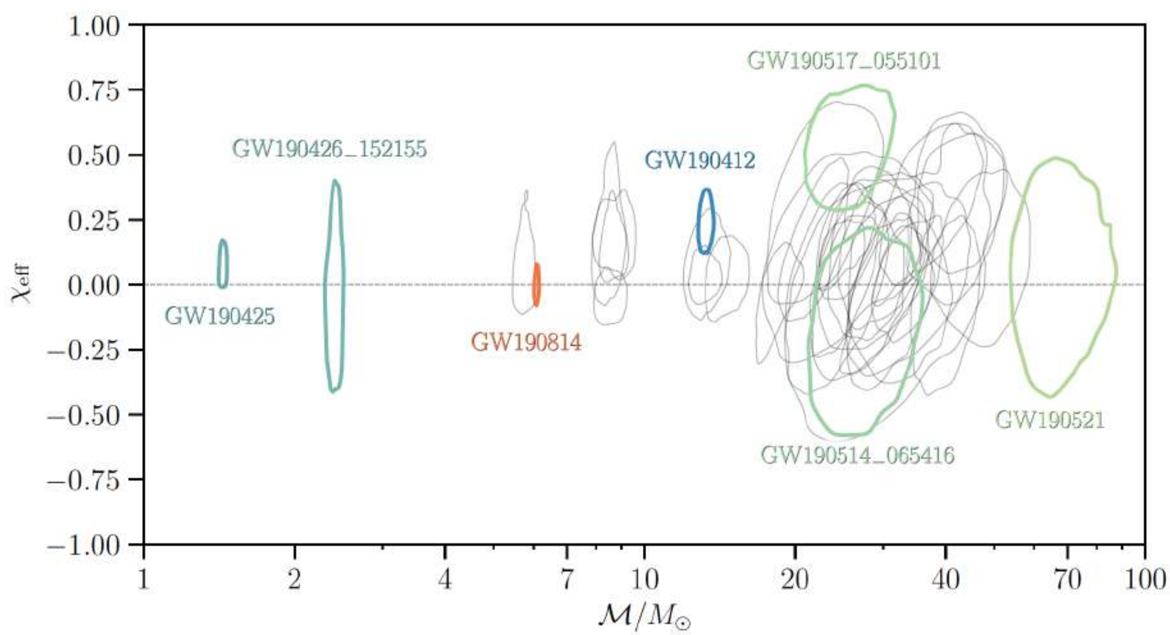

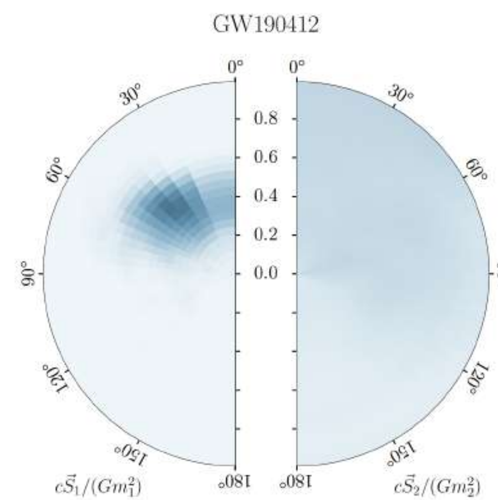

Intrepretation of BHBH mergers spins

Given that the far majority of all BH-BH mergers reported so far have near-zero effective spins leads to only three potential explanations (e.g. Belczynski et al., 2020):

<u>If the individual BH spin magnitudes are large, then:</u>
(i) Either both BH spin vectors must be nearly in the orbital plane, or
(ii) the spin angular momenta of the BHs must be oppositely directed and similar in magnitude.

Finally, there is also the possibility that:
(iii) the BH spin magnitudes are small.

Belczynski et al. (2020) demonstrate that they can reproduce the observed distribution of low $\chi_{\rm eff}$ values within the classical isolated binary evolution scenario (the CE channel) of BH-BH formation assuming effcient angular momentum transport.

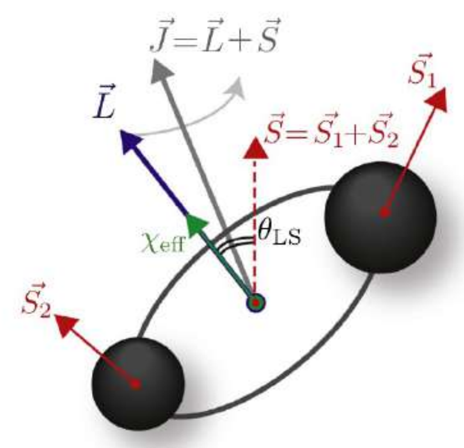

Expectations from stellar evolution:

See e.g.: Kushnir et al. (2016), Hotokezaka & Piran (2017), Zaldarriaga et al. (2018), Fuller & Ma (2019), Qin et al. (2019), Belczynski et al. (2020), Bavera et al. (2020)

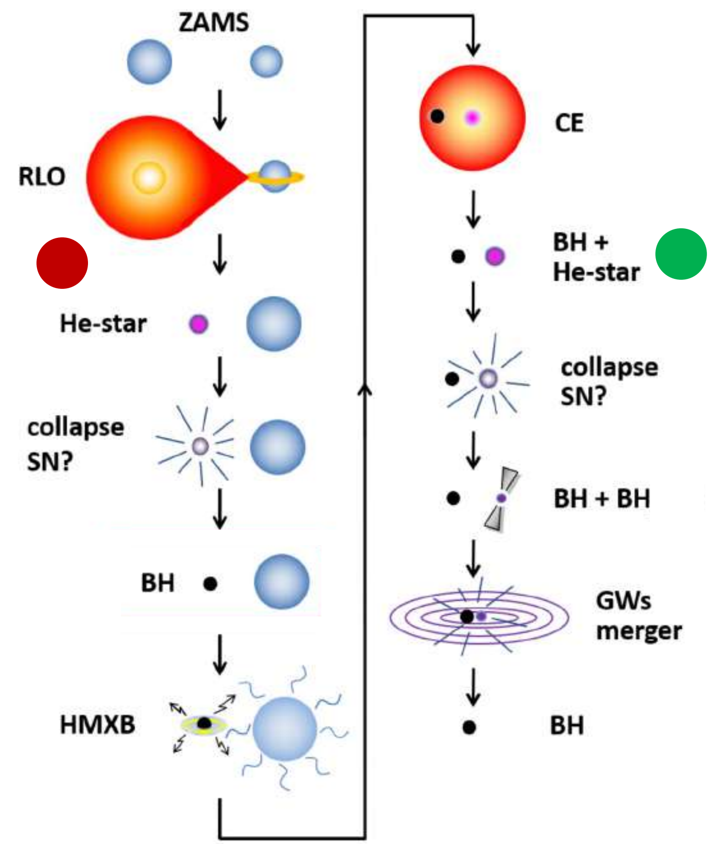

- First-born BH will be spinning rather slow
- Second-born BH will be spinning rather fast

1. Efficient angular momentum transport by viscosity will couple the stellar core to its envelope, thereby slowing the spin of the core as the envelope expands when it becomes a giant star. Contradiction *

2. Tidal interactions between the first-born BH and the close-by naked-core WR-star (progenitor of the second-born BH) causes the latter to spin up efficiently.

* In clear tension with observations of BH spins in HMXBs (see Lecture 9)

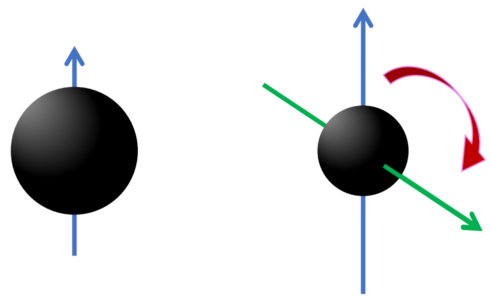

sort hul 1 sort hul 2

The Astrophysical Journal, 938:66 (14pp), 2022 October 10 https://doi.org/10.3847/1538-4357/ac86c8

Tossing Black Hole Spin Axes

Thomas M. Tauris
Department of Materials and Production, Aalborg University, Skjernvej 4A, DK-9220 Aalborg Øst, Denmark; tauris@mp.aau.dk
Received 2022 May 4; revised 2022 August 2; accepted 2022 August 2; published 2022 October 13

Abstract

The detection of double black hole (BH+BH) mergers provides a unique possibility to understand their physical properties and origin. To date, the LIGO–Virgo–KAGRA network of high-frequency gravitational-wave

The Astrophysical Journal, 938:66 (14pp), 2022 October 10 Tauris

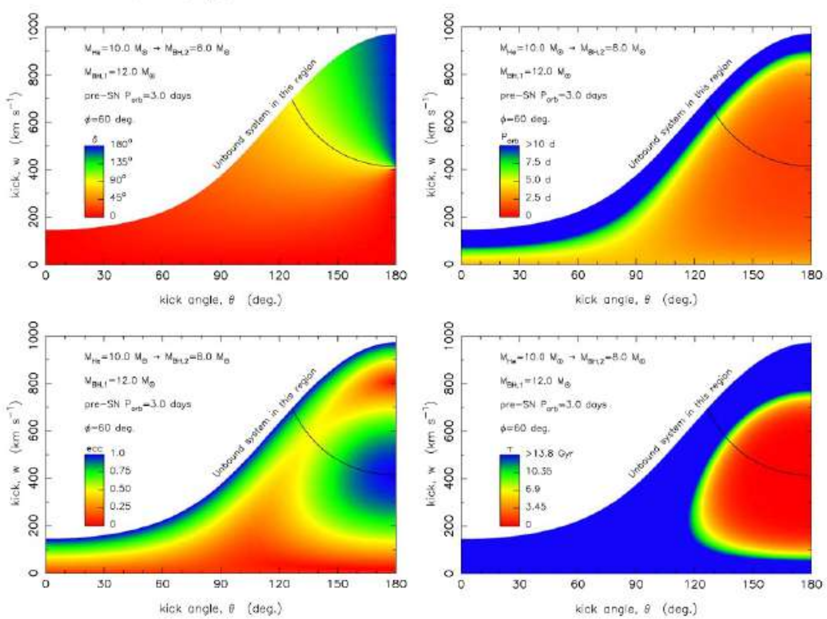

$$\chi_{\rm eff} \equiv \frac{(M_1\chi_1 + M_2\chi_2)}{M_T} \cdot \frac{\boldsymbol{L}}{|\boldsymbol{L}|}$$

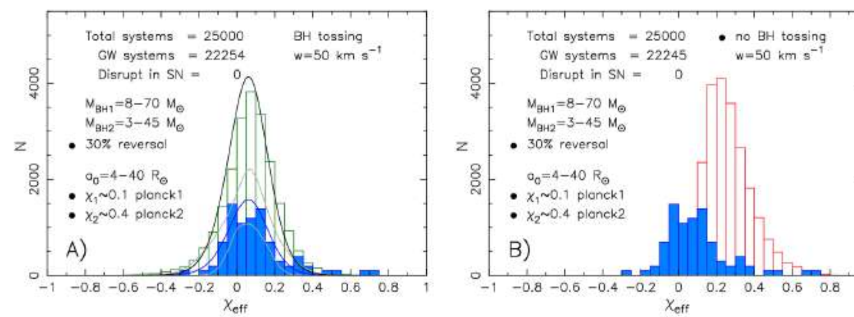

short Gamma-Ray Burst (sGRB)

sGRB may be launced (within 2 sec) via either:

a) Pair-annihilation of neutrinos

b) Strong (and twisted) B-field (Blandford-Znajek mechanism, MRI)

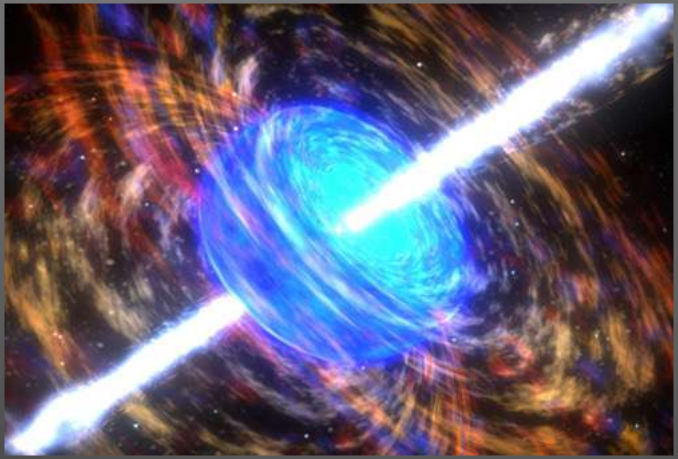

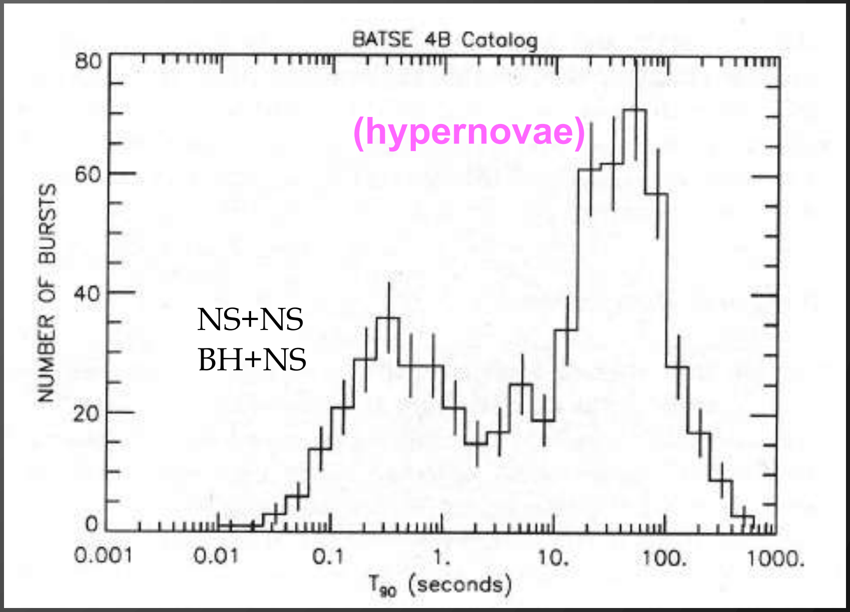

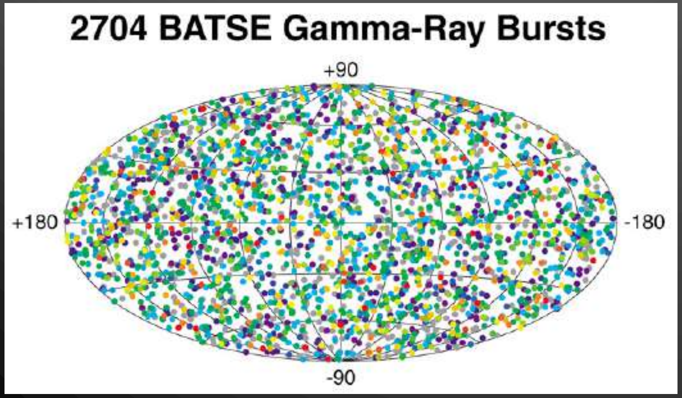

Unified Picture of Gamma-Ray Bursts

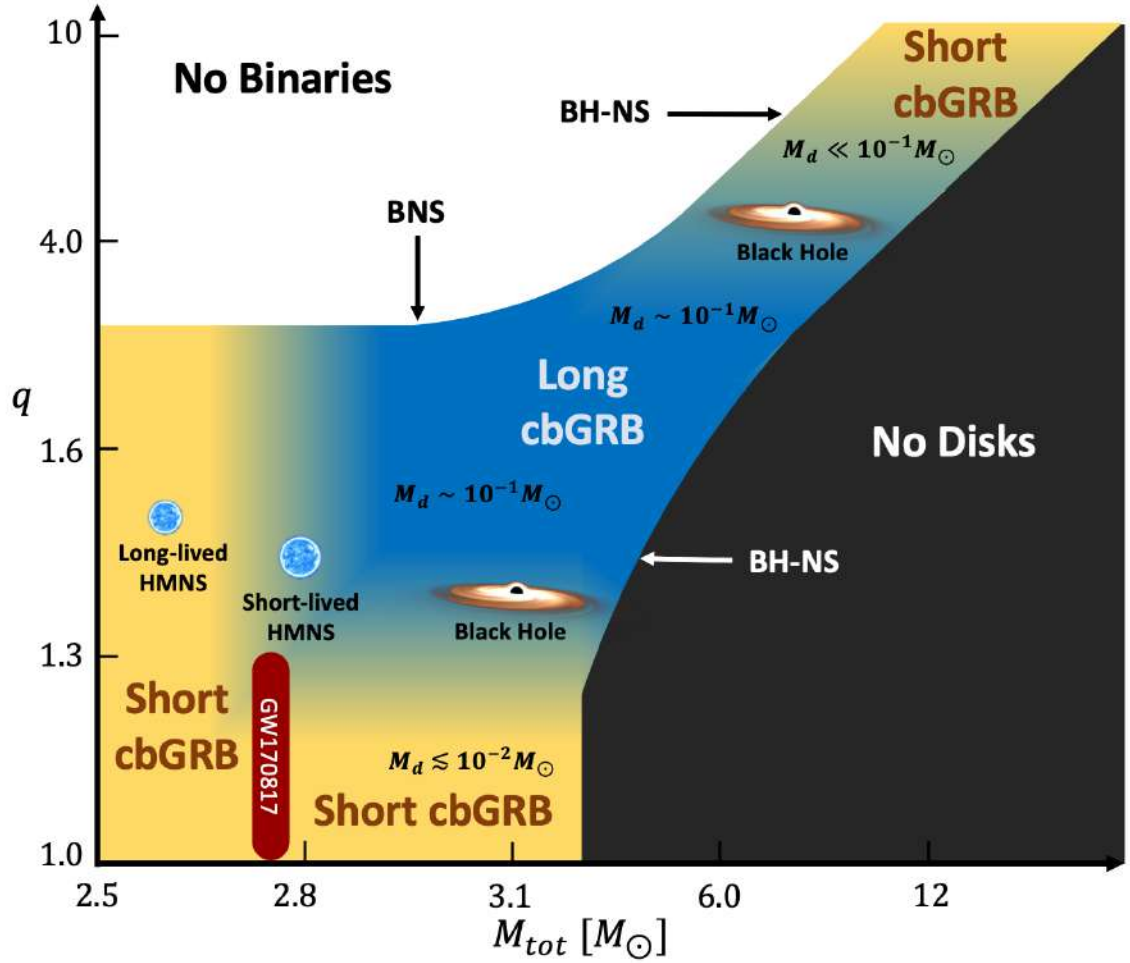

Figure 2. The outcomes of compact object mergers and their ability to power various cbGRBs sub-classes as a function of the binary mass ratio and total mass. lbGRBs occur in high $M_{\rm tot}$ and high q BNS mergers that form a massive BH disk, or in high pre-merger BH spin and low mass ratio BH–NS mergers (blue region). sbGRBs may arise either from equal mass ratio BNS mergers (bottom yellow region) and low pre-merger BH spin/high mass ratio BH–NS mergers (top yellow region), or by HMNS formed in BNS mergers with $M_{\rm tot} \lesssim 2.8\, M_\odot$ (left yellow region). The absence of evidence for distinct sub-classes of sbGRBs suggests that either BHs or HMNSs are likely to be the sole origin of these events, i.e. only one of the proposed sbGRB scenarios is correct. The Galactic BNS mass distribution, the bimodal GRB duration distribution, and GW170817 observations favor HMNSs as the engine of sbGRB jets.

Gottlieb et al. (2023)
https://arxiv.org/abs/2309.00038

Gottlieb et al. (2023)

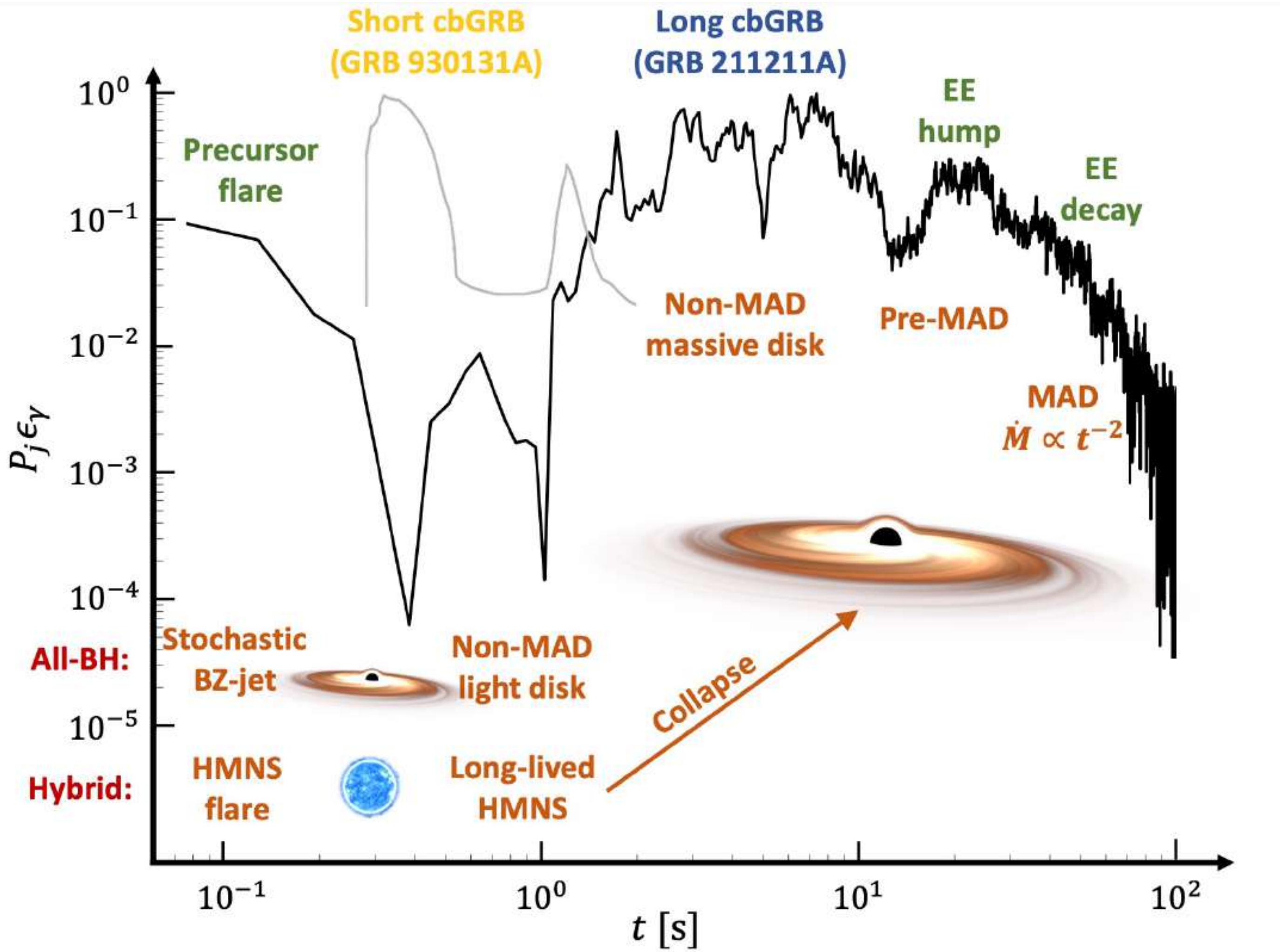

Figure 3. An illustration of how the underlying physics of the merger product (orange) in the hybrid and all-BH scenarios (red) translates into different phases in the cbGRB light curves: sbGRB (yellow), lbGRBs (blue) and preceding and succeeding phases (green). Representations of the light curves of the lbGRB 211211A (Rastinejad et al. 2022) and sbGRB 930131A (Kouveliotou et al. 1994) are shown in black and gray, respectively, in a log-log scale.

Gottlieb et al. (2023)

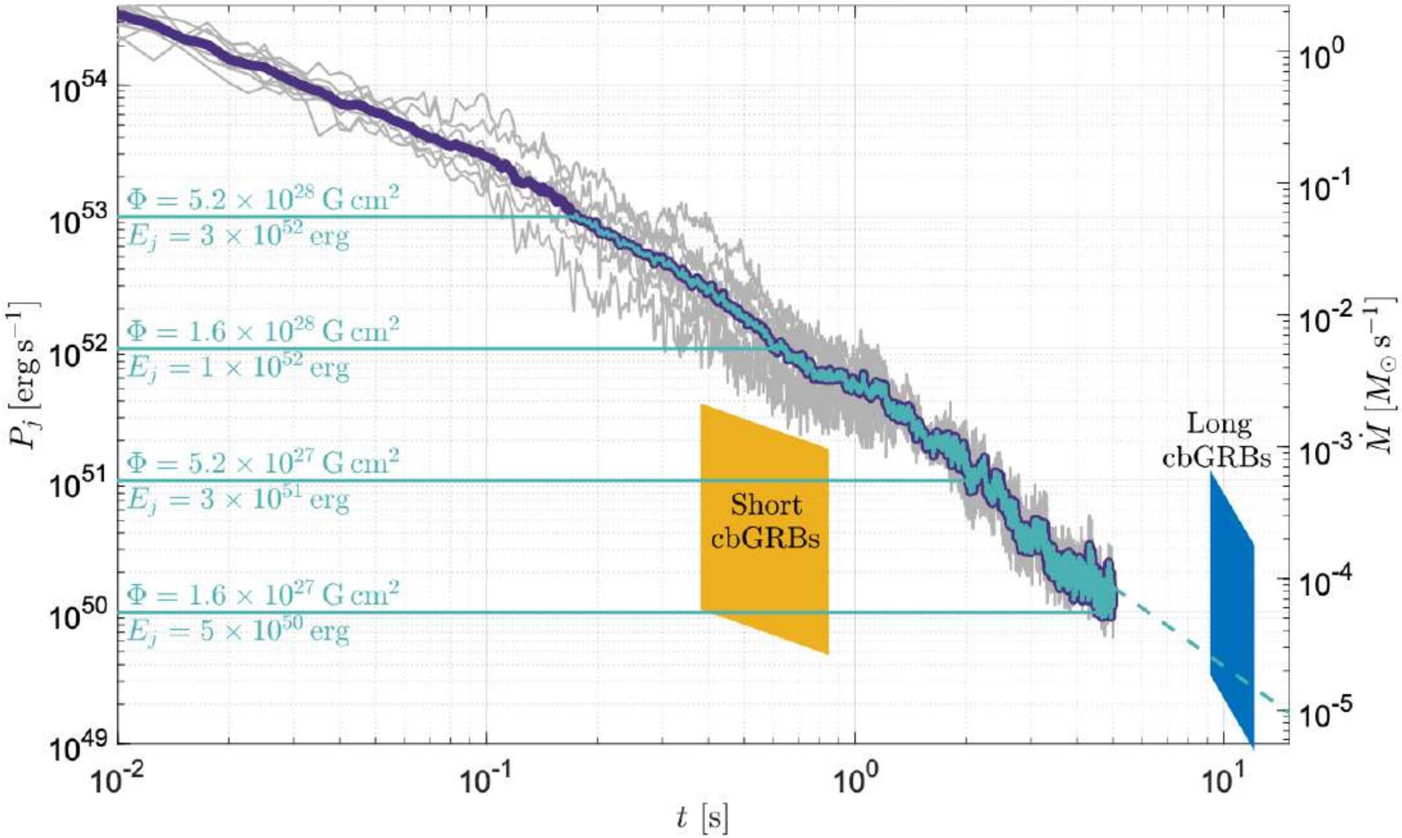

Figure 1. The jet power evolution of post-merger accretion disks for varying levels of magnetic flux ranging from non-MAD to MAD. Gray lines show the post-merger mass accretion rate evolution (right vertical axis) obtained for 4 BH–NS merger simulations (Gottlieb et al. 2023b) and the 5 BNS merger simulations presented here, all of which generate massive disks $M_d \approx 0.1\, M_\odot$. The purple line delineates the logarithmic average of these mass accretion rates, which constitutes the maximum jet power assuming $\eta_a = 1$ corresponding to a BH spin $a \approx 0.87$ (left vertical axis). Turquoise lines illustrate schematically the jet power evolution for different assumptions about the dimensional magnetic flux threading the BH, Φ, and the corresponding total jet energy, E_j. Since the magnetic flux on the BH is likely accumulated early and hence remains nearly constant before the disk transitions to MAD, the jet power, P_j, is also predicted to be roughly constant at these times. However, once the dimensionless magnetic flux saturates in the MAD state, the jet power saturates at $P_j = \dot{M}c^2$ and thus follows the mass-accretion rate $\dot{M} \propto t^{-2}$ thereafter (we have extrapolated P_j by a dashed line to later times). The yellow (blue) region outlines the estimated average jet power and duration T_{90} (T_{50}) of the sbGRB (lbGRB) population based on prompt emission and afterglow observations (see text). While the jets from such massive disks are either too powerful, or operate for too long, compared to the sbGRB population, BH accretion from such massive disks nicely matches the observed properties of lbGRBs.

Kilonovae

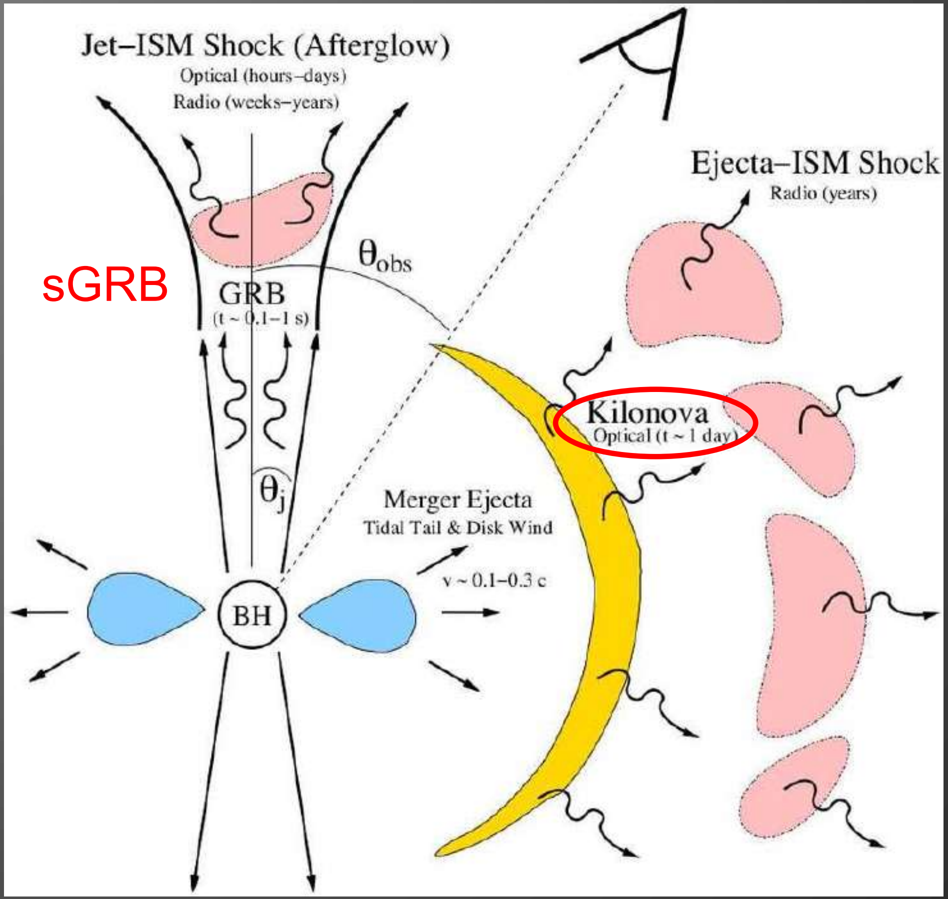

sGRB

Metzger & Berger (2012)

Excellent reviews:
Giacomazzo, Eichler & Arcones (2019)
Shibata & Hotokezaka (2019)

Optical near-IR kilonova (makronova / sGRB afterglow)

- 0.01-$0.1\ M_{sun}$ ejected as dynamic + viscous ejecta
  (more disk mass for aligned spin axes,
  also dependence on NS+NS vs BH+NS)

- r-process nucleosynthesis (heavy n-rich nuclei).

- The decay to stability powers an EM transient.
  (Abbott et al. 2017, Metzger 2017, Rosswog et al. 2018)

- Peaks at $L=10^{42}$ erg s^{-1} after about one day
  Faint (21-24 mag) and fast decay (hrs-days)
  The EM signal (kilonova) is affected by mass composition (Y_e), and temperature of ejecta.

- ISM powered X-ray and radio afterglow
  from synchrotron emission
  (a few 100 μJy, weeks-months)

- Neutrinos are not expected to be detected
  (even in next generation detectors) due
  to the large distances.

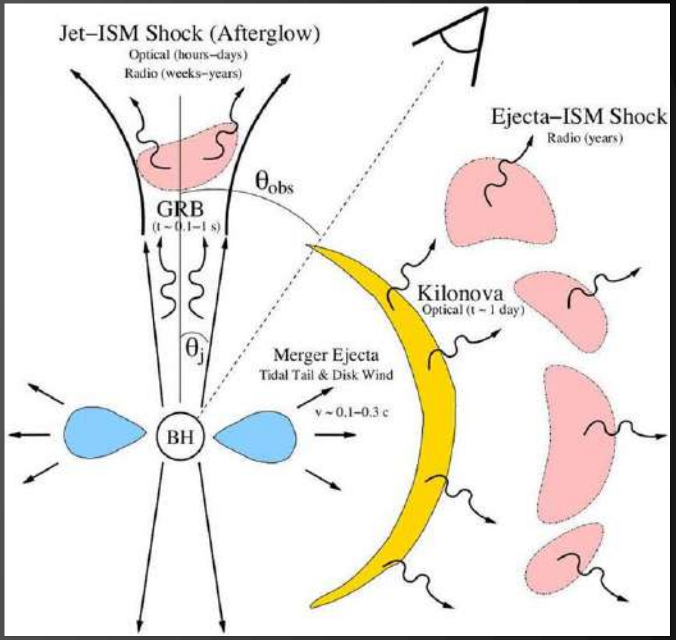

Metzger & Berger (2012)

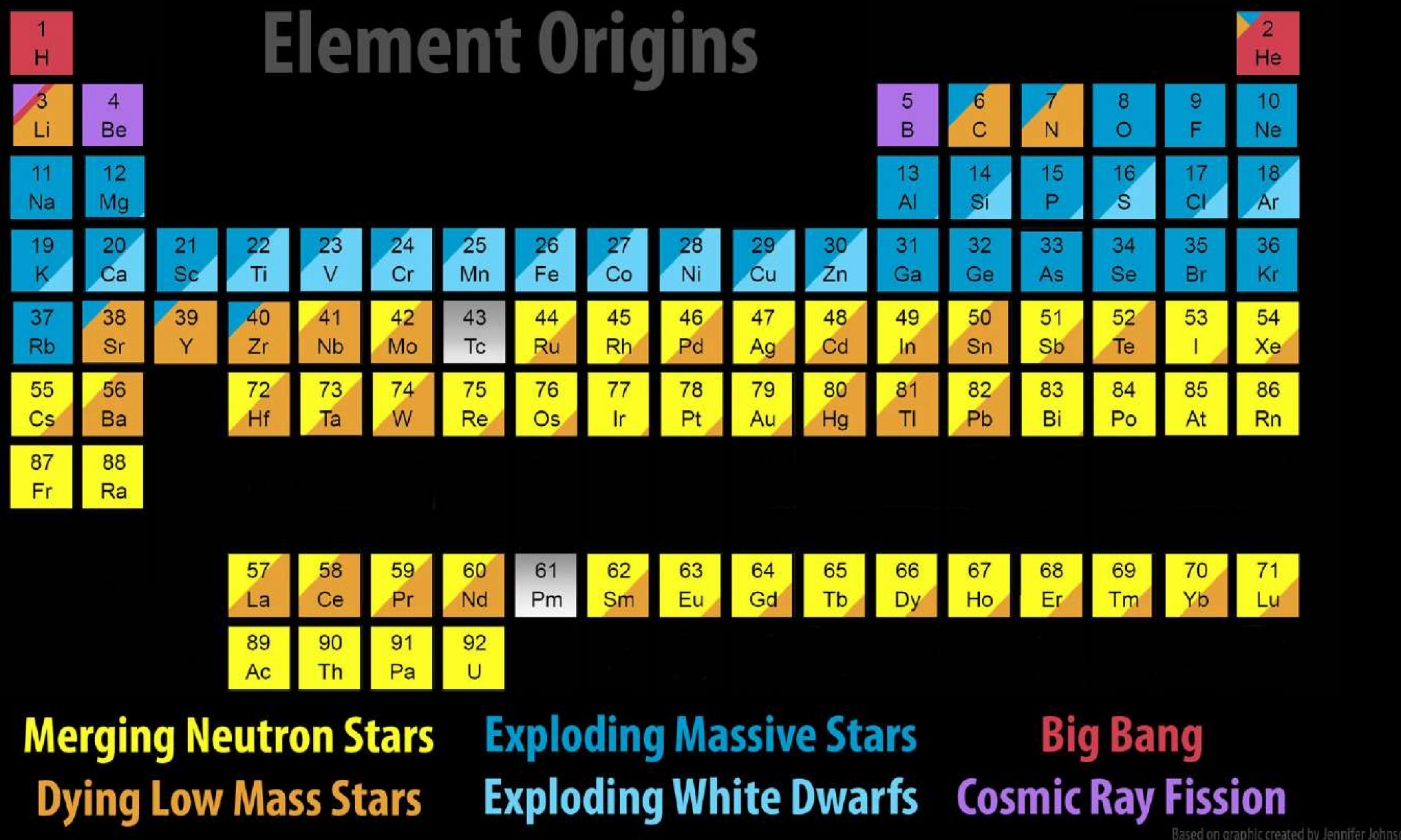

Metzger & Berger (2012)

The r-process (see Giacomazzo et al. 2019)

Rapid neutron-capture process (r-process) was proposed by Burbidge et al. (1957) and Cameron (1957). It occurs due to **fast neutron (n) captures in comparison to beta-decays,** and runs very close to the n-drip line.

Accumulation of material along the path occurs whenever isotopes with a closed **n-shell** are reached (affecting both the n-capture cross sections and the beta-rates).

After the intense supply of free neutrons has ceased, the extrenely n-rich isotopes undergo a series of beta-decays to stability.

The final average mass can be estimated from:

final average mass number (e.g. Pu-244)

initial seed nuclei (typical iron group, e.g. 60)

$$\langle A \rangle_f = \langle A \rangle_i + \left(\frac{Y_n}{Y_{seed}}\right)_i$$

ratio (e.g. 184) = $\dfrac{\text{neutron abundance}}{\text{summed up abundances of seed nuclei}}$

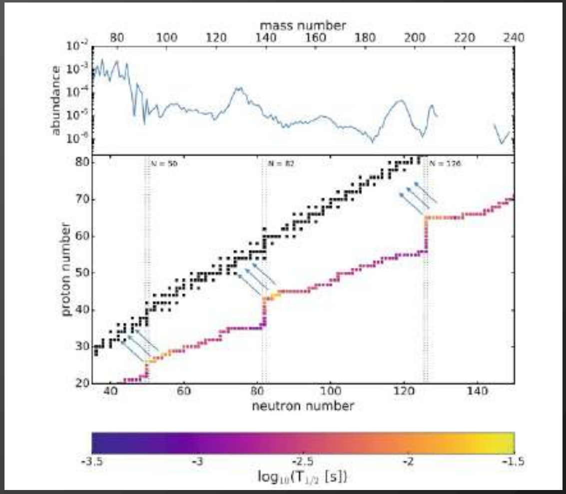

Note, a high Y_n is possible where Y_e is low (b/c charge neutrality), e.g. in NS merger ejecta.

Sometimes fission cycles occur in which A_f is divided in two and builds up again.

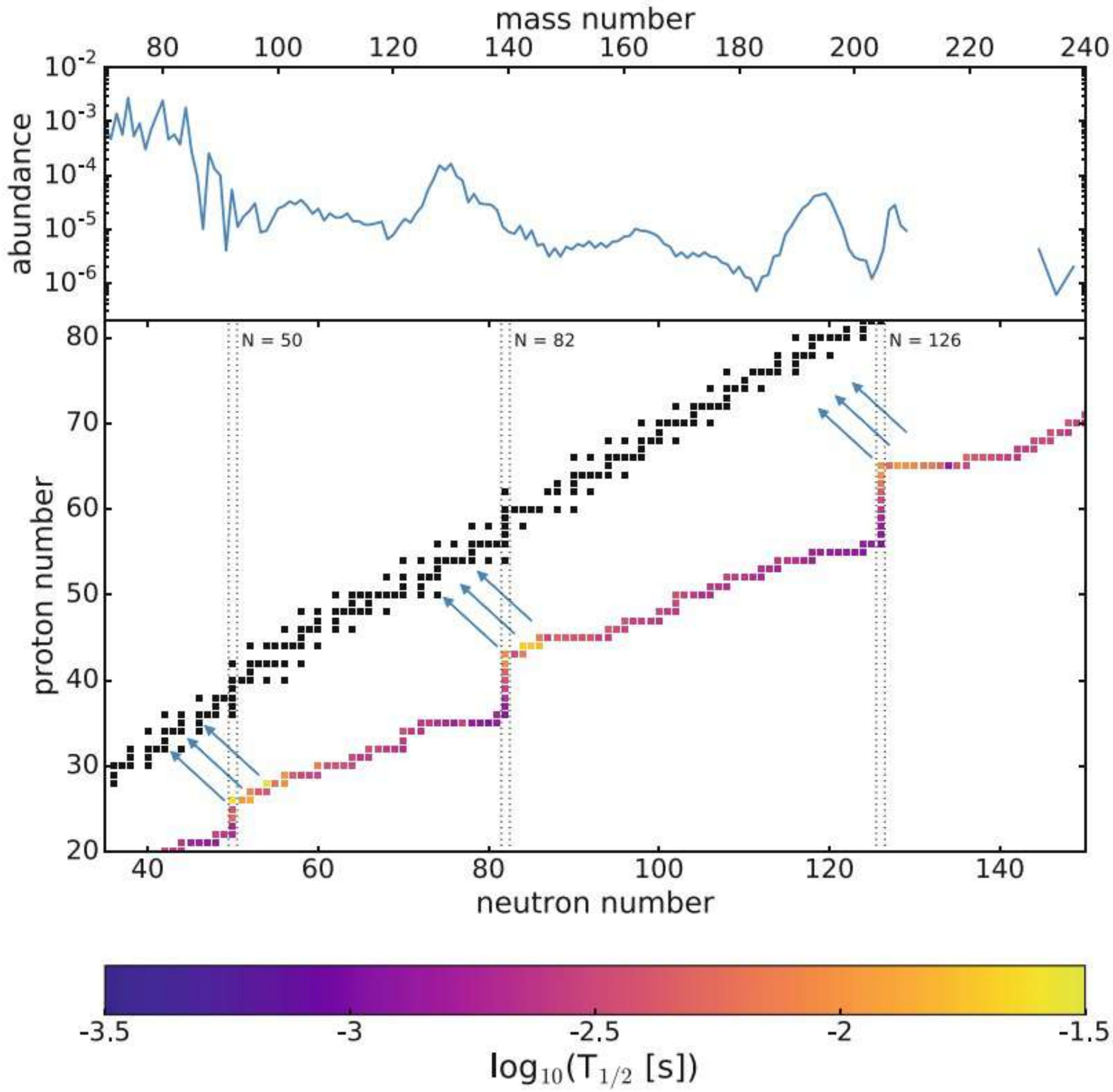

Fig. 11.2 Top panel: Solar r-process abundances as a function of nuclear mass number A. The values are taken from Sneden et al. (2008). Bottom panel: Typical r-process path in the nuclear chart and the corresponding β-decay half-lives according to Möller et al. (2003). Stable isotopes are marked in black and the magic neutron numbers are indicated by vertical dotted lines. The overlay of the two panels demonstrates how regions of large $T_{1/2}$ at the magic neutron numbers are responsible for the r-process abundance peaks after decay to stability

Modelling the r-process

Necessary information: characteristics of light to heavy nuclei between the valley of stability and the n-drip line.

Calibration: Solar spectroscopic data, meteoritic values, deep-sea sediments. In particular, the Galactic evolution of the Eu (Z=63) abundance is of interest.

The pattern of abundances of heavy n-capture elements (e.g. Z=58-76 or the Lanthanides) observed in r-process-rich metal-poor stars are remarkably similar to the Solar System measurements.

Actinides have a clear and unique r-process origin.

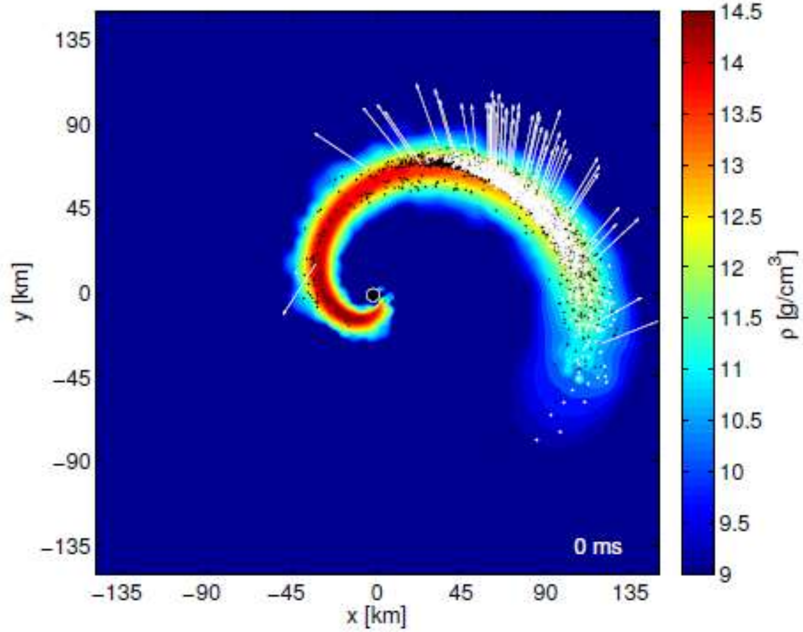

Just et al. (2015)

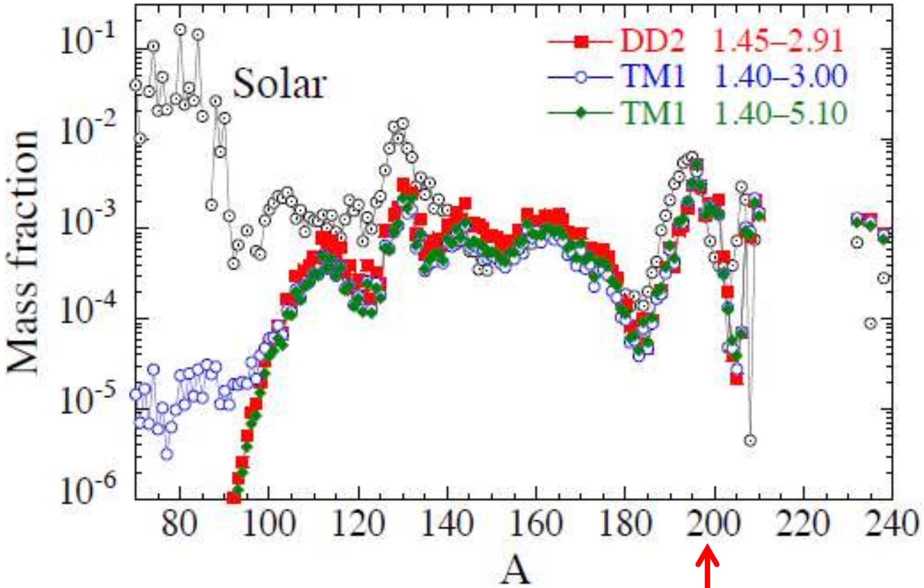

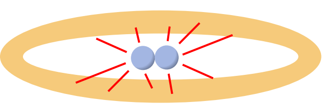

Double neutron star mergers:

→ ejection of $10^{-3} - 10^{-2}\ M_\odot$ heavy r-process elements

See also Rosswog (2013, 2013RSPTA.37120272R)

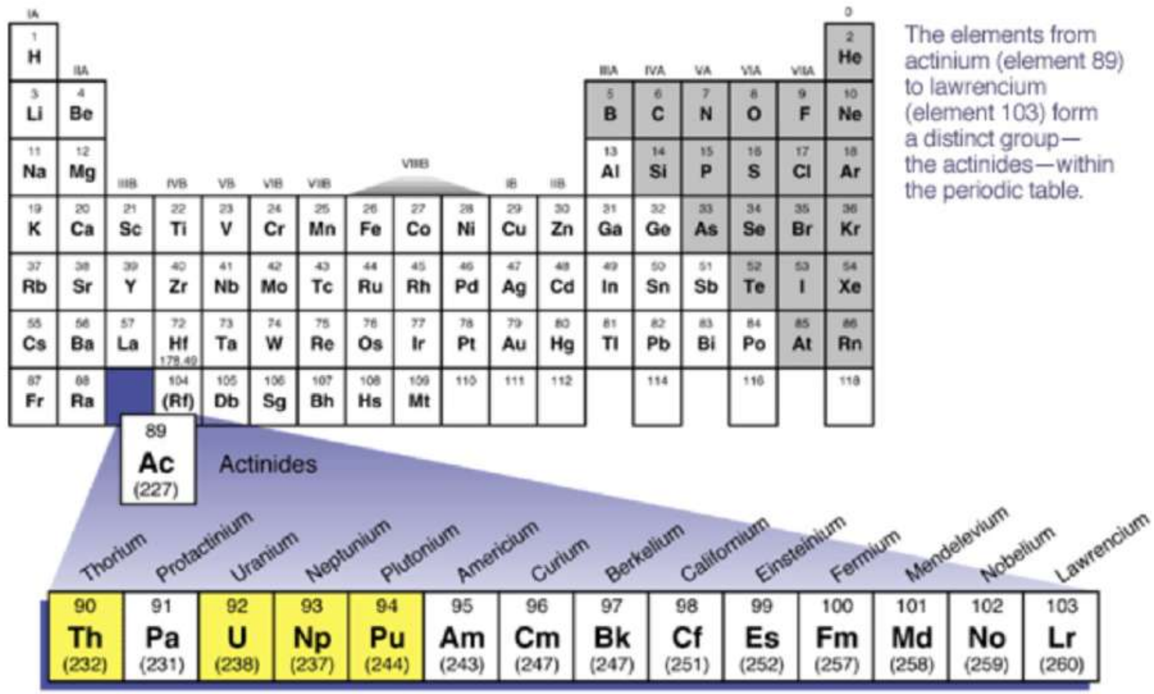

The elements from actinium (element 89) to lawrencium (element 103) form a distinct group—the actinides—within the periodic table.

Mass ejecta and electron fraction

1) Dynamical ejecta (tidal disruption)

2) Disk ejecta (viscous heating and MHD)

Total amount of ejecta (few 0.001 M_{sun} to 0.1 M_{sun}) depends on:

- NS+NS → prompt BH formation or MNS (meta stable, Δt = 10 ms – 10 s)
- Mass ratio (q < 0.8 leads to larger yield)
- NS radius and BH spin

Important output parameters are: mass, velocity and electron fraction (Y_e).

Y_e is of key importance for determing the abundance of r-process elements, which again determine the opacity of the EM emission.

Electron fraction and opacity

NS material: $Y_e = 0.05 – 0.1$

However dynamical ejecta could be influenced by weak processes (>10 MeV)

which drive $Y_e = 0.5$ $n + e^+ \rightarrow \; p + \bar{\nu}_e$ $n + \nu_e \rightarrow \; p + e^-$

n-rich matter (Y_e small): r-process elements with A > 120 are robustly synthesized

n-poor matter (Y_e large): only r-process elements with A < 130 are synthesized
(i.e. lanthenides are not produced)

Opacity (photon): large for lanthenide-rich ejecta (red colour)

small for lanthenide-poor ejecta (blue colour)

Shibata & Kotokezaka (2019)

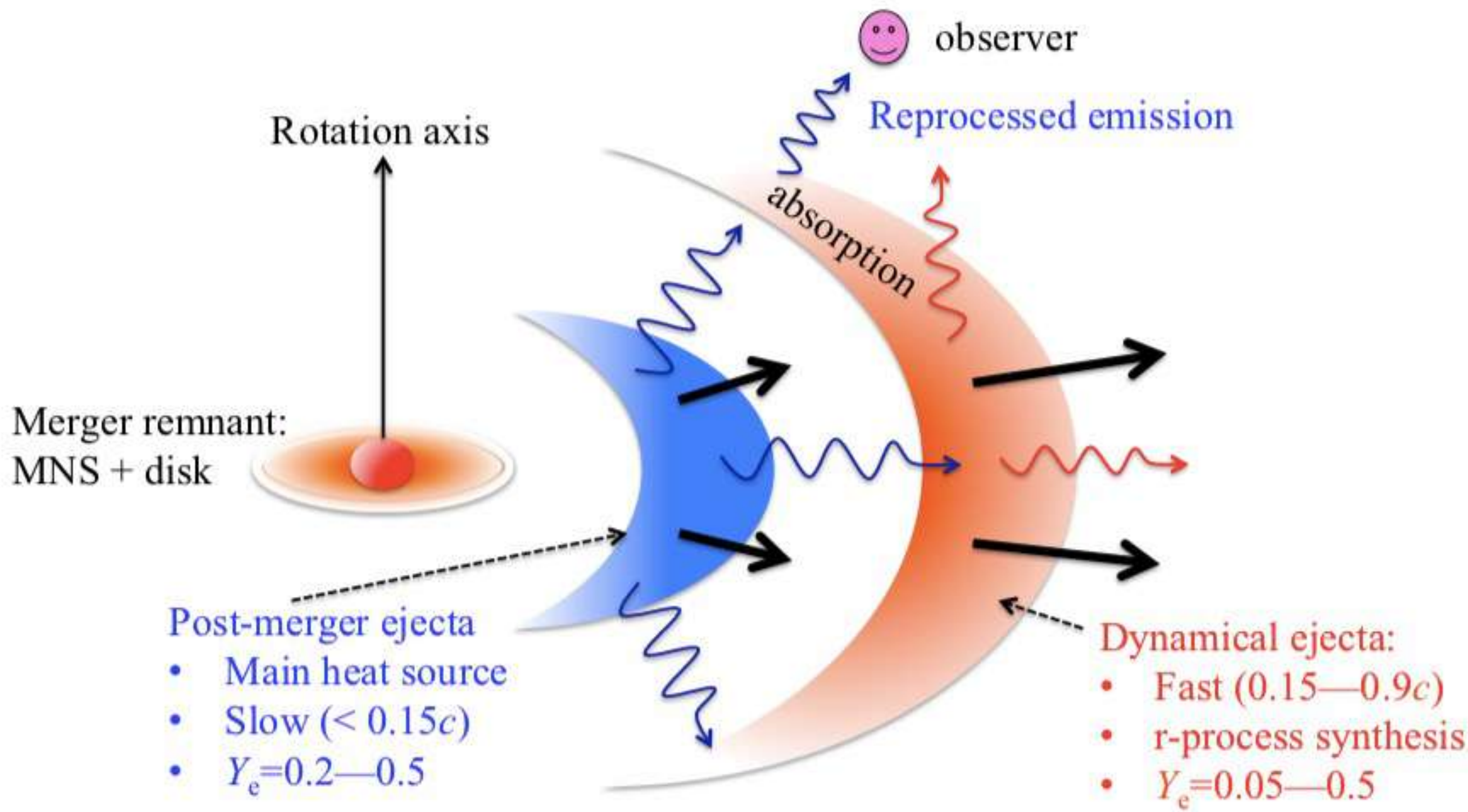

A<130 synthesized

A>120 synthesized (lanthanides)

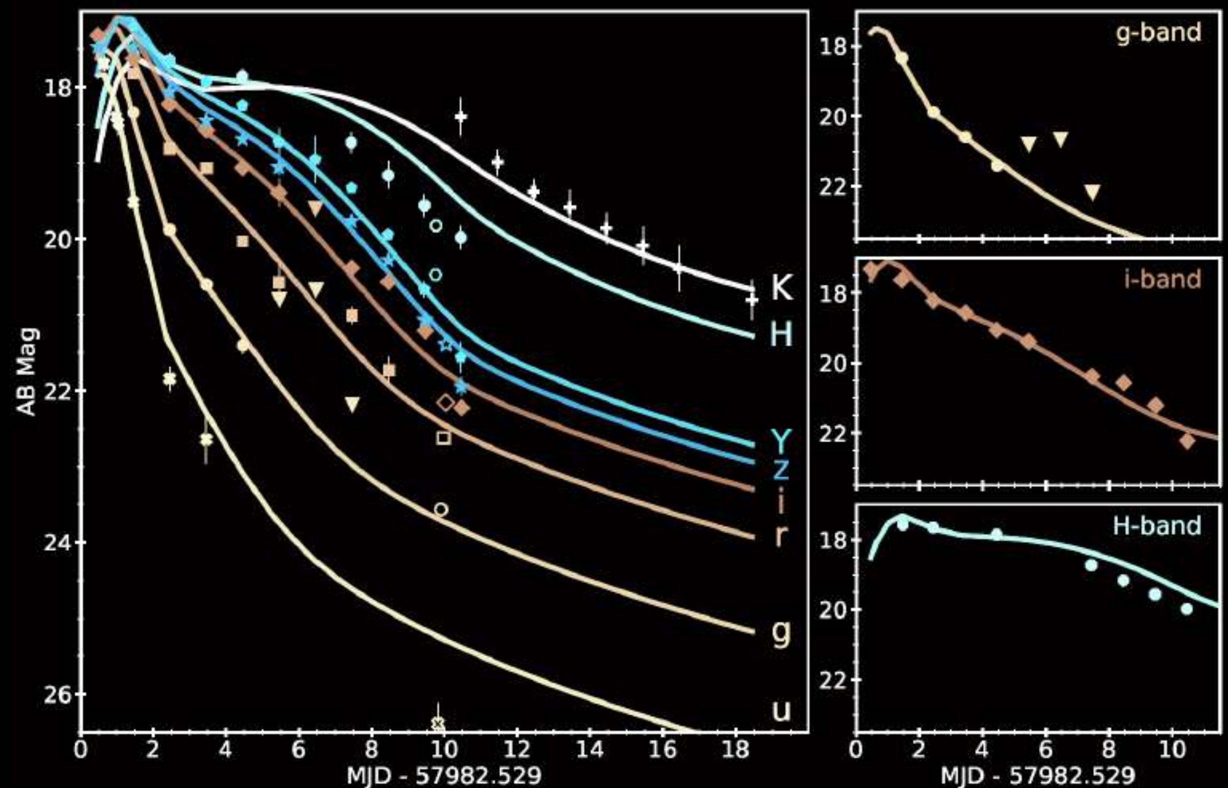

UV, optical, and near-IR spectra are well fit by a two-component kilonova

0.02 M_{sun} lanthanide-poor ejecta (blue) and 0.05 M_{sun} lanthanide rich ejecta (red)

Cowperthwaite,..., DAB et al. ApJ **848** L17 (2017)

The following 5 slides are provided by Duncan Brown.

Distance-constrained GW observations of viewing angle are consistent with EM observations

Mooley et al. report 14 - 28 deg from radio

Troja et al. report 21 - 29 deg from broad band observations

GW and EM observations support successful-jet cocoon model (structured jet)

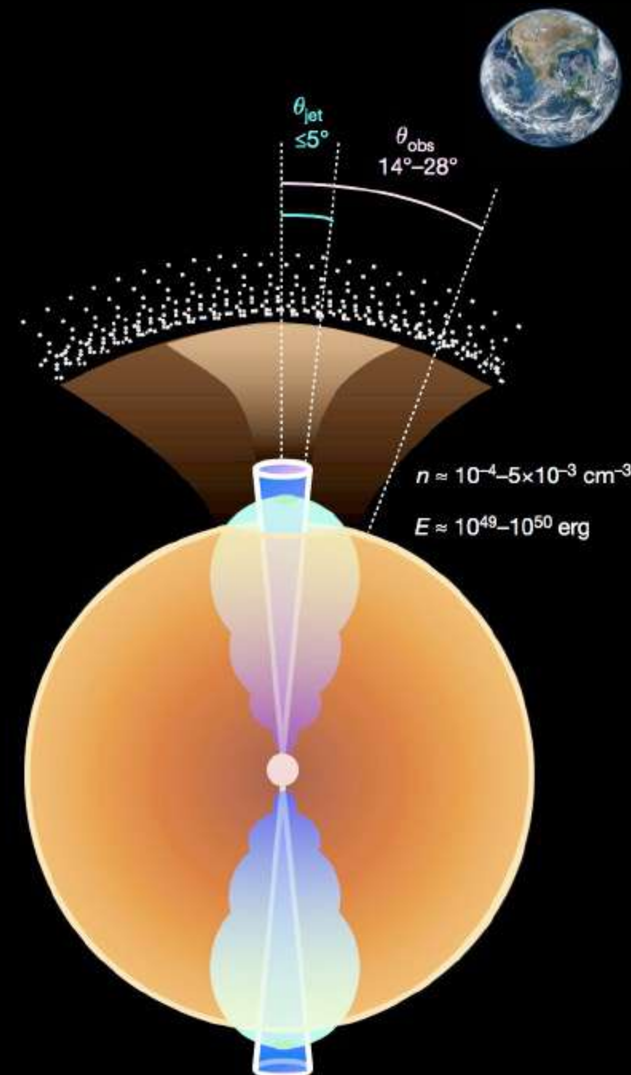

Mooley et al. Nature **561**, 355 (2018)

Troja et al. MNRAS arXiv:1808.06617

$v_{red} \sim 0.1$ c

$v_{blue} \sim 0.25$ c

Kilonova light curves suggest the existence of a hyper massive neutron star prior to collapse to a black hole

EM suggests neutron star merger

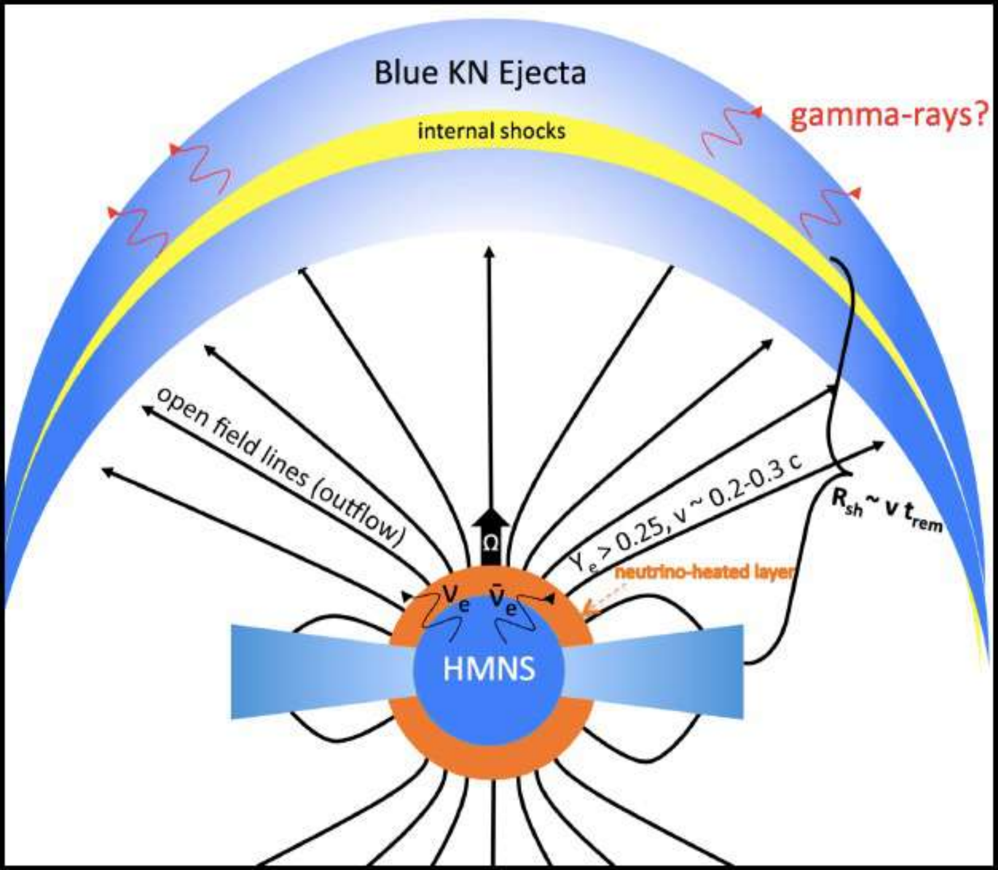

Metzger, Thompson, Quataert ApJL **856** 101 (2018)

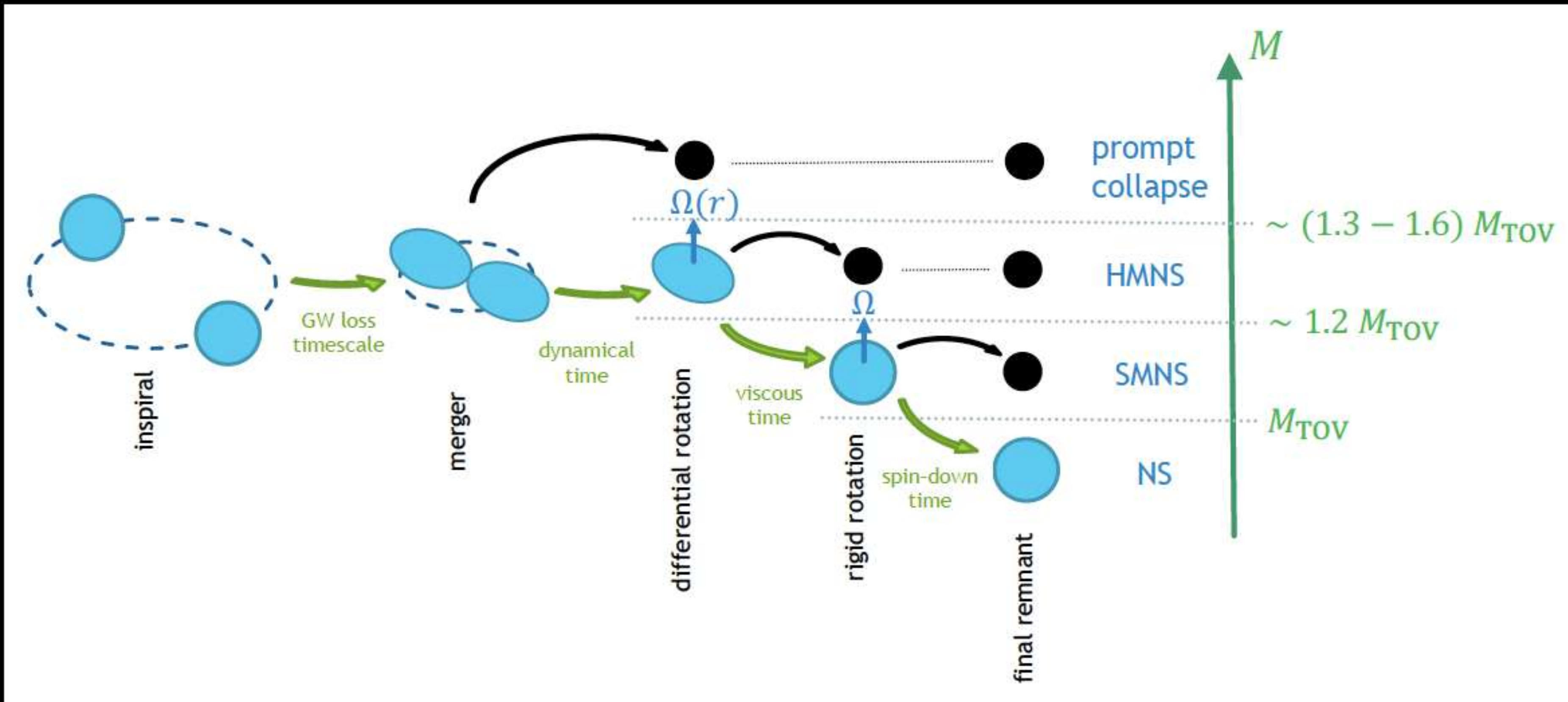

Ben Margalit

The merger remnant also places a constraint on the maximum neutron star mass

The remnant NS cannot be long lived, or there would be too much energy in the EM observantion

$$M_{\max} \leq 2.17 M_{\odot} \ (90\%)$$

Margalit and Metzger ApJL 850 19 (2018)

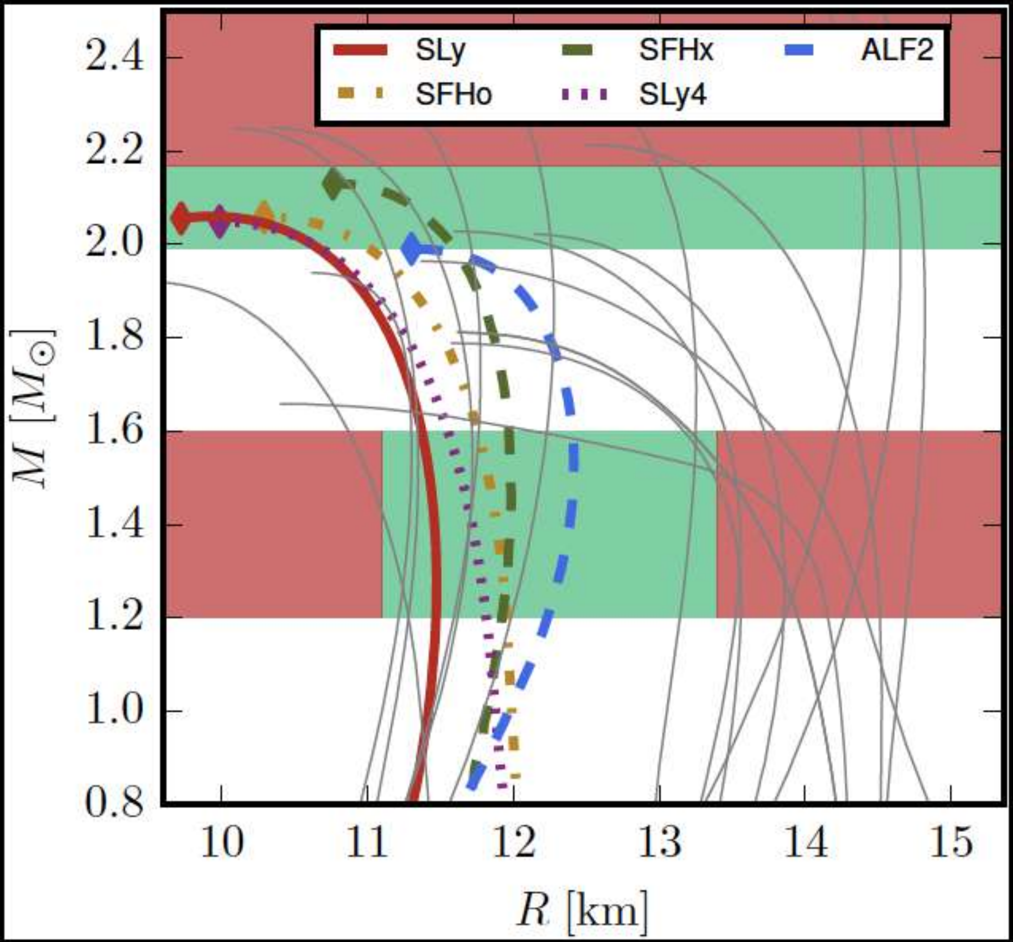

Coughlin, Dietrich, Margalit, Metzger arXiv:1812:04803

The r-process: observational evidence
NS mergers versus core collapse supernovae

GW170817: first firm detection of kilonova (EM transient).

Ejected mass $\Delta M_{eject} \geq 1.5 \times 10^{-2}\ M_{\odot}$ depending on amount of energy release ending up in the observed emission (Rosswog et al. 2017)

Heavy r-process elements are also observed in atmospheres of old stars and in the Solar system. If they are explained by core-collapse SNe the amount of enrichment per explosion is therefore about $10^{-5}\ M_{\odot}$ for a Galactic SN rate of about $0.01\ yr^{-1}$

However, studies of a group of stars in the dwarf galaxy Reticulum II supports rare events with large ejecta (NS mergers) compared to frequent events with little ejecta (core-collapse SNe), cf. Beniamini et al. (2016).

- **Spin distributions of BHs and NSs**

| $X_{\rm eff}$ | < 0.35 at the 90% credible level for all events!
(degeneracy between projected spins and
orbital inclination, masses)

$$\chi_{eff} \equiv \frac{1}{M}\left(m_1\chi_1 + m_2\chi_2\right)$$

3G ?

Provides a clue to their astrophysical origin
e.g. Baibhav et al. (2020)

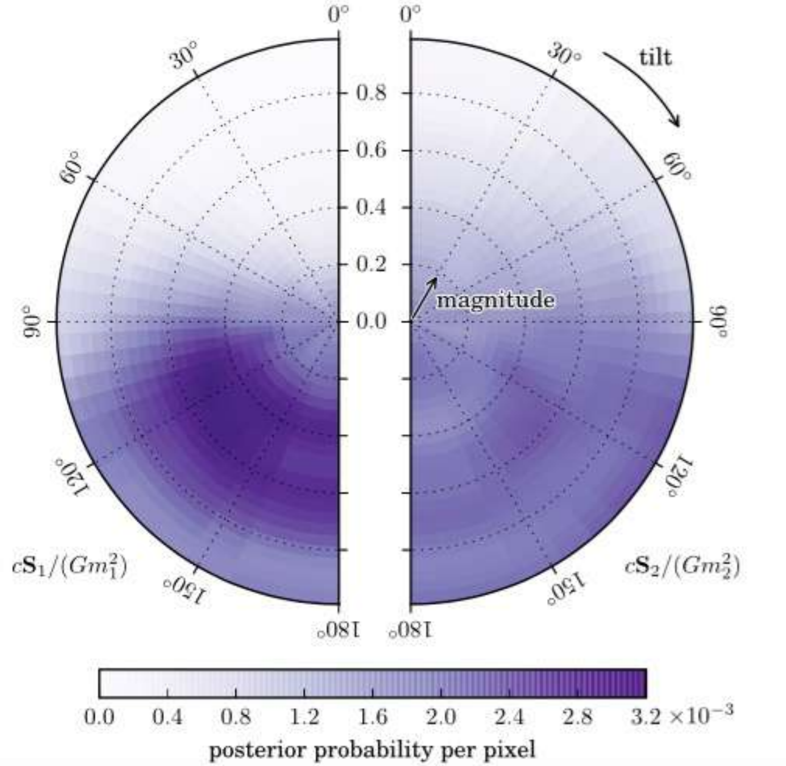

- **Tests of GR and other gravity theories**

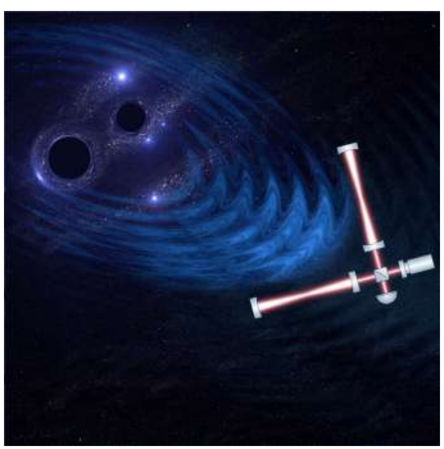

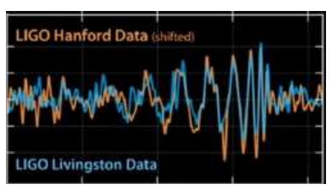

- **Multi-messenger astrophysics**
- ✓ GWs
- ✓ Optical
- ✓ X-rays
- ✓ Radio
- ✓ …more

LISA
~2034

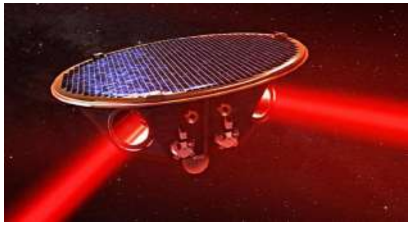

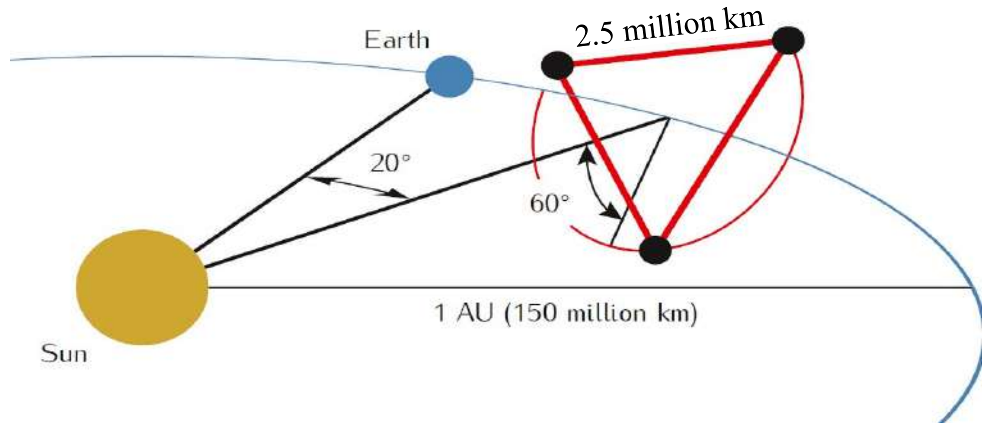

3G
~ ?

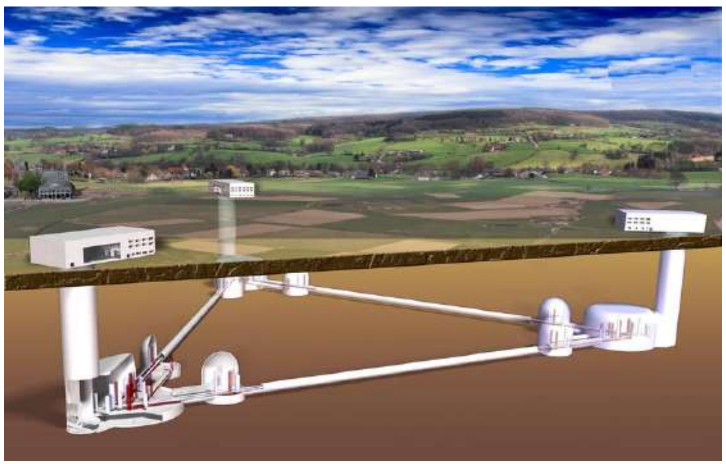

EINSTEIN TELESCOPE

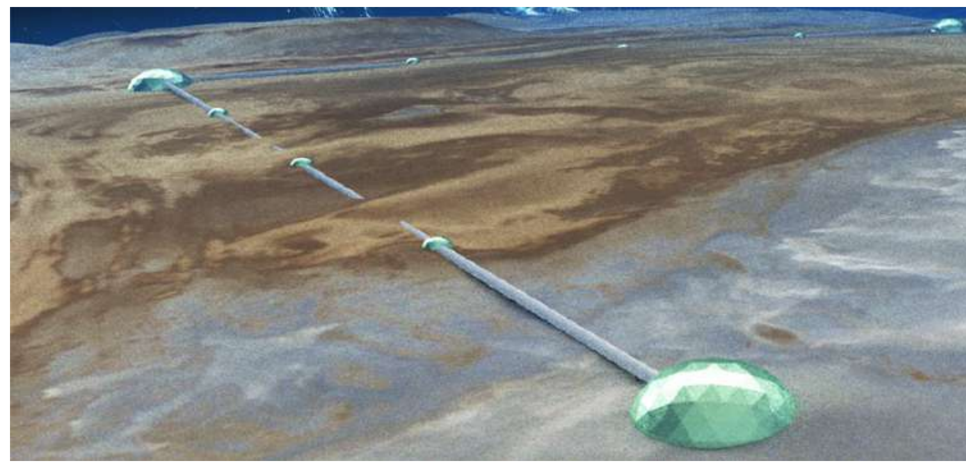

COSMIC EXPLORER

Ask for 3 detectors
(~ 1 billion € each)

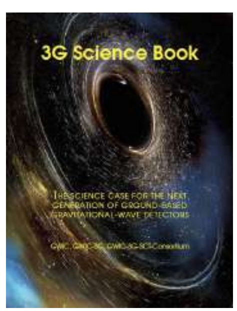

- Detect all BH-BH mergers out to $z \sim 20$
- Detect the BH seeds evolving into SMBHs
- Possibly detect primordial BHs
- Determine the NS EoS to extreme precision
- etc.

GW spectrum evolution

with finite-temperature effects (specific entropy) of the WD donor

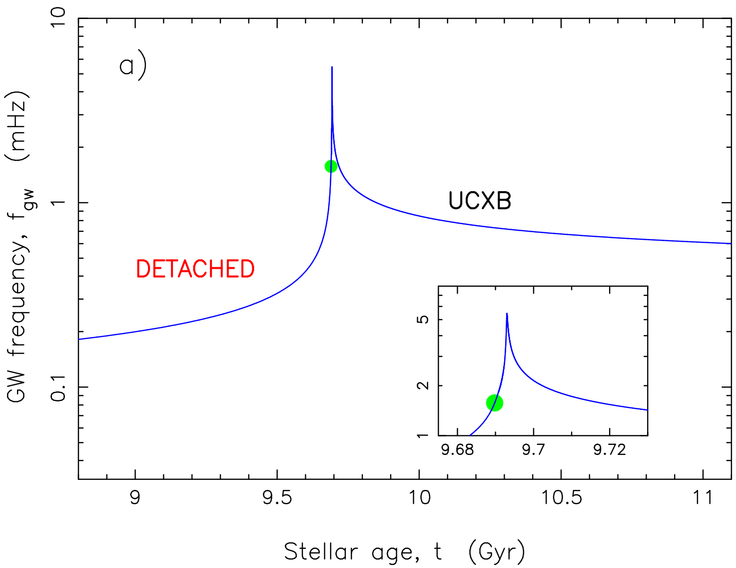

Tauris (2018), PRL

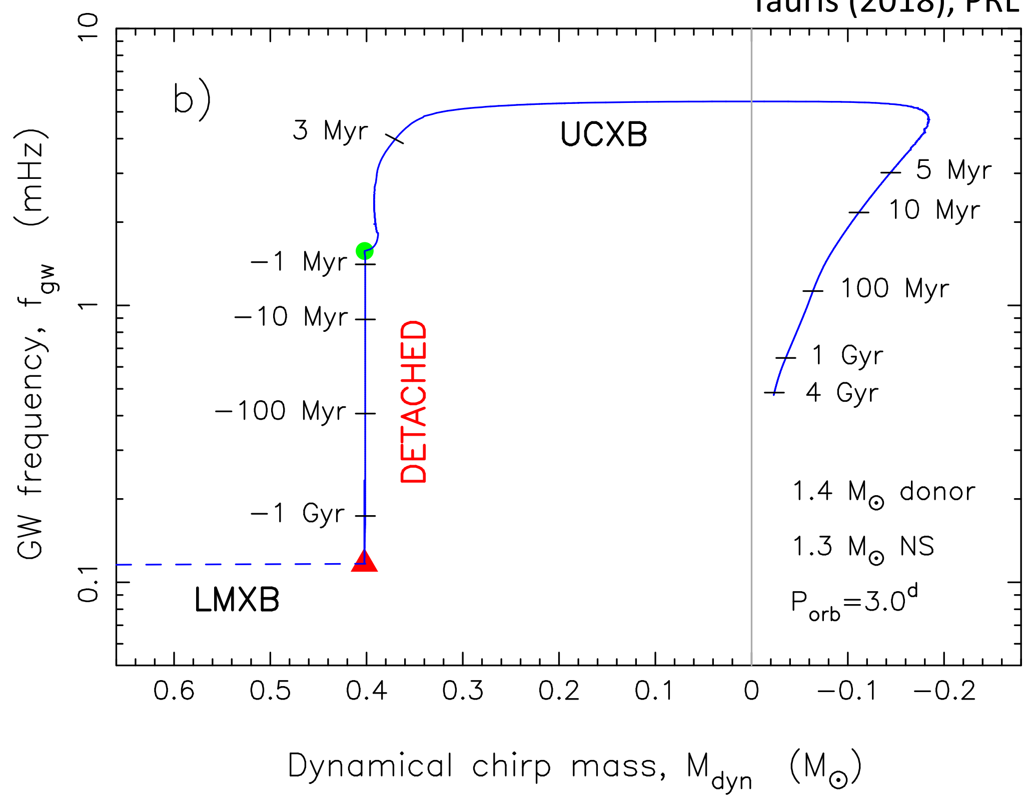

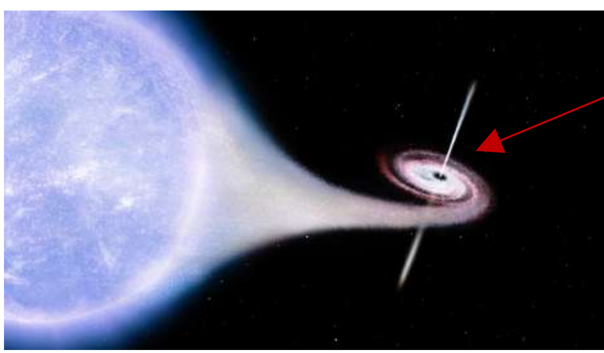

Determine NS the mass to a high accuracy via a new method

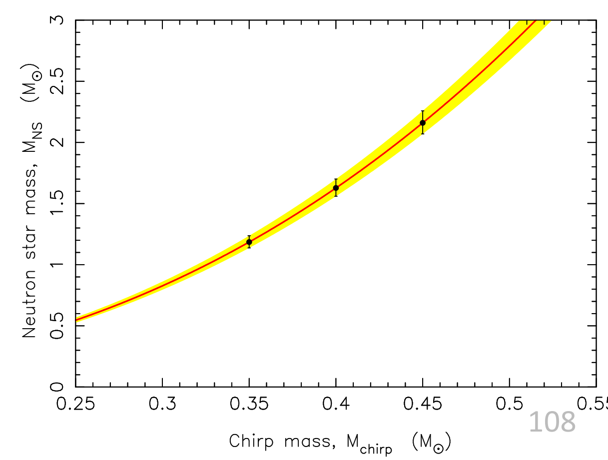

Tauris (2018), PRL

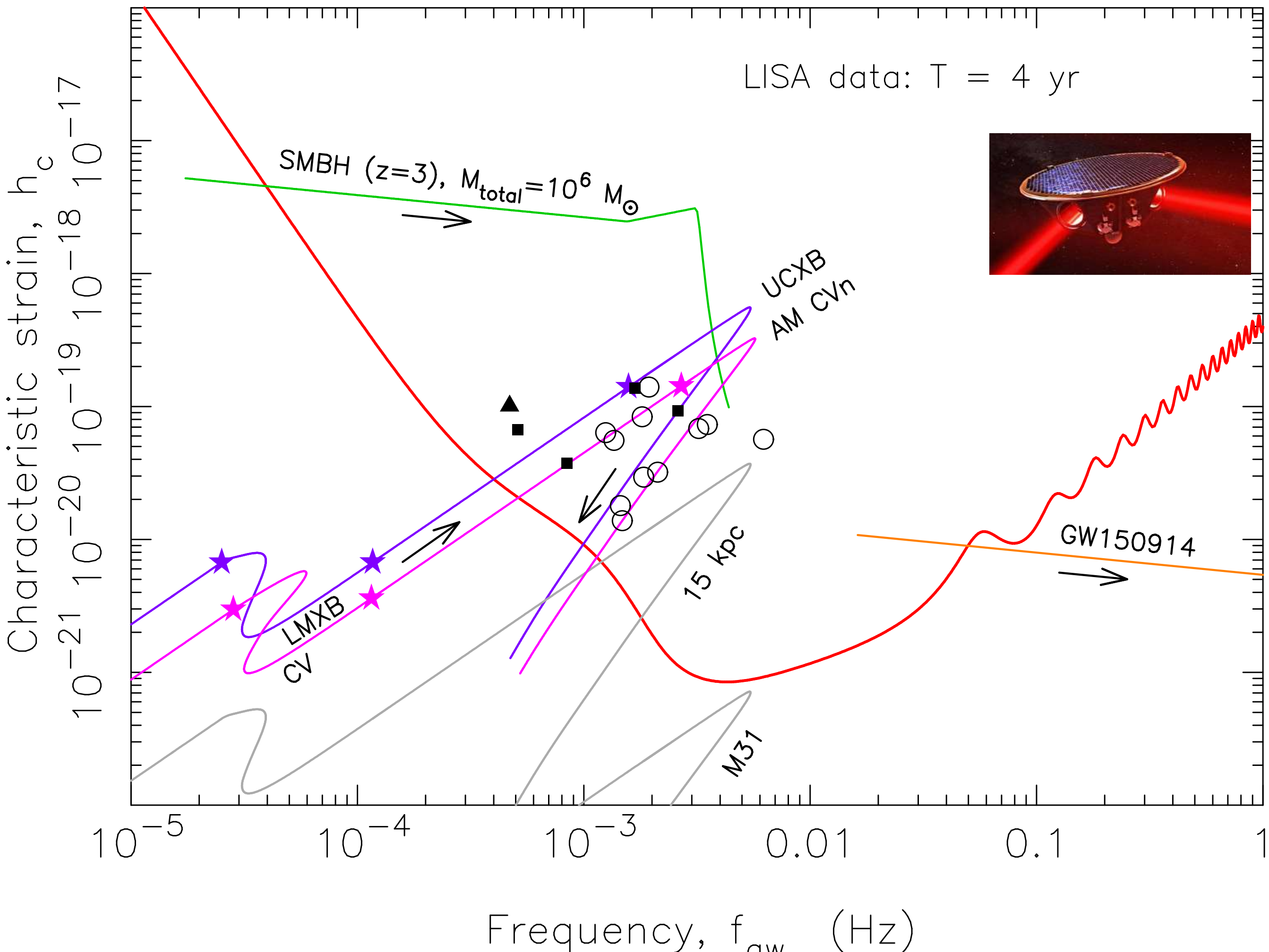

$$h_c \approx \sqrt{N_{cycles}}\,\sqrt{2}\,h_0 = \sqrt{2 f_{gw} T_{obs}}\,h_0 \qquad h_0 = \sqrt{\frac{32}{80}}\,\frac{\pi^{2/3} G^{5/3} f_{gw}^{2/3} M_{chirp}^{5/3}}{c^4\, d_L}$$

Physics of Compact Objects
week 10

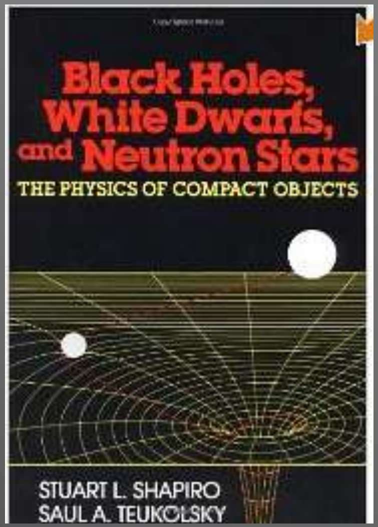

Shapiro & Teukolsky (1983), Wiley-Interscience

Curriculum
- Lecture notes
- Tauris & van den Heuvel (2023), Chapter 15
  (Shapiro & Teikolsky Chapter 16)
  (Riles 2013; Colpi & Senasa 2017)
  (LIGO-Virgo-KAGRA: GWTC-3: arXiv:2111.03634)

Exercises: # 7, 8

- Monday Nov. 13, 10:15-12:00
  + course evaluation

Stars

SNe

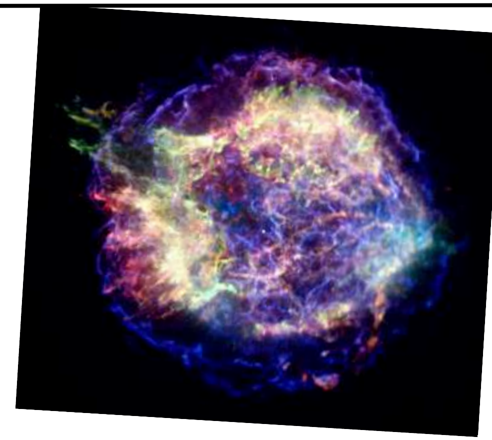

Compact Objects

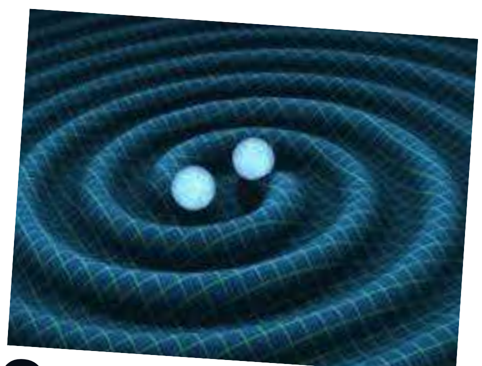

Gravitational Waves

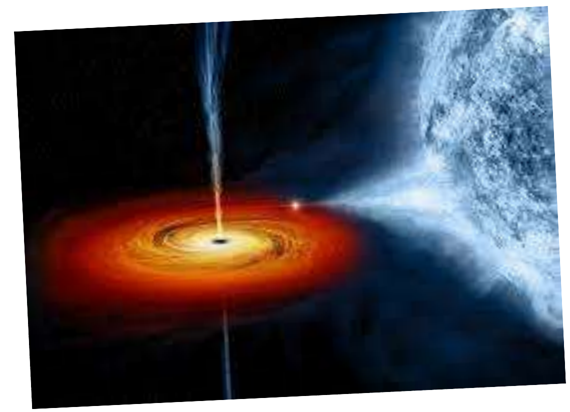

Binary Interactions

Programme

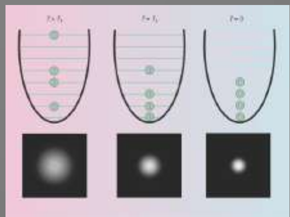

- * **Introduction**
- * **Degenerate Fermi Gases**

  Non-relativistic and extreme relativistic electron / (n,p,e^-) gases

- * **White Dwarfs**

  Structure, cooling models, observations

- * **Neutron Stars**

  Structure and equation-of-state
- * **Radio Pulsars**

  Characteristics, spin evolution, magnetars, observations

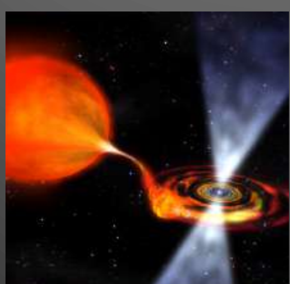

- * **Binary Evolution and Interactions**

  X-ray binaries, accretion, formation of millisecond pulsars, recycling
- * **Black Holes**

  Observations, characteristics and spins

- * **Gravitational Waves**

  Sources and detection, kilonovae
- * **Exam**

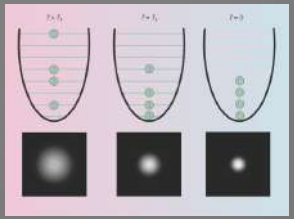

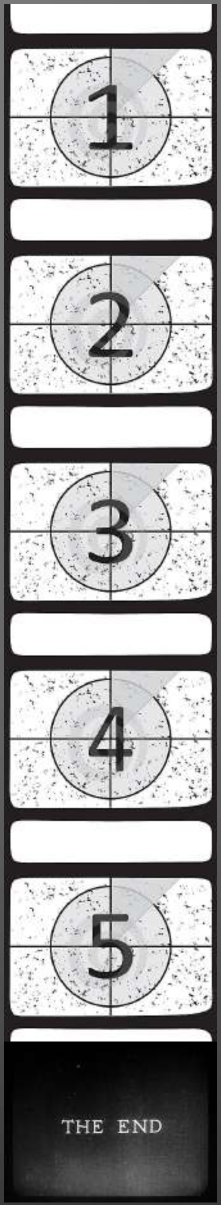

Thanks for joining!
Remember your evaluations